12th Early Career Planetary Scientists Meeting

UK Planetary Forum

19th-20th February 2015 | The University of Kent

Centre for Astrophysics and Planetary Science (CAPS) | University of Kent

SEPnet South East Physics Network

The Open University

The UK Planetary Forum

http://ukplanetaryforum.org | ukpf@hotmail.co.uk

Affiliated to the Royal Astronomical Society
http://www.ras.org.uk

The UK Planetary Forum (UKPF) was founded in 1996 as a representative body of the planetary science community. Its main aim is to promote planetary research in the UK among scientists and the public. UKPF is affiliated with the Royal Astronomical Society (RAS).

The UKPF maintains a website and mailing list through which announcements, news and opportunities are posted. There are over 350 members of the UKPF from institutions across the UK and the worldwide community of planetary scientists. The list also includes research council and media representatives. We are keen to develop innovative activities to promote planetary science in the UK and welcome suggestions and ideas from members.

How to Join

We urge all members of the planetary science community to join the UKPF. Email your name and research details to the address above, or contact one of the committee members directly.

UKPF Committee

Beth Steer (The Open University | beth.steer@open.ac.uk)
Louise Alexander (Birkbeck, University of London | l.alexander@bbk.ac.uk)
Richard Passmore (University of Oxford | passmore@atm.ox.ac.uk)

Acknowledgements

Sincere thanks go to Chrysa Avdellidou for facilitating the meeting and for her tireless efforts to make the meeting a success. Thanks for financial backing and support to SEPNET, the Centre for Astrophysics and Planetary Science group at Kent University, the Royal Astronomical Society and The Open University.

Cover Image: *Credited to ESA/Rosetta/NAVCAM taken on 20th November 2014.*

Meeting Timetable

Talks

Thursday	Speaker	Talk Title
11:00-12:15	REGISTRATION	
12.30 - 12.45	INTRODUCTION AND WELCOME	
12.45 - 13.15 (Keynote)	**Prof. Mark Burchell** University of Kent	Astrobiology and the Moon
13:15-13:30	**Lee White** University of Portsmouth	Experimental shock deformation of whole-rock samples to ascertain petrologically-resolved, impact-analogous deformation of micro-baddeleyite
13:30-13:45	**Tom Davison** Imperial College London	Impact bombardment of Ceres
13:45-14:00	**Annemarie Pickersgill** University of Glasgow	Experimental impact craters formed in the Shap granite
14:00-14:15	**Kim Birkett** Mullard Space Science Laboratory, UCL	Modelling neutral cometary sodium tails
14:15-14:30	**Leanne Staddon** University of Leicester	The primary and secondary mineralogy of augite basalt NWA 8159
14:30-15:00	BREAK	
15:00-15:15	**Emma Fegan** The Open University	Catenae: The grooves of Mercury
15:15:15:30	**Rebecca Thomas** The Open University	Explosive volcanism in impact craters on Mercury and the Moon
15:30-15:45	**Jonathan Mason** The Open University	An ultraviolet and visible spectrometer to improve trace gas climatologies and dust properties in the martian atmosphere
15:45-16:00	**Elliot Curtis-Harper** The Open University	The anaerobic community of an esturine environment: an analogue for life on Mars
16:00-16:15	**Frances Butcher** University of Cambridge	Are the Dorsa Argentea on Mars glacial eskers?
16:15-16:30	**Peter Fawdon** The Open University	Evolving magmas, explosive eruptions and hydrothermal deposits at Nili Patea Caldera, Syrtis Major,

		Mars
16:30-16:45	**Joel Davis** UCL	Stratigraphic evidence of episodic fluvial activity in the South Melas Chasma Basin, Valles Marineris, Mars
16:45-17:15 (Keynote)	**Dr. Peter Grindrod** Birkbeck, University of London	Selecting the landing site for the ESA 2018 ExoMars rover
17:15-19:15	POSTER SESSION AND LAB TOURS	
19:30	DINNER	
	END	
Friday	Speaker	Talk Title
09:00-09:30 (Keynote)	**Dr. Katherine Joy** University of Manchester	Big bangs in the solar system: the Moon as an archive of impact bombardment in the Solar System
09:30-09:45	**Graeme Poole** Imperial College London	Molybdenum isotopes in iron meteorites - Constraints on solar nebula heterogeneities and parent body processes
09:45-10:00	**Huma Irfan** Birkbeck, University of London	Characterisation of potential landing sites in the Lunar south pole region
10:00-10:15	**Francesca Mcdonald** University of Manchester	Volatiles in the Earth-Moon system: A halogen perspective
10:15-10:30	**Matthias van Ginneken** Imperial College London	The weathering of micrometeorites from the Transantarctic mountains
10:30-10:45	**Lotta Kemppinen** University of Glasgow	A Study of the alteration products within martian shergottite Dhofar 019
10:45-11:00	**Adrienne Macartney** University of Glasgow	Multi-generational carbonate replacement of glass in the martian meteorite Allan Hills 84001 precludes biological origin
11:00-11:30	BREAK	
11:30-11:45	**Jane MacArthur** University of Leicester	The thermal and alteration history for NWA 8114 martian regolith
11:45-12:00	**Roy Adkin** The Open University	Novel fluorescent sensors for the detection of organic molecules in extra-terrestrial samples
12:00-12:15	**Natasha Almeida** The Natural History Museum	Investigating porosity in ordinary chondrites with X-Ray micro-computed tomography (μCT)
12:15-12:30	**Jay Shah** Imperial College London	A micro-CT approach to the paleomagnetic conglomerate test applied to meteorites
12:30-12:45	**Nicholas Oliver Attree**	Collisional features in Saturn's F

	Queen Mary, UCL	Ring
12:45-13:00	**Angelos Tsiaras** UCL	Exoplanetary Spectroscopy with *HST*-WFC3/IR Spatial Scanning: The Super-Earth HD97658B
13:00-13:15	**Andrew McNeill** Queen's University, Belfast	Brightness variation distributions among main belt asteroids from sparse light curve sampling with Pan-STARRS 1
13:15-13:30	**Agata Rozek** University of Kent	Spin-state and thermophysical analysis of the near-Earth asteroid (8567) 1996 HW1
13:30-14:30	FINISH	

Poster Session

Poster Board No.	Presenter	Poster Title
1	**Alex Barrett** The Open University	Sorting Patterned Ground on Earth and Mars
2	**Alex Clarke** Manchester University	Analysis of Presolar Silicon Carbide Grains Using TOF-SIMS and NanoSIMS
3	**Chrysa Avdellidou** University of Kent	Survival of the Impactor During Hypervelocity Collisions
4	**Daniel Staab** The Open University	A Search for Disintegrating Exoplanets
5	**Epifanio Vaccaro** NHM/The Open University	Probing Meteorites Matrix using Non-Destructive Techniques
6	**George Jacobs** The Open University	Interactions between the interior and surface reservoirs for volatiles on Mars as recorded in martian meteorite NWA 7034
7	**James New** University of Kent	Dragons - Resistive Grid Calibration
8	**Jenna Pasini** University of Kent	Panspermia Survival Scenarios for Organisms that Survive Typical Hypervelocity Solar System Impact Events
9	**Jennifer Harris** Birkbeck, UCL	Multispectral Imaging of Hydrothermal Alteration Terrains Using an ExoMars Pancam Emulator
10	**Joel Davis** Department of Earth Sciences, UCL	Aram Dorsum: A Noachian Inverted Fluvial Channel System and Candidate Exomars 2018 Rover Landing Site
11	**Laura Brooker** The Open University	The History of Water at Lyot Crater, Mars: Possible Surface Manifestations of Ancient Groundwater and/or Recent Climate Change
12	**Marriana Felici** Mullard Space Centre, UCL	Survey of the Plasma Composition in Saturn's Magnetotail
13	**Meabh Hyland** Queen’s University, Belfast	The Photometric Properties of the Trans-Neptunian Object (145452) 2005 RN43

14	**Natasha Stephen** Plymouth University	Using the Martian Meteorites as a Ground Truth for Spacecraft Data; A multidisciplinary Approach
15	**Nick Rhys Thomas** University of Glasgow	Preservation of Soil Biomarkers Under Mars-Analogue Conditions: Astrobiological Implications
16	**Peter Fawdon** The Open University	The Hypanis fluvial deltaic system in Xanthe Terra: A Candidate Exomars 2018 Rover Landing Site
17	**Peter Woolman** The Open University	Subsurface Halophiles: An analogue for potential life on Mars
18	**Ricky Hibbert** University of Kent	The effects of temperature on the raman spectrum of high purity quartz crystals
19	**Roland Young** University of Oxford	Simulating Jupiter's global atmospheric dynamics and clouds using a general circulation model
20	**Thomas Barrett** The Open University	The Origin of Water and other Volatiles in the Inner Solar System as Shown by Howardite-Eucrite-Diogenite (HED) meteorites

EXPERIMENTAL SHOCK DEFORMATION OF WHOLE-ROCK SAMPLES TO ASCERTAIN PETROLOGICALLY-RESOLVED, IMPACT-ANALOGOUS DEFORMATION OF MICRO-BADDELEYITE (ZRO_2)

L. F. White[1], R. Hibbert[2], J. Darling[1], D. Moser[3], M. C. Price[2], M. J. Cole[2] & D. Bullen[1]. `
[1]University of Portsmouth, UK. Email: lee.white@port.ac.uk. [2]University of Kent. [3] University of Western Ontario, Canada.

Introduction: Despite its great promise as a chronometer and petrological recorder of planetary evolution [1] and common occurrence in mafic rock samples, very little work has been conducted on the effects of shock metamorphism on either the internal crystal lattice structure or isotopic systems (i.e. U-Pb) of micro-baddeleyite (monoclinic ZrO_2). Intriguingly, initial examination of samples collected from the 1.85 Ga Sudbury impact structure in Ontario reveal heterogeneity of the shock-state of baddeleyite and zircon on a ~200μm scale, with unaltered crystalline grains occurring in close proximity to heavily deformed and twisted crystals of the same composition. These grains, located within the same thin section, should theoretically have been exposed to identical pressure and temperature conditions derived from the impact event, though clearly wave propagation is substantially altered on the micro scale (nm - cm) as well as the macro (m – km). The application of shock experiments [2] may go some way to addressing this issue. By generating a substantial impact shock-wave (peak pressure conditions ~20 GPa) of known orientation in a well-characterised lithological sample, a great deal of the variables that effect natural samples are quantified. This facilitates the closer examination of fine-scale mineralogical relationships on the shock-state of accessory phases, aiding towards a greater understanding of the development of peaks (and troughs) of pressure and temperature as a direct result of shockwave propagation.

Method & Samples: In collaboration with the University of Kent, the experimental shocking of samples within a laboratory environment using the two-stage light gas gun technique [3] is possible. Reproducible shots, whereby 1mm in diameter stainless steel projectiles are impacted onto 50mm x 100mm rock cores, ensures that any heterogeneity in the shock-state of grains are purely a function of depth within the core and the refractive or reflective nature of the sample mineralogy. Additionally, the ability to conduct a 'hot shot' (impacting the sample following attendant heating to <1000°c) allows for the recreation of shock propagation at crustal depths where deformation would occur in a more plastic fashion than in brittle surface rocks. Multiple shots, varying either the speed of projectile (i.e. shock pressure) or attendant heating temperature (i.e. crustal depth) will be conducted to produce a comprehensive dataset for comparison to natural samples, acting to highlight potential P/T barometers for application to both terrestrial and extra-terrestrial shocked lithologies.

The concurrent analysis of micro-structural crystal lattice structure (i.e. Electron Backscatter Diffraction (EBSD)) with *in-situ* U-Pb isotope ratios (Laser Ablation Inductively Coupled Plasma Mass Spectrometry (LA-ICP-MS)) allows for the timing and severity of impact-derived deformation to be more accurately interpreted [1]. This technique, applied to both the experimentally and naturally shocked samples, will allow us to pick apart phases of shock metamorphism with a greater degree of precision, ideally being able to determine P/T conditions within these terrestrial shocked rocks before application to *ex-situ* meteoritic samples. Here we present an overview of micro-baddeleyite (and its importance to analysing solar system geochronology) as well as initial results from this ongoing study, highlighting this mineral phases ability to date a wide range of planetary processes, addressing long term issues such as planetary evolution and bombardment which have thus far remained unresolved.

[1] Moser. D. E. et al. 2013. *Nature*, 499: 454 – 457. [2] Langenhorst. F and Deutsch. A. 1998. *Advanced Mineralogy Volume 3*, 95 – 119. [3] Burchell. M. J. et al. 1999. *Measurement Sci. and Tech*, 10: 41.

IMPACT BOMBARDMENT OF CERES.

T.M. Davison[1], G.S. Collins[1], D.P. O'Brien[2], F.J. Ciesla[3], P.A. Bland[4] and B.J. Travis[2]. [1]Impacts & Astromaterials Research Centre, Dept. of Earth Science and Engineering, Imperial College London, UK. E-mail: thomas.davison@imperial.ac.uk. [2]Planetary Science Institute, Tucson, AZ 85719, USA. [3]Dept. of the Geophysical Sciences, The University of Chicago, Chicago, IL 60637, USA. Dept. of Applied Geology, Curtin University, Perth, WA 6845, Australia.

Introduction: The internal structure of Ceres is unknown, although several structures have been proposed. The most prominent in the literature include either a dry or hydrated silicate core with an icy mantle [1]. Different structures will lead to different impact crater morphologies. NASA's *Dawn* will enter orbit around Ceres soon and start sending the first images of craters on the surface, which can be used to infer the nature of the interior. Here, we use a statistical model to predict the largest impacts expected on Ceres during solar system history, and explore how internal structure affects crater morphology.

Predicting impactor sizes: Using the statistical framework presented in [2], the number, sizes and velocities of impacts on Ceres were estimated. The size- and velocity frequency distribution of impactors in the asteroid belt were estimated using dynamical and collisional evolution models of terrestrial planet formation [3, 4] and as predicted for Ceres [5]. The disruption threshold for Ceres was set using the criteria from [6] appropriate for icy worlds, although after 10^4 simulations of Ceres' impact history, no disruptive impacts occurred. Over the course of solar system history, Ceres could expect over 63000 impacts by impactors 300 m in diameter or larger. Over the same time period, on average Ceres would experience 3 impacts by objects one-twentieth its size (48 km), and have 1.3 impacts by objects one-tenth of its size (96 km).

The expected number of craters on Ceres today will also be dependent on the internal structure, as crater relaxation, especially near the equator, could remove evidence of craters > 4 km if they form in an ice layer [7]. Using the crater scaling parameters for ice from [8], the model predicts around two craters larger than ~ 700 km diameter. For small craters which form entirely in the ice mantle, this estimate is robust, but for larger craters (e.g. in which the core will play a role during the opening of the transient crater, or the curvature of the surface is significant), further modelling is required.

Impact modelling: The iSALE shock physics code [9–11] was used to simulate impacts into different possible internal structures for Ceres: (a) a dry silicate core with a radius of 369 km (using the ANEOS equation of state for dunite [12]) capped by an ice mantle (ANEOS equation of state for water), and (b) a hydrated silicate core of radius 426 km (using the ANEOS equation of state for serpentine [13]) capped by an ice mantle. The size of the cores was calculated to give a mass, surface gravity and bulk density consistent with those estimated for Ceres. A computational cell size of ~ 3 km was used, which means that Ceres was represented by 160 cells across its radius. iSALE was used in its 2D, axisymmetric formulation to reduce computational costs (thus imposing a normal incidence impact angle), although full 3D simulations are ongoing. The silicate cores were assigned strength using the model described in [9], with parameters for dunite taken from [14]; the ice mantles were assigned strength using the model developed for icy satellites [e.g. 15]. Material was weakened after impact using the block model of acoustic fluidization [16]. A gravity field was assigned at the start of the calculation and, due to the large mass difference between the impactor and Ceres, was not updated during the calculation. Crater scaling for icy targets [8] suggests that to form a final crater ~ 700 km in diameter, a projectile composed of ice around one tenth the diameter of Ceres is required to impact at 4 km s^{-1} (a typical impact velocity on Ceres [5]).

Results: Two preliminary simulations of a 96 km diameter projectile impacting Ceres at 4 km s^{-1} have been run: one with a serpentine core and one with a dunite core. During the opening of a transient crater the ice mantle is stripped away to expose the core in both cases, and in the serpentine case, a small crater is opened up in the core. In the serpentine case, the core remains exposed (or only thinly covered) over a region ~ 200 km in diameter. Figure 1 shows the scale of the final craters. The crater on the Ceres with a serpentine core has a rim-to-rim diameter of ~ 690 km, and the crater formed on the Ceres with a dunite core has a rim-to-rim diameter of ~ 760 km, consisent with the crater scaling estimate.

Discussion: Internal structure clearly plays a key role in determining final crater morphology. In large scale cratering events like those modelled here, no silicate material is ejected onto the surface, although some may be brought closer to the surface in a central uplift, beneath thinned mantle material. Modelling of larger impact events will place a constraint on the type of impact that could leave silicate ejecta on the surface, and thus be used in comparison with observations from *Dawn*. The uplift of core material will be observable in gravity anomaly measurements from *Dawn*, which can further be used to constrain the interior structure of Ceres. Further modelling will extend the parameter space over different impactor velocities, sizes and angles, and other internal structures (for example, a "convecting mudball" [17] or a homogeneous hydrated silicate body [18]).

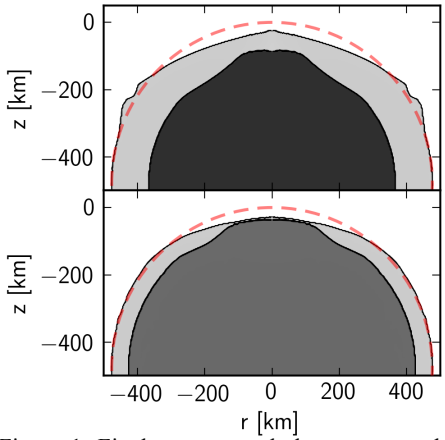

Figure 1: Final crater morphology compared to the pre- impact surface (red dashed line) for the dunite-core (top) and the serpentine-core (bottom) simulations.

References: [1] McCord TB & Sotin C (2005) *JGR Planets*, 110:E05009 [2] Davison TM *et al.* (2013) *MAPS* 48:1894–1918 [3] O'Brien DP *et al.* (2006) *Icarus* 184:39–58 [4] O'Brien DP (2009) *Icarus* 203:112–118 [5] O'Brien DP & Sykes MV (2011) *Space Sci. Rev.* 163:41–61 [6] Leinhardt ZM & Stewart ST (2009) *Icarus* 199:542–559 [7] Bland MT (2013) *Icarus* 226:510–521 [8] Kraus RG *et al.* (2011) *Icarus* 214:724–738 [9] Collins GS *et al.* (2004) *MAPS* 39:217–231 [10] Wünnemann K *et al.* (2006) *Icarus* 180:514–527 [11] Amsden AA *et al.* (1980) *Los Alamos National Lab. Report* LA-8095:101p [12] Benz W *et al.* (1989) *Icarus* 81:113–131 [13] Brookshaw L (1998) Working Paper Series SC-MC-9813 University of Southern Queensland, 12p [14] Ivanov BA *et al.* (2010) *Geol. Soc. Spec. Pap.* 465:29–49 [15] Bray, VJ *et al.* (2014) *Icarus* 231:394–406 [16] Melosh HJ (1979) *J. Geophys. Res.* 84:7513– 7520 [17] Bland PA *et al.* (2013) *LPSC abs.* #1447 [18] Zolotov MY (2009) *Icarus* 204:183–193.

EXPERIMENTAL IMPACT CRATERS FORMED IN THE SHAP GRANITE.

A. E. Pickersgill[1], P. Lindgren[1], M. Burchell[2], M. R. Lee[1], D. F. Mark[1], M. Price[2], [1]School of Geographical & Earth Sciences, University of Glasgow, Gregory Building, Lilybank Gardens, Glasgow G12 8QQ, U.K. [2]School of Physical Sciences, University of Kent, Canterbury, Kent CT2 7NZ, U.K. a.pickersgill.1@research.gla.ac.uk.

Introduction: The effects of shock metamorphism on feldspar group minerals have not been studied extensively in the past. However, they are being increasingly investigated for use as shock barometers due to their importance in planetary studies and meteoritics, where rocks often contain little or no quartz [e.g., 1]. This provides the motivation to examine more closely the effects of high-velocity impact of a projectile, in the method of [2], into a feldspathic target, in order to examine the resultant deformation.

Geological context: The Shap Granite has been widely studied and provides some of the most-well characterized alkali-feldspar to date. The pre-existing in-depth understanding of their microstructures, and the lack of regional deformation resulting in little evidence of tectonically induced strain prior to the impact experiments [e.g. 3, 4] makes them excellent candidates for this project. This study targets alkali feldspar phenocrysts of 1-3 cm size range, with bulk composition of ~$Or_{75}Ab_{25}$ [3].

Methods: *Impact experiments* were conducted on three target blocks, two of which measured 3.5 × 3.5 × 2 cm, and one 2 × 2 × 1.5 cm. The surface of each block was polished flat prior to the experiments. Impacts were carried out at the University of Kent using a horizontally firing two stage light gas gun, capable of firing millimetre sized projectiles at speeds from 1 to 8.5 km/s. Speed of the projectile is determined to accuracy better than 1% [5]. The projectile does not slow down during flight due to both the gun range and the target chamber being evacuated to a pressure of 20 Pa [5]. All targets were impacted normal to the polished surface using a 0.8 mm stainless steel projectile. Projectile speed is given in Table 1.

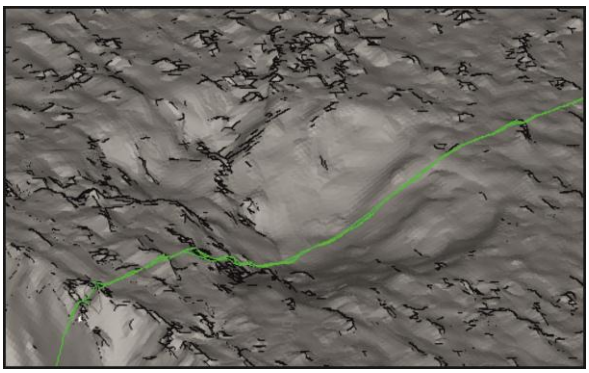

Figure 1: 3D model of Crater B, approximately 1 cm in diameter, with a green line indicating the cross-sectional cut that was made after initial analyses.

Table 1: Crater dimensions and projectile speed

Crater	Speed (km/s)	L (mm)	W (mm)	D (mm)	*L'*	*W'*	*D'*
A*	1.64	8.5	6.5	2.8	10.6	8.1	3.5
C	2.09	19.1	9.5	2.0	23.9	11.9	2.5
B	2.94	11.4	10.3	1.7	14.3	12.9	2.1

Uncertainty in each dimension is ±0.2 mm. L –the longest dimension; W – the widest dimension orthogonal to L; D – the surface to the deepest point of the crater. *L', W', D'* – length, width, depth normalized to projectile diameter. *This crater formed over the edge of the block, so the measurements are incomplete and not indicative of a crater formed in an infinite

3-Dimensional Laser Scanning of the resultant craters was carried out using a NextEngine 3D Scanner HD at the University of Glasgow, with a texture density of 400 DPI and dimensional accuracy of ±0.005 inches. 3D scans were processed using ScanStudio HD and MiniMagics software (Figure 1).

Electron Microscopy Analyses were undertaken at the University of Glasgow using a Carl Zeiss Sigma Variable Pressure field emission analytical Scanning Electron Microscope with Oxford Microanalysis. Craters were carbon coated, then studied initially in plan view through backscatter electron (BSE) and secondary electron (SE) imaging at 20 kV and in high vacuum mode. Following these initial analyses, each crater was cut through its centre to make a cross-section as indicated in Figure 1. The cut sections were then polished, carbon coated, and studied again in the SEM via BSE and SE imaging in order to examine microstructural deformation at depth below the crater.

Observations: Each of the three impacts listed above resulted in the formation of a small crater, the dimensions of which are summarized in Table 1. None of the targets were completely shattered. Shapes of the three craters vary, from equant (B) to extremely elongate (C). The dimensions of A suggest an equant shape, but as the crater overlaps with the edge of the block, it is not possible to measure the true dimensions.

Intense brecciation of the target was observed up to a depth of 760 µm (0.95 projectile diameters) underneath the floor of the crater. The brecciated zone transitions into a zone of intense fracturing which continues to 2 mm (2.5 projectile diameters) below the crater floor. The deepest radial fractures end 4 mm (5.0 projectile diameters) below the crater floor, with a total length of 4.7 mm (5.9 projectile diameters).

There were no changes observed in the microstructure of the impacted feldspar crystals. Exsolution lamellae maintained the same orientation and density as in unaffected parts of the crystal (i.e. those farthest from the impact). No melt of any composition was identified, though particulate matter of a similar composition to the impactor was observed in plan view.

Future work: Future work will include targeting more feldspar phenocrysts at a wider range of impact speeds. This work will include orienting the crystals differently to the projectile in order to account for the anisotropic strength of the crystal, and will include a wider range of speeds of projectile in order to have greater variation in shock effects produced.

References: [1] Jaret S. *et al*. (2014) *MAPS*. 49:1007-1022. [2] Lindgren P. *et al*. (2013) *EPSL*. 384:71-80. [3] Lee M. R. and Parsons I. (1997) *J. Geol. Soc. London.* 154:183-188. [4] Waldron K. *et al.* (1994) *Contr. Min. Petr.* 116:360-364. [5] Burchell M. *et al.* (1999) *Meas. Sci. Technol.* 10:41-50.

Acknowledgements: We gratefully acknowledge funding from the Natural Sciences and Engineering Research Council of Canada (NSERC), The Science and Technologies Facility Council (STFC), and the University of Glasgow College of Science and Engineering. We would like to thank P. Chung from the Imaging Spectroscopy and Analysis Centre at the University of Glasgow for assistance with the SEM.

MODELLING NEUTRAL COMETARY SODIUM TAILS.

K. S. Birkett[1,2] (Email: k.birkett.12@ucl.ac.uk), G. H. Jones[1,2] and A. J. Coates[1,2]. [1]Mullard Space Science Laboratory, University College London. [2]The Centre for Planetary Sciences at University College London/Birkbeck.

Introduction: Neutral sodium is typically easy to detect in active comets around perihelion, due to the very high efficiency of the sodium D transition, and at some comets a distinct neutral sodium tail is observed. The first distinct neutral sodium tail images were apparent in comet Hale-Bopp (C/1995 O1) data taken using CoCam [1], but since this initial detection similar features have been observed at near-Sun comets using the LASCO coronagraph on SOHO. A full picture of the distribution and evolution of neutral cometary sodium may best be established using a combination of spectra and images in different filters at multiple times throughout the orbit.

The high efficiency of the sodium D transition has allowed it to be detected in systems, even if the column density of sodium is extremely low. In these instances it is sometimes possible to determine some of the system's characteristics from the sodium emission detection, such as in Io's plasma torus [2]. It is hoped that a similar approach may be applied to the active cometary environment but at present the production of neutral sodium is unknown. Various authors [3-7, thorough review presented in 8] have suggested various combinations of sources of neutral sodium in the nuclear region, near-nuclear region, dust tail and ion tail.

Our Model: In order to understand the wide variety of cometary observations of neutral sodium available we have developed the first fully three dimensional, heliocentric distance dependent, versatile Monte Carlo neutral sodium tail model known as COMPASS (Cometary Orbital Motion at Perihelion: an Adaptable Sodium Simulation), which incorporates the unintuitive variation in radiation pressure influences on sodium atoms with different heliocentric velocities. Our model was initially based on that of Brown et al [5].

Results: We present a comparison between COMPASS, the Brown et al model [5] and observational data. We have found agreement with the overall morphology and brightness of the neutral sodium tail observed at comet Hale-Bopp (C/1995 O1, for which this phenomenon was studied most extensively) and COMPASS. Furthermore we have found that COMPASS more accurately reproduces the variations in relative brightness with distance from the nucleus observed at comet Hale-Bopp than the Brown et al model [5]. Therefore we conclude that the inclusion of orbital motion and observational perspective enable a significant improvement in the understanding of neutral cometary sodium observations. The versatility of COMPASS allows it to be easily adapted to any other cometary sodium observations, and we have begun to extend the model to other comets of interest.

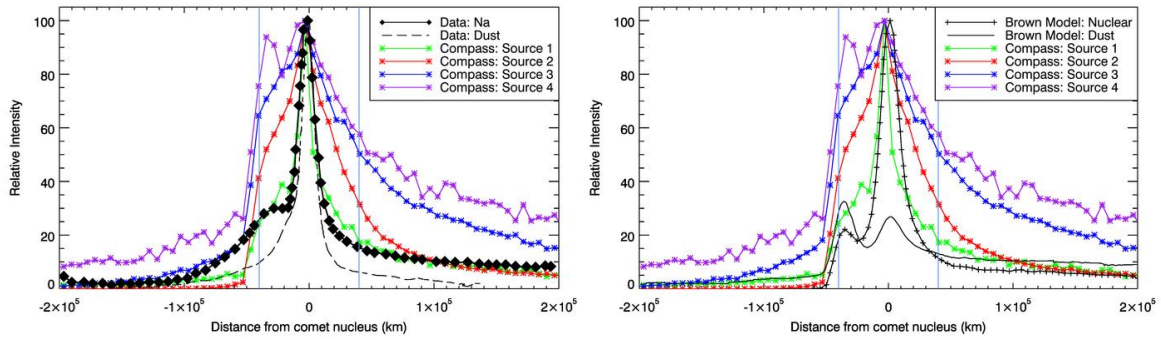

Figure 1: Comparison of COMPASS results for a variety of different neutral sodium sources for comet Hale-Bopp with observations presented in [5] (left). Comparison of COMPASS results with Brown et al [5] model results for comet Hale-Bopp at the same time (right). COMPASS source 1 (representative of simplistic dust source) provides best fit to observational data.

Acknowledgements: Project supported by the UK Science and Technology Facilities Council. CoCam data courtesy Hale-Bopp international team.

References: [1] G. Cremonese, H. Boehnhardt, J. Crovisier et al 1997, ApJ, 490, L199-202. [2] M. Mendillo, S. Laurent, J. Wilson et al 2007, Nature, 448, 7151, 330-332**.** [3] M. Combi, M. DiSanti, U. Fink 1997, Icarus, 130, 336-354**.** [4] C. Arpigny, H. Rauer, J. Manfroid 1998, A&A, 334, 53-56**.** [5] M. Brown, A. Bouchez, H. Spinrad et al 1998, Icarus, 134, 228-234**.** [6] H. Rauer, C. Arpigny, J. Manfroid 1998, A&A, 334, L61-64**.** [7] H. Kawakita, M. Fujii 1998, ApJ, 502, L185-188**.** [8] G. Cremonese 1999, Space Science Reviews, 90, 1-2, 83-89.

THE PRIMARY AND SECONDARY MINERALOGY OF AUGITE BASALT NWA 8159

L. G. Staddon[1], J. C. Bridges[2] and A. D. Saunders[1]. [1]Department of Geology, University of Leicester, LE1 7RH UK. Corresponding Author E-mail: ls261@student.le.ac.uk. [2]Space Research Centre, University of Leicester, LE1 7RH UK.

Introduction: Found in Morocco in 2013, NWA 8159 is the first martian augite basalt[1,2]. Radiometric dating has yielded an early Amazonian age of 2.3±0.5Ga[3], meaning it is one of the oldest known martian samples. Previous analysis[1,2] has suggested both chemical and physical affinities to nakhlites[4], including pyroxene zoning trends, oxygen fugacity and similar shock pressures. Within this study, mineralogical and geochemical characteristics of a ~5 x 3.5mm thin section are being determined and compared to other martian meteorites. Does this sample correlate with other SNCs, or does it represent a previously unsampled portion of martian crust?

Primary Phases: Optical microscopy and SEM analysis of the primary phases indicate a modal mineralogy of ~45% subhedral augite, 40% lath-shaped plagioclase, 5% sub/euhedral olivine, 3% Fe-oxides and 2% orthopyroxene. The remaining 5% is a Fe-oxide rich lithology, named here an 'intergrowth'. Unlike studies of other fragments of this meteorite[1], plagioclase has not undergone transformation to maskelynite. Disequilibrium of olivine suggests this phase may be xenocrystic. Some olivines display orthopyroxene/magnetite reaction 'mantles', as previously described[1,2], and some also contain orthopyroxene inclusions. The sample also displays three different crystal sizes, with the fine grained main thin section, a finer-grained area with the same modal abundances as the main thin section, and the finest grained intergrowths.

Mineral Analysis: Studies of pyroxenes match published data[1], which show evidence of extreme Fe enrichment of augite rims. This is a trait also observed in nakhlites[4], although the pyroxene compositions of NWA 8159 are distinct (Fig. 1). Augites within this meteorite show complex chemical zoning, with decreasing Mg, Al and Cr contents away from the crystal cores. Pyroxene compositions within the fine-grained portion of the sample match the rest of the thin section, although the rims are slightly lower in Ca. This may reflect crystallisation following the formation of the earlier, larger augites which left the melt Ca-depleted. Plagioclase within this sample is labradorite (~An54), though some plagioclase inclusions within augites are tentatively identified as more Na-rich andesine.

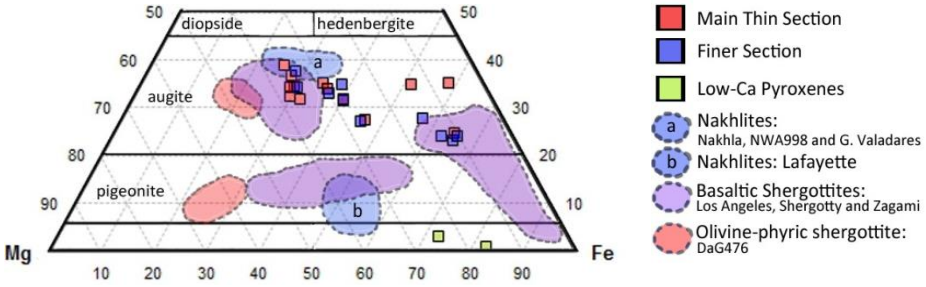

Figure 1: Pyroxene Quadrilateral: Fields taken from [4] and [5]. Data overlaps with SNCs but no definitive correlation with any group. [2] reports greater correlation with MIL 03346 mesostasis.

Secondary Mineralogy: This sample of NWA 8159 also contains abundant evidence of secondary alteration. Randomly-orientated carbonate veins up to 50µm across are prevalent. These veins are also associated with alteration observed in some of the olivines, where textures similar to serpentinisation are present (Fig. 3). Further work is needed to determine if the secondary alteration within this meteorite is terrestrial or martian.

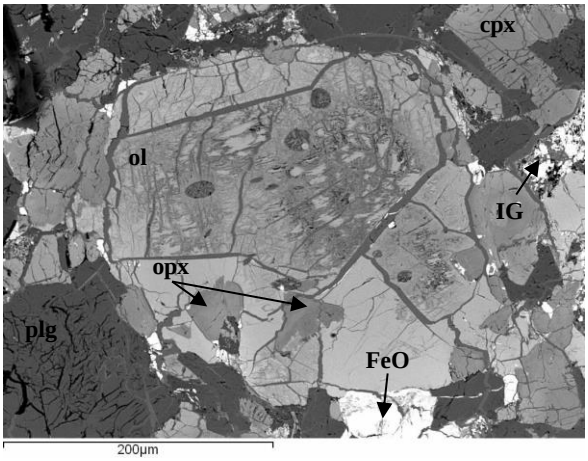

Figure 2: BSE image of alteration of olivine (**ol**) controlled by carbonate veins. This olivine does not show reaction 'mantle' of orthopyroxene and magnetite. Also marked: Augite (**cpx**), Low-Ca pyroxene (**opx),** Labradorite (**plg**), 'intergrowths' (**IG)** and Fe-oxides (**FeO)**.

Future Work: This study will focus on the nature of the olivines within NWA 8159. This is to determine if they represent xenocrysts or phenocrysts, whether they show any chemical zoning and attempt to determine if their alteration is martian. SEM, electron microprobe and ICP-MS data will then be interpreted and continue to be compared to other SNCs to determine if this meteorite truly represents a previously unsmapled portion of the martian crust.

References: [1] Agee C. B et al. 2013. Abstract #2036. 45th LPSC. [2] Herd C. D. K. et al. 2013. Abstract #2423. 45th LPSC. [3] Simon. J. I. et al. 2013. Abstract #5363. 77th AMSM. [4] Treiman A. H. 2005. *Chem. der Erde.* 65:203-270. [5] Bridges J. C. and Warren P.B. 2006. *JGS*. 163(2):229-251.

CATENAE: THE GROOVES OF MERCURY.

E. R. Fegan[1], D. A. Rothery[1], S. J. Conway[1] and M. Anand[1,2], [1]Department of Physical Sciences, The Open University, Milton Keynes, MK7 6AA, UK (emma.fegan@open.ac.uk). [2]Department of Earth Science, The Natural History Museum, Cromwell Road, London, SW7 5BD, UK.

Introduction: Catenae are chains of more-or-less coalesced craters found on the surfaces of various planets and moons in the solar system. These can be chains of secondaries linked to a primary (commonly seen on Earth's Moon), while on the Martian moon Phobos it has been hypothesised that they are secondary impact chains the primary craters for which are located on the surface of Mars [1]. On Jovian moons Callisto and Ganymede, comets fragmented by Jupiter's gravitational field are thought to have formed catenae by serial impact [2].

Catenae are more common on the surface of Mercury than previously identified (only 3 have been formally named [3]). Those that are proximal, straight and radial (or nearly radial) to impact craters are almost certainly chains of secondaries. However, there are others that are apparently unrelated to any potential primary impact feature (see Fig. 1). Similar features on the Moon have been suggested to have formed by an internal process such as subsidence of the surface [4] rather than by impact processes. This work documents the occurrence of catenae across the Hermean surface and investigates whether they have a preferential orientation, or are more common on certain geologic units, as these data may help establish whether they are formed by impact processes.

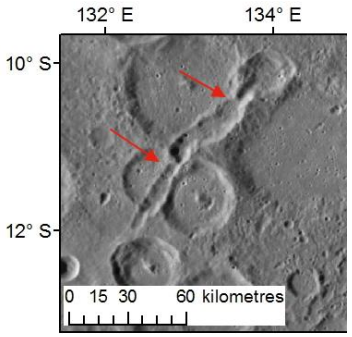

Figure 1: An un-named catena on Mercury, indicated by red arrows. MDIS mosaic, equirectangular projection. A landslide in the crater at the southern end of the catena may have been triggered by its emplacement [3]

Method: We conducted a global survey of catenae by visually examining the surface using the MESSENGER (MDIS global mosaic v9) in ArcMap and digitising catenae. Next, we calculated the strike of each of the catenae to see if there is a global trend in orientation. Finally we examined the geological units in which catenae are most commonly found by calculating the average line density for certain geologic units [5]. Note that this map covers 45% of the surface, so only a subset of catenae are included in this last stage.

Results/Discussion: The global survey, which includes 399 identified catenae, and global line density results are as follows: Catenae are seen all over the surface, they range from 5-300 km in length and are between 10 and 30 km in width. There are pronounced clusters. Chains formed by the impact of large secondary fragments would be expected to form proximal and radial to a large primary impact crater [6], and should therefore be found in clusters around basins. In some cases this is so, in which case the catenae in that cluster are almost certainly all secondary impact chains, but not all. Globally, the orientations of catenae appear to show a preference for NNE-SSW and NNW-SSE. If they were all secondary chains, one would expect a random mixture of orientations. The features are large enough that we do not expect lighting bias to be playing a significant role. Perhaps the responsible process for a significant number of catenae might be similar to that suggested for the Jovian satellites [2] – comets or asteroids are fragmented by the Sun and impact upon the surface of Mercury creating crater chains without a primary crater. Catenae are most numerous on the Intercrater Plains (the oldest terrain on the surface [7]) and Crater Materials (a unit consisting of all craters and associated ejecta blankets) units. This is not simply because these units cover the greatest area (although Crater Material unit is very extensive, see Table 1); the line density of features is higher on these units than on the Smooth plains (see Table 1). It should also be noted that we have found very few catenae on the Caloris plains (see Fig. 2), which might suggest that the responsible process occurred mainly pre-Calorian.

Unit	Mean line density (per km^2)	Areal extent (km^2)	Relative age
Global	0.000458	7.58×10^7	
Smooth plains	0.000065	1.01×10^7	Youngest
Crater materials	0.000173	1.80×10^7	
Intercrater plains	0.000207	1.25×10^7	Oldest

Table 1: Mean line density of catenae on selected geological units, and area/relative age of those units

Preliminary Conclusions:

- Catenae are relatively common on Mercury; we identified 399 in our survey. They are found mainly on older plains and material associated with impacts (ejecta). They are not common on smooth plains, and are very rare on the Caloris Plains. This suggests that the processes forming them were more common pre-Calorian.
- They are not evenly distributed across the surface, which would support their origin as secondary impact chains if these clusters all surrounded impact structures. At this early stage it appears that some catenae cannot be easily explained as secondary impact chains.
- Our work so far suggests that the mechanism of formation could be secondary chains for some catenae, but that other processes (such as the impact of fragmented comets/asteroids, or an internal process) could also play a role.

References: [1] Murray J. B. and Iliffe J. C. 2011. *Geological Society, London, Special Publications, 356,* 21-41 [2] Melosh H. J. 1998. *Nature, 394,* 221-223. [3] Rothery D. A. 2015. *Planet Mercury,* Springer-Praxis 180pp. [4] Masursky H. et al (eds) 1987. *Apollo over the Moon (NASA SP-36),* Sci and Tech Information Office, NASA. [5] USGS (2010) *Mercury Geology Downloads* http://webgis.wr.usgs.gov/pigwad/down/mercury_geology.htm. [6] Heiken G. H. et al 1991. *Lunar Sourcebook,* Cambridge University Press 736pp. [7] Trask N. J. and Guest J. E. 1975. *JGR, 80(17),* 2461-2477.

EXPLOSIVE VOLCANISM IN IMPACT CRATERS ON MERCURY AND THE MOON

Rebecca. J. Thomas[1], David A. Rothery[1], Susan J. Conway[1] and Mahesh Anand[1,2], [1]Dept. of Physical Sciences, The Open University, Milton Keynes, MK7 6AA, U.K. (rebecca.thomas@open.ac.uk), [2]Dept. of Earth Sciences, The Natural History Museum, London, SW7 5BD, U.K.

Introduction: On both Mercury and the Moon, pyroclastic deposits centred on endogenic vents are commonly found within impact craters (e.g., [1], [2]). It has been hypothesized that this colocation results from stalling of ascending magma in the relatively low-density brecciated zone beneath craters prior to explosive volcanic eruption [3–5]. However, the specific localization of vents, the presence or absence of crater floor fractures and the inferred style of explosive volcanism differ on the two bodies, indicating differences in the nature of sub-surface magma storage. To investigate this, we compare the morphology, scale and tectonic association of pyroclastic deposits and vents in 16 complex craters on Mercury and 15 on the Moon (Fig. 1).

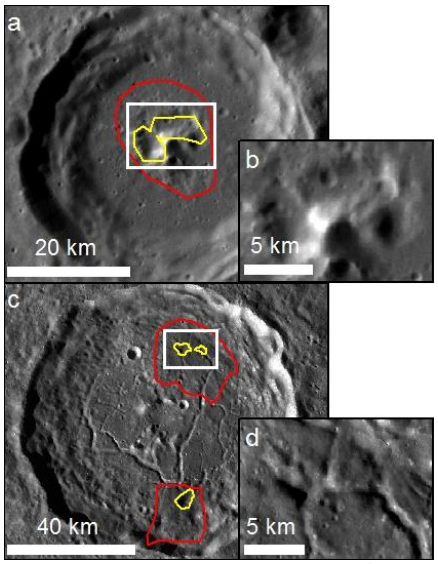

Figure 1: Characteristic appearance of crater-hosted explosive volcanic vents (yellow outlines) and deposits (red outlines) on a. Mercury (MESSENGER NAC images, NASA/JHUAPL/ Carnegie Washington) and c. the Moon (LROC WAC mosaic), with close-ups of vents, b. and d., indicated by white rectangles.

Results and implications for style of volcanism: On Mercury, our observations (Table 1) are consistent with eruption after sufficiently long residence time in a sub-surface magma chamber for large bubbles to form and for fractional crystallization to lead to concentration of volatiles in the remaining melt. These inferences are made on the basis of evidence for high-energy eruption (large ballistic range of particles [6] and large vents) and deposit morphology consistent with a predominantly large particle size [7] resulting from bubble coalescence prior to eruption. On the Moon, the lower values for maximum particle range and vent size are consistent with a lower concentration of volatiles in the magma prior to eruption, and deposit morphology is consistent with intermittent Vulcanian eruption [3].

Implications for the nature of sub-surface magma storage and controls on its depth: The lunar sites are predominantly within floor-fractured craters (FFCs), with vent-formation in circumferential fractures. This suggests that shallow intrusion of magma has uplifted the crater floor, providing pathways for magma ascent towards the surface at the outer edges of the intrusion. In contrast, we detect no floor-uplift or fracturing in host craters on Mercury, and vents are commonly at the crater centre. We have considered several explanations for this disparity, and find that the most probable explanation is that magma storage is deeper on Mercury than on the Moon, despite higher gravity (which would tend to lead to shallower intrusions).

On Earth, upper-crustal magma storage is shallower in extensional than in compressive regimes. In a compressive regime, as has existed on Mercury through much of its geological history, magma is stored deeper and magma chamber rupture occurs only where pre-existing structures are present in the overlying rock [8]. In contrast, the Moon is not in a state of significant global compression [9]. Many of the examples studied here and lunar FFCs in general occur at the margins of mare-filled basins [4]. It has previously been noted that flexural extension due to the mare-load may favour magma ascent from depth at these locations [10]. This comparison with Mercury highlights the possibility that this stress state additionally favours unusually shallow magma storage. This is also consistent with the observation of FFCs with a probable magmatic genesis in areas in extension on Mars [11]. The regional stress regime is therefore a potential controlling factor on the depth of intrusions beneath impact craters on terrestrial bodies.

Table 1. Comparison between explosive volcanism within complex craters on Mercury and the Moon.

	Mercury	**Moon**
Median vent volume (summed by site) / km^3	3.61 (11.43)	0.12 (0.65)
Median maximum ballistic range of ejected particles / km	18.6	10.7
Relief of deposits	No relief, or low relief (≤ 3.5°) within 6.5 km of the crater rim, a fraction of the radius of the spectral anomaly.	Low relief (< 2°) over the extent of the spectral anomaly
Tectonic modification of the host crater	Minor thrusts in 2 (compressional)	14 are floor-fractured craters (extensional)
Location within the host crater	Most (14) at crater centre. At 3 sites, vents at floor margin.	Most (10) at crater floor/wall margin. 2 at crater central uplift.

References: [1] L. R. Gaddis, M. I. et al. (2003) *Icarus*, 161(2), 262-280. [2] L. Kerber et al. (2011) *Planet. Space Sci.*, 59(15), 1895–1909. [3] J.W. Head and Wilson, L. (1979) *Lunar Planet. Sci. Conf. Proc.*, 10, 2861–2897. [4] L.M. Jozwiak et al. (2012). *J. Geophys.Res.*, 117(E11), E11005. [5] R.J. Thomas et al. (2014) *J. Geophys. Res.* 119(10), 2239-2254. [6] L. Wilson (1980. *J. Volcanol. Geotherm. Res.*, 8, 297-313. [7] L. Wilson and J.W. Head (1981) *J. Geophys. Res.*, 86 (B4), 2971–3001. [8] E. Chaussard and F. Amelung (2014) *Geochemistry, Geophys. Geosystems*, 15,(4), 1407–1418. [9] S. C. Solomon (1977) *Phys. Earth Planet. Inter.*, 15, 135–145. [10] P. J. McGovern et al. (2014) *Lunar Planet. Sci. Conf.*, 45, 2771. [11] M. Bamberg et al. (2014) *Planet. Space Sci.*, 98, 146–162. –162.

AN ULTRAVIOLET AND VISIBLE SPECTROMETER TO IMPROVE TRACE GAS CLIMATOLOGIES AND DUST PROPERTIES IN THE MARTIAN ATMOSPHERE

J. P. Mason[1], M. R. Patel[1,2], A.C. Vandaele [3] M. R. Leese[1],B. H. Hathi[4], D. Dawson[1], E. Neefs[3], F. Daerden[3], J.-J. López-Moreno[5], J. Rodriguez Gomez[5], G. Bellucci[6], and the NOMAD team. [1]The Open University, Walton Hall, Milton Keynes, MK7 6AA. E-mail: jon.mason@open.ac.uk. [2]Rutherford Appleton Laboratory, Harwell Oxford, Dicot, OX11 0QX. [3]Belgian Inst. for Space Aeronomy, Planetary Aeronomy, Bruxelles, Belgium. [4]Mullard Space Science Laboratory, Holmbury St. Mary, Dorking, RH5 6NT.[5]Instituto de Astrofisica de Andalucia IAA-CSIC, Granada, Spain. [6]Istituto di Astrofisica e Planetologia Spaziali, Roma, Italy

Introduction:

UVIS is an ultraviolet and visible spectrometer forming part of the NOMAD instrument (the NADIR and Occultation for Mars Discovery) due to fly on the ExoMars Trace Gas Orbiter (TGO) in 2016. An illustration of TGO and NOMAD is shown in Figure 1. UVIS will take frequent, high resolution (1 nm) spectra over the wavelength range of 200 - 650 nm. UVIS will map the presence and variation of ozone (O_3) and will be used to refine the optical properties of the martian airborne dust, which is poorly constrained in the UV. Cloud properties will also be investigated, potentially differentiating between those composed of H_2O and CO_2 ice.

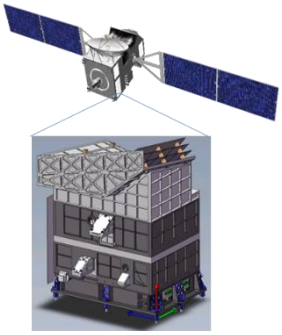

Figure 1: Image of TGO and a CAD model of NOMAD. Image courtesy of OIP.

Observation modes:

UVIS observation modes complement each other and provide information in different spatial dimensions and at flexible temporal sampling rates. Solar Occultation provides high spatial resolution vertical profiles of trace gas absolute abundances together with aerosol extinction at a vertical sampling equal to or lower than 1 km. Nadir mapping mode provides total vertical column abundances. The nadir mode will provide detailed trace gas mapping enabling the identification of potential source regions of the trace gases and provide crucial information on the nature of the processes involved.

Spatial and temporal coverage: From a 74° inclined orbit, the latitudes covered in solar occultation range from 87°N to 88°S with good revisit time at various solar longitudes. The nadir coverage between ±74° latitude provides global spatial sampling on average every 3 to 4 sols with varying local times. Due to the nature of the orbit, there will be occasional repeated ground tracks offering better temporal sampling of a given region.

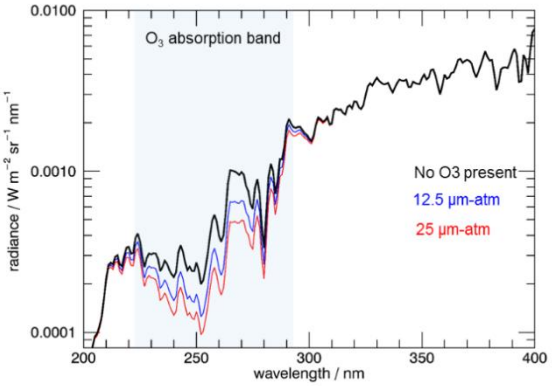

Figure 2: Simulated UV radiance spectra showing the absorption of UV radiation by O_3between 220-290 nm

Detection of Trace Gases:

UVIS is sensitive to O_3, one of the most reactive species in the martian atmosphere. O_3 absorbs UV radiation in the wavelength range 220 – 290 nm. Figure 2 shows a simulated NADIR spectra for different O_3 abundances. The spectra show that O_3 causes a significant reduction in the detected amount of UV radiation between 220 and 290 nm. By comparison of this reduction in the UV radiance to modelled spectra, the O_3 abundance can be retrieved. The sensitivity of UVIS may allow for the potential detection of SO_2, a gas which can be related to volcanism. Its detection or negative detection is vital to verify any low-level present or recent volcanic activity on Mars.

Dust properties:

The accurate determination of ozone abundance is complicated by airborne dust, Figure 3, which both radiatively scatters and absorbs throughout the wavelength range observed by UVIS. Figure 3 shows that the characteristic reduction in radiance around 255 nm as a result of O_3 is modified due to the presence of dust, therefore accurate modelling of the dust optical properties is required. The dust optical properties have been reasonably constrained in the visible [1, 2, 3], however, they are poorly constrained in the UV [4, 5, 6]. UVIS provides the capability to constrain the UV optical properties of the dust over a wide wavelength range, a key component for the accurate retrieval of O_3.

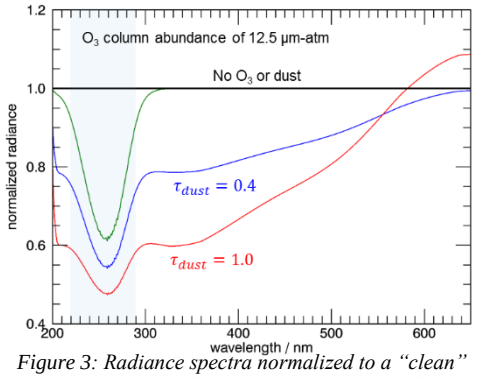

Figure 3: Radiance spectra normalized to a "clean" atmosphere. Dust modifies the spectra across the full UVIS wavelength range

Conclusion:

UVIS provides the first high resolution (1 nm) ultraviolet and visible spectrometer (200-650 nm) to orbit Mars. UVIS will extend the existing atmospheric climatologies for O_3, and other trace species (SO_2). An improved O3 climatology will advance our understanding of photochemical processes in the martian atmosphere, as well as the UV levels on the surface, through the use of radiative transfer modeling of the atmosphere. In addition UVIS will constrain the optical properties of airborne dust in the UV spectral region and further expand our knowledge of the optical properties in the visible.

References: [1] Pollack J. B. et al. 1995. *JGR.* 100:5235-5250. [2] Ockert-Bell M. E. et al. 1997. *JGR.* 102:9039-9050. [3] Wolff M. J. et al. 2009. *JGR.* 114:E00D04. [4] Goguen J. D. et al. 2003. *BAAS.* 35:914. [5] Mateshvili N. et al. 2007. *ASR.* 40:869-880. [6] Wolff M. J. et al. 2009. *ICARUS.* 208:493-503.

The anaerobic community of an estuarine environment: an analogue for life on Mars.

E.Curtis-Harper, V.K.Pearson, S.P.Schwenzer and K.Olsson-Francis. The Open University. Walton Hall, Milton Keynes, MK7 6AA, UK; E-mail: Elliot.curtis-harper@open.ac.uk

Introduction:
The first step in finding potential extant, and/or extinct, life on Mars is to understand the potential biological processes that may have occurred on Mars and identify biosignatures that such processes would generate. This is dependent on identifying and characterising microbial life in suitable terrestrial analogue environments and reliably distinguishing between biotic and abiotic processes. Chemolithotrophic anaerobic microorganisms, such as methanogens, are ideal organisms for investigating potential life in the martian sub-surface[1] as they represent deeply branched terrestrial species that would likely survive there. Furthermore, the carbon dioxide and hydrogen required for their metabolism are provided by the approximately 96% carbon dioxide atmosphere[2] and hydrogen produced in serpentinisation and other reactions[3].

In this study, we used a community of anaerobic microorganisms (Fig.1), which were isolated from below the redox potential discontinuity (RPD) layer of the River Dee estuary, UK. The anaerobic conditions, the 11-15˚C temperature and high salinity (37g/l NaCl) make the sub-RPD zone an ideal analogue for the martian subsurface.

Methods:
Using MiSeq sequencing we investigated the composition of the microbial community, which included sulfate reducing bacteria (Fig. 1). Anaerobic growth experiments were conducted using a minimal growth medium containing dd H_2O, sodium lactate (carbon source), ammonium chloride (nitrogen source) and thioglycollate and ascorbic acid reducing agents. The remaining bioessential elements were provided by a Mars analogue rock mix consisting of a non-amygdaloidal terrestrial basalt from Le Cheix Quarry and aegirine in the ratio 1.75:1 respectively. These geological substrates were geochemically characterized by XRF and XRD and shown to be a compositional analogue for the Rocknest site on Mars[4].

Growth was measured using cell counts. The dissolution kinetics will be determined by analysing the release of key elements, such as Si, Ca, K, Fe in the growth medium with ICP-AES (results pending). Gas Chromatography was carried out on aliquots of the headspace gas to investigate the presence of methane, which is a byproduct of methanogen metabolism.

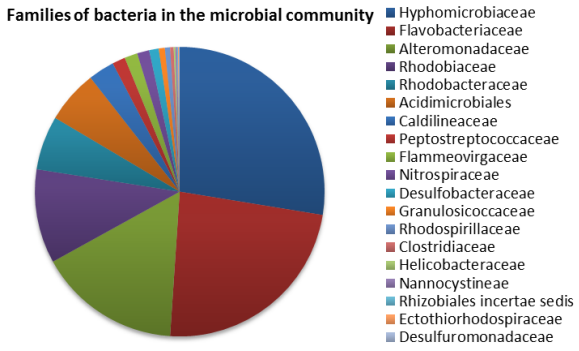

Figure 1. MiSeq analysis on DNA extracted from the River Dee sub-RPD sample.

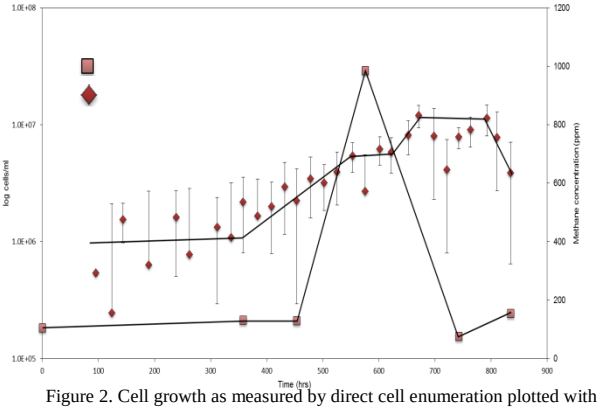

Figure 2. Cell growth as measured by direct cell enumeration plotted with CH_4 concentrations in the gas headspace over time

Results/Discussion:
The growth curve displayed in Fig. 2 demonstrates that the microbial community was able to grow in the nutrient poor minimal growth medium, utilising the bio-essential elements provided by the Mars analog substrates. Abiotic controls were treated identically and no growth was observed. Thus a varied anaerobic microbial community, which contains chemolithotrophs, can utilize a Mars analogue rock substrate.

The growth curve suggests a possible biphasic growth. The simultaneous fluctuations in methane concentrations may suggest a relationship between methanogenic and methanotrophic microoorganisms whereby the secondary exponential growth phase can be attributed to methanotrophs utilizing methane produced when the methanogenic archaea exponentially grow. MiSeq sequencing has already been used to identify the presence of methanotrophic bacteria in our samples and further analysis of the archaeal community, using MiSeq analysis, will confirm whether methanogenic archaea are present.

Further experimental work will focus on identifying geochemical biomarkers formed as a result of the presence of the microbial community by comparing ICP-AES data for media aliquots taken from biotic and abiotic samples.

Conclusions:
This study demonstrates that the microbial community below the RPD of the River Dee Estuary can act as an informative analogue in studies of Martian habitability and life detection. Thus it should be possible to identify biosignatures in the Mars analogue substrate to inform future Mars life detection missions.

References: [1] Weiss B. P., Yung Y. L. and Nealson K. H. 2000. *PNAS.* 97(4):1395–1399. [2] Mahaffy P. et al 2013 *Science,* 341(1997): 263-266 [3] Hellevang H., Huang S. and Thorseth I. 2011 *Astrobiology* 11(7): 711-724. [4] Schmidt M., Campbell J. and Gellert R. 2014 *Journal of Geophysical Research: Planets* 119(1): 64-81

ARE THE DORSA ARGENTEA ON MARS GLACIAL ESKERS?

F. E. G. Butcher[1]. [1]University of Cambridge. E-mail: fegb2@cam.ac.uk.
S. J. Conway[2]. [2]Department of Physical Sciences, Open University.

Introduction: The Dorsa Argentea are a suite of ridges occupying a topographic low within the Dorsa Argentea Formation (DAF) [1] adjacent to the south polar cap of Mars. The DAF is distributed in the region -83° to -57°, 252° - 130°W, extending northwards from its margin with the South Polar Layered Deposits [1]. Previous analyses have found evidence for meltback of an extensive Hesperian-aged (> 2Ga) ice cap terminating at the distal margins of the DAF. Further they proposed the Dorsa Argentea ridges were putative eskers [1]. Eskers are ridges formed by sediment deposition in basal conduits of an ice-body by the flow of meltwater [2].

Qualitative analysis using Mars Orbiter Laser Altimeter (MOLA) data has found similarities between the DAF ridges and terrestrial eskers, including relationships between ridge morphology/dimensions and the surrounding topography [3]. However no quantitative assessment of these relationships has been presented and a mantling deposit may have influenced the interpretation of the relationship between crest morphology and underlying topography. This study further tests the esker hypothesis, by extensively re-mapping the Dorsa Argentea ridges with more recent images from the Mars Reconnaissance Orbiter Context Camera (CTX) at 6 m/pixel. Using this new map we quantitatively assess the influence of local topographic slope upon ridge dimensions and morphology using MOLA topographic data.

Methods: Ridges exceeding 10 km in length were digitised onto a CTX image-mosaic overlain with the ~115m/pixel and ~230m/pixel polar MOLA gridded topographic data. Associated ridge segments were grouped into continuous ridge "routes". Ridge cross-sectional topographic profiles were obtained at ideally ~1 km spacing, and zones with MOLA data-gaps were excluded. The base elevation for each profile was taken to be the average elevation of the two base points selected with reference to MOLA topography and CTX imagery, and surrounding surface slope was calculated between successive profiles on the same ridge segment. Each profile was assigned a crest morphological type (round-, broad-or multiple-crested) according to the criteria of Bernhardt et al [4].

Results: The DAF ridges [Fig 1a] exhibit an average continuity (ratio of total length of ridge segments to length of ridge segments plus gaps) of 91% ±6%, and an average sinuosity of 1.10±0.12, being significantly more continuous, and exhibiting lower sinuosities than terrestrial eskers such as those of New York State [5].

Topographic relationships: The ridges are observed to rise over highs in the underlying topography. "Ridge 1" of our dataset shows a tendency for increased ridge height on downhill slopes and decreased ridge height on uphill slopes (R-sq = 52%, p = 0.00). Such a relationship is common in terrestrial eskers, and is due to pressurized flow of water in subglacial conduits [2].

Crest morphology: The DAF ridges exhibit round, broad and multiple-crest morphologies. Round ridge sections exhibited an average height of 46±2m, compared to 30±3m for broad ridge sections and 25±1m for multiple-crest types, but exhibited no statistically significant difference in width. Shreve [2] found broad-crested terrestrial eskers to exhibit greater widths and lower heights than round-crested sections. No such difference in width was found for the DAF ridges. As "ridge 1" [Fig 1b] ascends over rim of the infilled crater, its morphology transitions from a round to a broad morphology, before transitioning back to a round morphology as it descends on the distal side of the crater rim. Such morphological relationships to surrounding topography were observed by Shreve [2] for terrestrial eskers and are related to changes in conduit wall-melting processes with underlying slope. However, quantitative analysis of all cross-sectional topographic profiles revealed no significant difference in surrounding surface slope between crest morphological types,

Layering: Layering is observed in some ridge sections [e.g. Ridge 2, Fig 1a] supporting a fluvial origin. "Ridge 2" sits on a layer of material extending from the ridge into a topographic depression. These features could be interpreted as evidence of inverted channel topography. However, the ridge is less sinuous than typical terrestrial river systems, and the pedestal lacks evidence of inverted scroll bar topography that characterizes flood plains material associated with inverted channels [6].

Conclusions: Our study therefore supports an esker origin for the Dorsa Argentea ridges, although similarities to terrestrial eskers in the relationship between crest morphological type and surrounding surface slope may not be as strong as previously suggested [3].

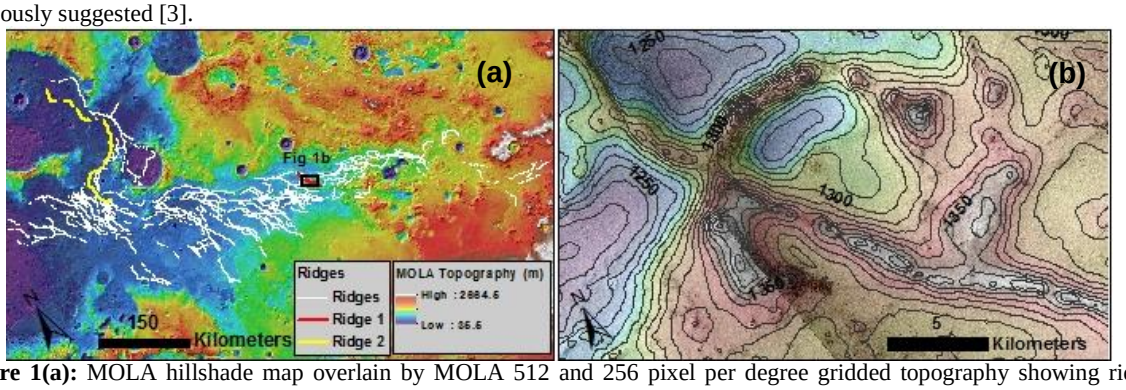

Figure 1(a): MOLA hillshade map overlain by MOLA 512 and 256 pixel per degree gridded topography showing ridge population. Ridge 1 is highlighted in red and ridge 2 highlighted in yellow. **Figure 1(b):** Contour map of ridge 1 (see Fig 1a) passing through an infilled crater. Contour interval 10m. MOLA 512 pixel per degree gridded data overlaying CTX images B12_0148285_1025_XN_77S026W and B12_014351_1024_XN_77S028W.

References: [1] Head III J. W. and Pratt S. 2001. *JGR.* 106(E6):12275-12299. [2] Shreve R. L. 1985. *Geol. Soc. Am. Bull.* 96(5):639-646. [3] Head J. W. and Hallet B. 2001. Abstract #1373 32nd LPSC. [4] Bernhardt H. et al. 2013. *Planet. Space. Sci.* 85:261-278. [5] Metzger S. M. 1992. 23rd LPSC. pp. 901-902. [6] Burr. D. M. 2009. *Icarus.* 200:52-76.

EVOLVING MAGMAS, EXPLOSIVE ERUPTIONS AND HYDROTHERMAL DEPOSITS AT NILI PATEA CALDERA, SYRTIS MAJOR, MARS.

P. Fawdon[*1], J. R. Skok[2], M.R. Balme[1], C. Vye-Brown[3], D.A. Rothery[1], C.J. Jordan[4]. [1]Department of Physical Sciences, The Open University, Walton Hall, Milton Keynes, UK. MK7 6AA; peter.fawdon@open.ac.uk, [2]Department of Geology & Geophysics, Louisiana State University, Baton Rouge, LA 70803., [3]British Geological Survey, Murchison House, West Mains Road, Edinburgh, UK. EH9 3LA, [4]British Geological Survey, Nicker Hill, Keyworth, Nottingham, NG12 5GG.

Introduction: Nili Patera is a 45 km diameter caldera at the center of the Syrtis Major Planum volcanic province [1]. Nili Patera is unique amongst martian volcanic terrains in that it is now below the surrounding planum and hosts a diverse range volcanic landforms and mineralogies. We present a geological stratigraphic history of the Nili Patera in which these geological findings are put into a nine-part geological history (figure 1). Additionally, we consider the implications of the caldera's evolution for; habitability, the evolution of Syrtis Major Planum and Highland Patera style volcanoes in general.

Conclusions (letters refer to figure 1)**:**

• Nili Patera formed between 3.28 (+0.80, -0.13 Ga) and 3.1 (+0.13 -0.22) G. by trapdoor collapse (b-c) into a thermomechanically weakend volcano-tectonic depression achieved by intrusion and magma advection (a).

• The bright fractured unit (*Bfu*) is either part of a felsic pluton exposed during caldera formation or remnants of a welded ignimbrite. Both derived from melting in the Noachian highland basement.

• There were five episodes of magmatic action: (i) a basaltic unit erupted from tuya-like vents in the north of the caldera (d); (ii) Nili Tholus and the evolved flow unit (*Efu*) erupted from an isolated magma chamber (e); (iii) intrusion formed a ~300 m high elliptical dome (f); (iv) a basaltic unit (*Mvu*) was emplaced from small cones in the east (g); and (v) an olivine-bearing unit (*Oru*) formed on the western caldera ring fault (i).

• The ductile layer beneath Syrtis Major, and evolved magma compositions and hydrothermal deposits, imply interaction with subsurface volatiles. Evidence for water and hydrated materials at an elevated geothermal gradient presents a possibile habitable environment (sampled by the hydrothermal deposits in Nili Patera).

• The similarities to other highland paterae imply a similar causal mechanism and thus astrobiological potential for those edifices too.

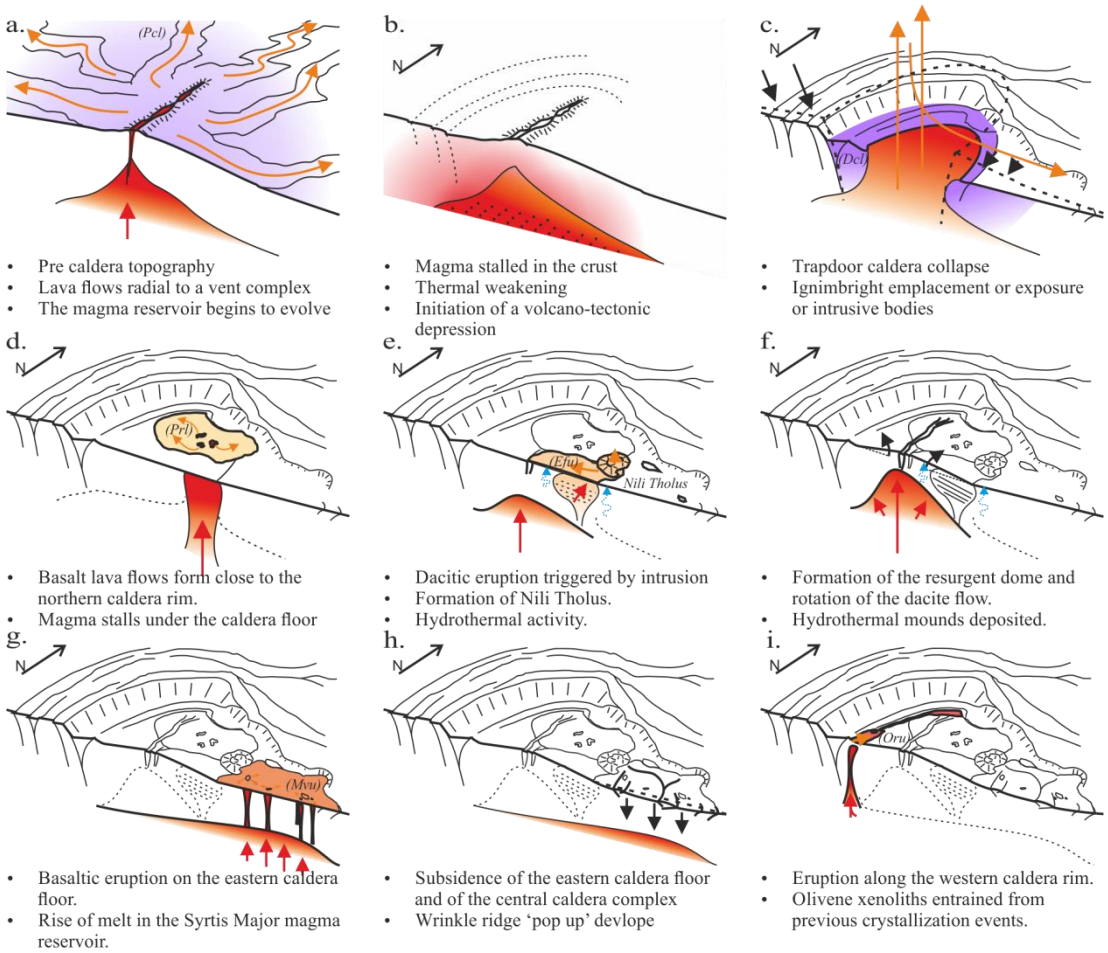

Figure 1: *Block diagrams a - i illustrating the volcanic history of the Nili Patera. The diagram is 50 km wide and has 5 times vertical exaggeration. Arrows show the direction of travel for: (Orange) erupted products, (red) magma, (Blue) hydrothermal fluids, and (black) tectonic or structural movement.*

STRATIGRAPHIC EVIDENCE OF EPISODIC FLUVIAL ACTIVITY IN THE SOUTH MELAS CHASMA BASIN, VALLES MARINERIS, MARS **J. Davis**[1, 2], P. Grindrod[2, 3], R. Williams[4], S. Gupta[5], and M. Balme[6]. [1]Dept. of Earth Sciences, University College London, London, UK, [2]Centre for Planetary Sciences at UCL-Birkbeck, University College London, London, UK, [3]Dept. of Geology and Planetary Science, Birkbeck, London, UK, [4]Planetary Science Institute, Tucson, AZ, USA, [5]Dept. of Earth Science and Engineering, Imperial College, London, UK, [6]Dept. of Physical Sciences, The Open University, Milton Keynes, UK.

Introduction: The South Melas basin is an enclosed topographic depression hanging on the southern wall of Melas Chasma, Valles Marineris. It is widely recognised to have been host to past aqueous activity [1, 2]. The South Melas basin contains a complex stratigraphy, which includes a series of sedimentary fans located on both the east and west side of the basin that originate from a network of valleys. Previous work has suggested that both the fans and the valley networks had an aqueous origin [1, 2]. It was recently proposed that the basin could have undergone multiple aqueous events throughout its history [3]. Our work builds on this interpretation by examining the stratigraphy within the basin at high resolution and characterising the valleys network to the east.

Methods: The South Melas Basin has exceptional image coverage in both CTX and HiRISE due to its candidacy as a landing site for MER, MSL and Mars 2020 [4]. These data were used to map the stratigraphic succession and the extent of the eastern channel networks at a greater resolution than previous work. Stereo pairs were also used to produce digital elevation models in order to determine stratigraphic relationships and make structural measurements within the basin.

Results and Discussion: The frequent variation in sediment texture throughout the sequence, from smooth and flat to rough, polygonalised and mottled, at both the western and eastern edges of the basin suggests that many further fan deposits are mixed in with the lacustrine sediment. This trend is particularly clear in the lower half of the sequence; less so in the upper half. Additionally, several fan-limb and lobe-shaped mounds have been found at the basin floor that may be the remnants of larger, more extensive fan deposits that are more resistant to erosion.

Midway up the sequence, there is a noticeable change in the dip direction of the lacustrine stratigraphy. This could be an angular unconformity, representing a break in lacustrine deposition and a drying-out of the basin, during which subsidence and/or erosion of the sediment may have occurred. Stratigraphically, the aqueous fans on the eastern margin of the basin lie on deposits above the unconformity, whereas the aqueous fans on the western margin lie below it.

Evidence for a break in deposition is supported by the occurrence of an exhumed palaeo-dune covered layered, identified by [3] at a similar stratigraphic position within the succession, which indicates sub-aerial exposure, presumably caused by the desiccation of the lake.

Previous work at MOC and THEMIS resolutions found the valley networks to the east of the palaeolake to be poorly integrated systems with low drainage densities [1]. These valley networks are in contrast to those to the west of the palaeolake, which are fourth to fifth order systems, consistent with surface runoff and precipitation, and more representative of a poly-phase fluvial system (i.e. they comprise of long, broad and shallow channels that then have been incised by more narrow and deep channels).

We have produced a new channel map at HiRISE and CTX resolution of the eastern valley networks. The valley networks and channels are fourth to fifth order systems, have high drainage densities, and show well defined drainage divides. Although the eastern valley networks are not as well preserved as the western valley networks, they show many of the same characteristics, which have been used to infer poly-phase fluvial activity in the western networks [3].

Furthermore, the narrow and deep channels in the east are surrounded by bright-toned material, similar to deposits on the western channels. Further downstream, some channels have deposited similar material on the canyon wall rock. Our map also shows that some of the eastern channels can be correlated to specific fan deposits at the eastern edge of the palaeolake. The bright deposits are also found in these channels, suggesting that the fan may have formed in one of the later fluvial phases in the basin.

Summary: The reflection in the shift in channel characteristics on either side of the basin indicates that water may have been flowing concurrently into the palaeolake from both the east and the west. If this were the case, any localised precipitation that could be responsible for the surface water would be across the entire ~ 300 km^2 area. Williams and Weitz [3] estimated a formation time of 10^2-10^5 years for the delta and submarine fans structures in the eastern and western parts of the basin. An unconformity lying between these two groups of fans could mean that there were at least two periods of sustained fluvial flow into the palaeolake.

References: [1] Quantin *et al.*, 2005, *JGR* 110 E12S19; [2] Metz *et al.*, 2009, *JGR* 114 E10002*;* [3] Williams and Weitz, 2014, *Icarus* 242 19-37; [4] Williams *et al.*, 2014, *Mars 2020 Landing Site Workshop*, Crystal City, VA; [5] Kirk *et al.*, 2008, *JGR* 113 E00A24.

MOLYBDENUM ISOTOPES IN IRON METEORITES – CONSTRAINTS ON SOLAR NEBULA HETEROGENEITIES AND PARENT BODY PROCESSES.

G. M. Poole[1], M. Rehkämper[1], T. Goldberg[1] and B. J. Coles[1]. [1]Department of Earth Science and Engineering, Imperial College London, London SW7 2AZ, UK. (g.poole11@imperial.ac.uk)

Introduction: Numerous recent studies have identified planetary-scale nucleosynthetic isotope anomalies for some refractory elements (e.g., Cr, Ti). Such anomalies are typically interpreted as representing an initial state of heterogeneity in the solar nebula. Molybdenum is ideally suited as a tracer of planetary-scale isotopic heterogeneity as its seven isotopes were produced by distinct nucleosynthetic processes, yet previous investigations have presented conflicting Mo results [1-3]. Here we present Mo isotope data with improved precision and for a larger range of iron meteorites than in previous studies, to inform the debate about nucleosynthetic isotope anomalies. The inheritance of solar nebula signatures can be investigated further by examining mass-dependent stable isotope anomalies. To this purpose, we have investigated mass-dependent Mo isotope fractionations for the same samples, based on additional stable isotope analyses via the double-spike technique.

Analytical techniques: Iron meteorite samples (1 to 15 g) were digested in aqua regia. Separation of Mo was achieved by a two-stage anion exchange procedure and the Mo isotopic compositions were measured by MC-ICP-MS. To determine nucleosynthetic Mo isotope anomalies, instrumental mass bias was corrected by internal normalisation to $^{98}Mo/^{96}Mo$, and data are reported in $\varepsilon^{i}Mo$ notation (Fig. 1). For stable Mo isotope measurements, samples were mixed with a ^{100}Mo-^{97}Mo double spike [4] prior to the separation chemistry, and data are reported in $\delta^{98}Mo$ notation (Fig. 2). The measured stable and nucleosynthetic Mo isotope results were combined to determine purely mass-dependent Mo isotope fractionation, by 'removing' any mass-independent effects.

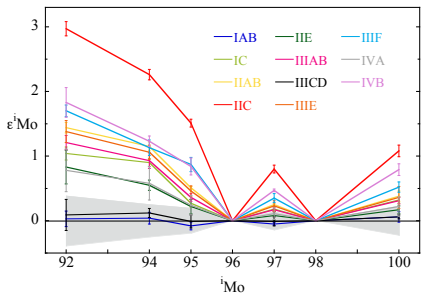

Fig. 1: Mean nucleosynthetic Mo isotope anomalies for iron groups, with 2se error bars. Grey shading defines 2σ of the bracketing standard (NIST SRM 3134) measurements. $\varepsilon^{i}Mo = [(^{i}Mo/^{96}Mo)_{smp} / (^{i}Mo/^{96}Mo)_{std} - 1] \times 10^{4}$.

Results: Following internal normalization to $^{98}Mo/^{96}Mo$, the Mo isotope data for all magmatic iron groups display the typical 'w-shaped' isotopic patterns associated with s-process deficits (Fig. 1). Whilst meteorites from the same group display consistent anomalies, the different groups show variable s-process deficits. These results are in agreement with some published data [2, 3] but stand in contrast to others [1]. Like [3], we also find that the non-magmatic IAB and IIICD irons do not show anomalies.

Fig. 2 displays the stable fractionations. The $\delta^{98}Mo$ values for magmatic iron meteorites vary within a limited range, from -0.39‰ to +0.02‰. The non-magmatic irons show more variation (-0.17‰ to +0.46‰), whilst troilites (FeS) from Toluca IAB display the greatest range (-0.56‰ to +0.42‰) and exhibit the lightest and nearly the heaviest $\delta^{98}Mo$ values.

Discussion: The magnitude of the observed nucleosynthetic isotope anomalies appears to correlate with metallographic cooling rate, and hence inferred size, of the associated parent bodies (e.g., [5]). Such a correlation may reflect progressive homogenization of the solar nebula over the timescale of iron meteorite parent body accretion, possibly due to late injection of s-process material into the protosolar disc. Alternatively, the correlation may imply more efficient homogenization in larger or more densely populated parent body feeding zones.

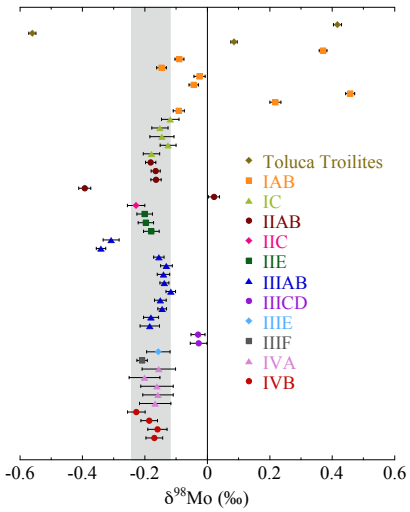

Fig. 2: Mean $\delta^{98}Mo$ value for each sample. Error bars are 2se. Grey shaded field defines 2σ uncertainty of the mean $\delta^{98}Mo$ -0.18‰ of the magmatic iron groups. $\delta^{98}Mo = [(^{98}Mo/^{95}Mo)_{smp} / (^{98}Mo/^{95}Mo)_{std} - 1] \times 10^{3}$.

In our study of stable Mo isotope compositions, the iron meteorite groups (except IAB/IIICD) provide a mean $\delta^{98}Mo$ of –0.18 ± 0.06‰ (2σ). As Mo is moderately siderophile, the $\delta^{98}Mo$ value of the bulk parent body is (essentially) identical to the isotope composition measured for the core. Given the consistency of the results, our mean $\delta^{98}Mo$ value for iron meteorite groups may closely approximate the solar system average.

The large range of $\delta^{98}Mo$ values observed for the Toluca troilites are most likely due to Mo isotope fractionation during metal–sulfide partitioning, whereby the observed variability may reflect both kinetic and equilibrium isotope effects. Similarly, the IAB/IIICD group shows highly variable $\delta^{98}Mo$ with both isotopically heavy and light Mo. This stands in contrast to the results of [6], who found only heavy Mo isotope signatures for this group, which were interpreted to reflect evaporative loss of isotopically light Mo during energetic impacts. Based on our new data, we conclude that the large range of $\delta^{98}Mo$ values observed for IAB/IIICD irons is best explained by segregation and crystallization of S-rich melts on the parent body [7] and associated metal–sulfide partitioning.

In addition, we also found small but resolvable and systematic variations of $\delta^{98}Mo$ within magmatic iron groups. Here, the greatest variability is displayed by meteorites towards the Ni-rich end of the associated parent body fractional crystallization trend (e.g., [8]). Sulfur is incompatible in solid metal and thus becomes enriched in the liquid metal during fractional crystallization of cores. We therefore propose the variations within magmatic iron meteorite groups represent processes associated with increased liquid metal S content, most likely metal–sulfide partitioning of Mo.

References: [1] Becker, H. and Walker, R. J. (2003) *Nature,* 425:152-155. [2] Dauphas, N., et al. (2002) *ApJ,* 565:640-644. [3] Burkhardt, C., et al. (2011) *EPSL,* 312:390-400. [4] Goldberg, T., et al. (2013) *JAAS,* 28:724-735. [5] Rasmussen, K. L., et al. (1995) *GCA,* 59:3049-3059. [6] Burkhardt, C., et al. (2014) *EPSL,* 391:201-211. [7] Benedix, G. K., et al. (2000) *MAPS,* 35:1127-1141. [8] Wasson, J. T. (1970) *Icarus,* 12:407-423.

CHARACTERISATION OF POTENTIAL LANDING SITES IN THE LUNAR SOUTH POLE REGION.

H. Irfan[1,2], I. A. Crawford[1,2], P. M. Grindrod[1,2], D. De Rosa[3] and J. D. Carpenter[3], [1]Department of Earth and Planetary Sciences, Birkbeck, University of London, Malet Street, London, WC1E 7HX, UK. [2]Centre for Planetary Sciences, UCL/Birkbeck, London, WC1E 6BT, UK. Email: huma.irfan.09@ucl.ac.uk. [3]European Space Agency, ESTEC, Keplerlaan 1, 2200 AG, Noordwijk ZH, The Netherlands.

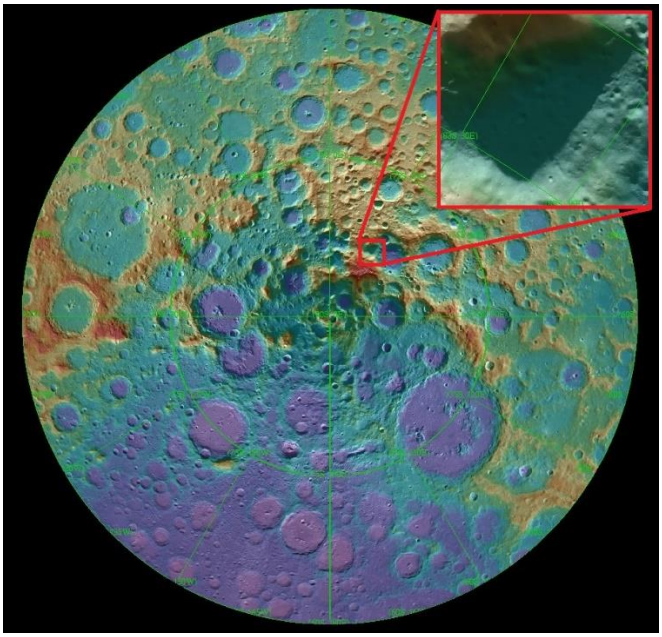

Figure 1. Region of interest location in the lunar South Pole.

Introduction: The objective of this study is the detailed investigation and characterisation of potential landing sites in the lunar South Pole, which is being conducted in collaboration with the European Space Agency (ESA). A prospective region of ~30 x 40 km, centred at 82.7°S, 33.5°W (Fig. 1) is being examined for these studies, which is located on the western limb of the Scott crater in the lunar South Pole, this location has been highlighted previously as an example of a possible site of interest in light of the Russian Luna-Resurs mission. The aim is to investigate and characterise smaller sub-sites of ~3 x 3 km within this locality that satisfy the criteria for the landing site selection, which take into account a risk assessment perspective and proximity to the scientifically interesting features that include: favourable illumination conditions, safe topography, technical constraints for spacecraft landing precision, and a proximity to the scientifically significant features which hint of a possible presence of water ice and/or volatiles and any latent scientifically interesting mineralogy. The lunar South Pole is a scientifically interesting region for future landing missions, within which, cold regions containing crater cold-traps have been suggested by the Diviner Lunar Radiometer Experiment data surface-temperature observations, where the temperatures can reach as low as 38 K in the permanently shadowed regions [1]. It is believed that within these crater cold-traps, cryogenically trapped water ice and/or volatiles of a primitive origin may have been derived from impacts and believed to have been preserved for billions of years. Suitable temperatures for volatile stability may also be found in the subsurface in some illuminated areas. In the light of these observations and assumptions, the site considered for this study presents interesting possibilities which are being investigated in detail in this study.

Datasets and Methodology: For a comprehensive analyses of this region and the sub-sites within it, various lunar remote sensing datasets have been utilised to ascertain the merit of the potential landing sites based on the aforementioned criteria including data from Lunar Reconnaissance Orbiter Camera (LROC) Narrow Angle Camera (NAC), Lunar Orbiter Laser Altimeter (LOLA), Diviner Lunar Radiometer Experiment and NASA's Moon Mineralogy Mapper (M3) hyperspectral data aboard the Chandrayaan-1 mission. USGS Integrated Software for Imagers and Spectrometers (ISIS), NASA Ames Stereo Pipeline (ASP), ArcGIS and Envi software are used to process and analyse the data, including generating DTMs, crater and boulder size-frequency distributions, slope and roughness maps, permanently shadowed regions and illumination conditions.

References: [1] Paige, D. A. et al. (2010) *Science, 330,* 479-482. [2] Tran, T. et al. (2010) *41st LPSC,* Abstract#2515. [3] Schmidt, R. et al. (2012) *XXII ISPRS Congress,* Vol XXXIX-B4, 506-510.

VOLATILES IN THE EARTH-MOON SYSTEM: A HALOGEN PERSPECTIVE.

F. E. McDonald[1], P. L. Clay[1], K. H. Joy[1], C. J. Ballentine[2] and R. Burgess[1]. [1]School of Earth, Atmospheric and Environmental Sciences, University of Manchester, Williamson Building, Oxford Road, Manchester, M13 9PL, UK. [2]Department of Earth Sciences, University of Oxford, South Parks Road, Oxford, OX1 3AN, UK.
Email: francesca.mcdonald@postgrad.manchester.ac.uk

Introduction: The volatile elements are an important constituent of the Earth and the Moon, having a major influence on their thermal and chemical processes such as melting, rheology and volcanism [1, 2]. Determining and comparing the volatile budgets of the lunar and terrestrial mantles will provide an understanding of volatile behaviour and distribution during the formation and evolution of the Earth-Moon system.

Volatiles In The Earth-Moon System: There are two main arguments concerning the origin of the Earth-Moon system volatile elements (each with their own variations) [3]: either they were accumulated during the main accretionary phase during early planetary formation from solar and chondritic material [4, 5], or the purported Earth-Moon forming impact(s) [6, 7] caused major degassing by hydrodynamic escape, with volatiles being subsequently acquired by both bodies as a "late veneer" of chondritic material [8], post-dating planetary formation and pre-dating mantle closure [9, 10, 11].

The Halogens As Tracers Of Volatiles: The halogens are a reactive group due to their high electronegativity and are themselves moderately to highly volatile. However, because the halogens have such large ionic radii (particularly the heavy halogens, Cl, Br and I), they are highly incompatible. This means that their distribution is strongly influenced by fluid mobility and planetary processes such as fractionation and degassing, making the halogens very good tracers for other volatile elements (e.g., H, C, N) [12]. Hence, by constraining halogen compositions of the terrestrial and lunar mantles it is possible to derive volatile budgets for the Earth-Moon system.

Terrestrial and Lunar Samples: Ancient terrestrial komatiites and lunar mare basalts which are rich in olivine hosted melt inclusions have been targeted in this study. The melt inclusions should have remained relatively unaltered/undegassed since their time of entrapment, protected within the olivines [13].

Terrestrial komatiites. A range of Archaean komatiites have been sourced from different greenstone belts around the world (i.e., Canada, S. E. Baltic Shield and South Africa). This sample set varies in age (3.3 Ga to 2.4 Ga) and flow depth to provide a global representation of the primitive terrestrial mantle and insight into its heterogeneity and evolution through time.

Lunar samples. Olivine rich mare basalts from a range of Apollo missions (aged 4.2 – 3.2 Ga) have been selected to represent different lunar mantle source locations, depths and variation in chemistry. Analysis of Apollo 17 picritic glass beads also provides further insight into degassing behaviour of volatiles on ascending to, erupting on, and ponding near to the lunar surface.

Petrography and Halogen Determination: All samples are petrographically and compositionally characterised using environmental scanning electron microscopy (ESEM) and electron microprobe techniques.

Halogen determination. The analytical technique used to determine halogens is Neutron Irradiation Noble Gas Mass Spectrometry (NI-NGMS) [14]. The initial neutron irradiation of samples converts the halogens Cl, Br and I into their respective noble gas isotopes, Ar, Kr and Xe, which are then readily measured by NGMS at the University of Manchester. Fusion by CO_2 laser or furnace step heating releases the noble gas component for measurement, which is then used to determine the original halogen abundances [15]. This method is particularly sensitive and able to detect the least abundant and most difficult to measure halogen, iodine, with a detection limit of ~1 ppb per 1 mg of sample material.

Targeting melt inclusions. Adapting the NI-NGMS to carry out *in-situ* UV laser ablation of melt inclusions hosted in individual olivine grains, enables determination of halogen concentrations representing primitive mantle compositions.

Scientific Implications: The questions I am aiming to address with this research include: What did the original halogen budgets look like and how depleted have they become? How heterogeneous are the lunar and Earth mantles with respect to halogens and to each other? How did the halogens respond to differentiation and the formation of a crust? What proportions of the halogens are/were degassed during volcanism? Are there large halogen fractionations related to volatility difference (i.e. I/Cl) due to impact cratering processes?

References: [1] Hirth, G. A. and Kohlstedt, D. 1996. *Earth Planet. Sci. Lett*. 144:93–108. [2] Saal, A. E. et al. 2008. *Nature. Lett.* 454:192-195. [3] Hauri, E. H. et al. 2015. *Earth Planet. Sci. Lett.*, 409:252-264. [4] Mukhopadhyay, S. 2012. *Nature. Lett*. 486:101-104. [5] Pepin, P. O. 1991. *Icarus.* 92:2-79. [6] Hartman, W. K. and Davis, D. R. 1975. *Icarus.* 24:504-515. [7] Canup, R. M. 2014. *Phil. Trans. R. Soc.* A372:20130175. [8] Holland, G. et al. 2009. *Science*. 326:1522-1525. [9] Tartèse, R. and Anand, M. 2013. *Earth Planet. Sci. Lett*. 361:480-486. [10] Marty, B. 2012. *Earth Planet. Sci. Lett.* 313-314:56-66. [11] Albarède, F. 2009. *Nature*. 461:1227-1233. [12] Kendrick, M. A. 2012. *Chemical Geology*. 292-293:116-126. [13] Bucholz, C. E. et al. 2013. *Earth Planet. Sci. Lett*. 374:145-155. [14] Burgess, R. et al. 2002. *Earth Planet. Sci. Lett.* 197:193-203. [15] Ruzie, L. et al. 2014. Abstract.#2145. Goldschmidt.

Acknowledgements: For their generous donation of komatiite samples, I am most thankful to Gary Byerly, Igor Puchtel, Bernard Marty, Euan Nisbet and Mary McGee. We thank CAPTEM and NASA for allocation of Apollo basalts.

THE WEATHERING OF MICROMETEORITES FROM THE TRANSANTARCTIC MOUNTAINS.

M. van Ginneken[1,2], M. G. Genge[1], L. Folco[3] and R. P. Harvey[4]. [1]IARC, Imperial College, London, UK. [2]NHM, London, UK. E-mail: m.van-ginneken@imperial.ac.uk. [3]Università di Pisa, Italy. [4]Case Western Uni., USA.

Introduction: The dry, cold and clean conditions in Antarctica make it particularly favorable for the preservation of meteorites and micrometeorites. Despite the favorable conditions, effects of terrestrial weathering are frequently observed in Antarctic meteorite finds [1]. Micrometeorites recovered in similar environments, such as on ice-free tops of nunataks for the Transantarctic Mountains (TAM) collection and in glacial moraine for the Larkman nunatak (LK) collection, may have old terrestrial ages [2], and yet there have been no systematic studies of their alteration. Here we present a study focusing on the weathering of micrometeorites from Antarctica.

Methods: 388 micrometeorites from LK and 25 from the TAM were studied. Micrometeorites were studied by SEM-BSE for structural and textural observations and WDS to determine their chemical composition. EBSD was used to study the crystallinity of secondary phases in 10 glass cosmic spherules. FTIR was used on 4 cosmic spherules to study olivine alteration.

Results:

Weathering of cosmic spherules. FeNi metal and sulphides, when present in metal droplets [3], are first to weather and form Fe-oxide. Glass in all cosmic spherule types weathers by hydration and formation of a hydrous gel similar to palagonite [4]. In olivine-bearing cosmic spherules, etch-pits typical of congruent dissolution are observed large crystals of olivine [5]. FTIR spectra show that congruent dissolution also occurs in fine-grained olivine. The sequence of alteration of glass and olivine is mainly controlled by fayalite (Fa) content of olivine, with olivine weathering before glass when Fa content is typically <30, and vice versa when Fa-content >30. In all particles, magnetite is unaffected by weathering. As a consequence, metal-free I-type cosmic spherules from LK appear unweathered.

Weathering of scoriaceous micrometeorites. The presence of jarosite in vesicles of TAM particles suggests that these are efficient structures for the circulation of weathering fluids. As a consequence, the decrease in porosity is an important aspect of weathering in scoriaceous micrometeorites. FeNi metal and sulphides weather first. Congruent dissolution of olivine also commonly occurs.

Weathering of unmelted micrometeorites. Fine-grained UMM from the TAM and LK collections studied here appear unweathered. Weathering of chondritic coarse-grained micrometeorites is similar to that of chondritic meteorites [1]. First FeNi metal and sulphides are altered to form Fe-oxides. Then congruent dissolution of olivine occurs. Pyroxene and glass/feldspar are more resistant to weathering than olivine. As weathering progresses, Fe in silicate is oxidized and Mg, Si and other lithophile elements are progressively removed from the system.

Discussion: MMs generally consist of several mineral phases and as a consequence are affected by differential weathering. By studying MMs exhibiting different degrees of weathering, we have been able to determine a sequence of alteration of their various mineral phases. In CSs, the sequence of alteration for CSs and ScMMs is as follow: FeNi metal<sulphide<olivine<glass<<magnetite (for olivine with <Fa25). CgMMs generally have a slightly more complex mineralogy than CSs and ScMMs. The sequence of alteration of their mineral phases is: FeNi metal/sulphide < olivine < feldspar/glass < pyroxene.

Determining the rate of weathering of MMs from the LK and TAM collection was not possible. In order to do so, future work may consist in the development of techniques that allow constraining the absolute age of individual particles exhibiting various degrees of weathering. Furthermore, despite the high variability in mineralogy and chemistry between the different groups of MMs, we propose a weathering scale for MMs based on both the degree of weathering (i.e. loss and/or alteration of primary material) and the level of encrustation by secondary phases. The following stages of weathering are distinguished: 0: No visible loss and/or alteration of primary material; 1: Minor loss and/or alteration of primary material (mainly silicate phases); 2: Moderate loss and/or alteration of primary material (20-60%); 3: Severe loss and/or alteration of primary material (>60%). These stages are then combined with the level of encrustation surrounding the particles, which is divided into three different stages: A: No visible encrustation; B: Partial encrustation; C: Complete encrustation.

Finally, we have determined environmental factors controlling the weathering of micrometeorites:

- Mineralogical and textural evidence indicates that water as the main agent controlling the weathering of MMs.
- The observation of etching pits in olivine show that the weathering occurred in an abiotic environment.
- The presence of jarosite and the congruent dissolution of olivine show that the water controlling the weathering of MMs was acid.
- The chemistry of secondary mineral phases show that weathering occurs in an open system, which in turn show that large scale melting of snow produced abundant liquid water in the first few centimetres of the LK moraine and in the micrometeorites traps of the TAM.
- The observation of laminations in palagonite and of several types of weathering related to different water/ratios in individual V-type CSs show that in addition to seasonal variations, climatic variations over long periods of time played an important role in the weathering of MMs.

Acknowledgments: This work was supported by the *Science and Technology Facilities Council* (STFC) [grant number: PS5337]. LF is supported by the Italian *Programma Nazionale delle Ricerche in Antartide* (PNRA) through the PEA2013 AZ2.04 "Meteoriti Antartiche" project, and by Pisa University's *Fondi di Ateneo*.

References: [1] Bland P. A. et al. 2006. In Meteorites and the early solar system II:853-868. [2] Rochette P. et al. 2008. Proceedings of the National Academy of Sciences 105: 18206-18211. [3] Genge M. J. and Grady M. M. 1998. Meteoritics and Planetary Science 33:425-434. [4] Stroncik N. A. and Schmincke H.-U. 2002. International Journal of Earth Sciences 91:680-697. [5] Velbel M. A. 2009. Geochimica et Cosmochimica Acta 73:6098-6113.

A STUDY OF THE ALTERATION PRODUCTS WITHIN MARTIAN SHERGOTTITE DHOFAR 019.

L.J.Hallis [1], L.I.M. Kemppinen [1], and M.R. Lee [1].
[1] Department of Geographical and Earth Sciences, University of Glasgow, Gregory Building, Lilybank Gardens, Glasgow G12 8QQ, UK. Lydia.Hallis@glasgow.ac.uk

Introduction: Dhofar 019 (Dh019) is an olivine-phyric basaltic shergottite, which was recovered in the desert in Oman on the 24th of January, 2000 [1] [2]. Identifying alteration products within Martian meteorites is essential for the study of the planet's past conditions and potential habitability.

Observations: Dh019 resembles EETA79001 lithology A and SaU 005 mineralogically and texturally, but contains spherical structures superficially similar to the pre-terrestrial carbonate assemblages found in nakhlite Allan Hills 84001, referred to as orangettes [3] [2]. The orangettes within Dh019 display concentric compositional zoning (smectite, calcite and gypsum) and are enclosed within matrix maskelynite (diaplectic feldspathic glass) at its contacts with large pyroxene grains (see image 1). Following its fall, Dh019 was exposed to extensive terrestrial weathering within a hot desert environment and this resulted in the pervasive alteration of the rock [4]. The affected components include the orangettes. The studied features and clay compositions are different from known Martian alteration products.

Methods and results: A FIB section through an orangette (image 1) was produced and TEM was used to analyze the clay contents which were found to be Mg, rather than Fe-rich, like known martian clays. SEM chemical results also revealed the carbonate to be calcite (~30-45 Ca wt.%), rather than iron-rich siderite. The studied Ca-carbonate within Dh019 will have entered the rock from the surrounding terrestrial desert soil, along with the smectite which is Mg-rich (~16.5-22.5 Mg wt.%), unlike known iron-rich Martian clays The surrounding maskelynite contains no Mg (plagioclase Na:Ca 3.1:6.8 wt.%).

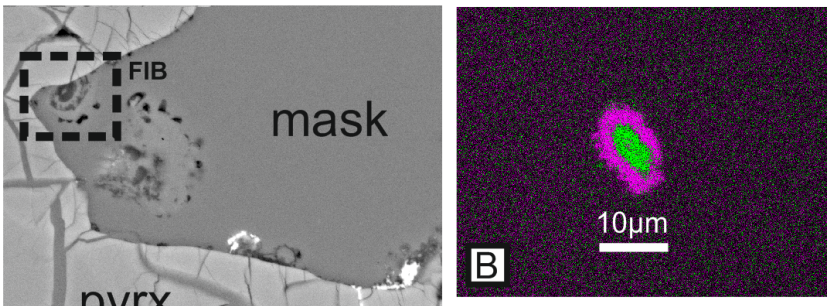

Fig.**1. A.** Shown within dashed line is an orangette formed at a boundary between matrix maskelynite (mask) and large pyroxene (pyrx) grains. A FIB section was made across the sequence of layers. **1. B.** False-colour BSE image of an orangette showing Ca-rich carbonate (in magenta) rimming an Mg-rich (in green) smectite core.

Conclusion: The reported difference between martian and terrestrial alteration minerals can be explained by the higher temperature and water-rock ratios on earth than on Mars. Martian alteration minerals have only so far been reported in meteorites of the nakhlite group and ALH 84001 e.g. [5]. The relative absence of Martian alteration products in shergottites can be explained by their younger age of <600 million years [6], as the Martian surface is known to have dried out dramatically over time. Members of this meteorite group may yet contain evidence for water - and possibly life - having existed on Mars until around 5 million years ago (the approximate ejection assigned age for the shergottites; e.g. [7]). This is important, especially as remote sensing images and interpretations of recently formed gullies have suggested that the martian surface is even today not entirely dry [8], [9].

[1] Taylor et al., 2000 [2] Grossman, 2000 [3] Mikouchi and Miyamoto, 2000 [4] Taylor et al., 2002 [5] Wentworth, Thomas-Keprta and McKay, 1998? [6] Nyquist, L.E. 2006 [7] McSween and Huss, 2010 [8] McEwen et al., 2011 [9] Christensen, 2003

MULTI-GENERATIONAL CARBONATE REPLACEMENT OF GLASS IN THE MARTIAN METEORITE ALLAN HILLS 84001 PRECLUDES BIOLOGICAL ORIGIN.

A. Macartney[1], M. R. Lee[1], E. R. D. Scott[2], D. Mark[3]. [1]The University of Glasgow. E-mail: a.macartney.1@research.gla.ac.uk. [2] Hawai'i Institute of Geophysics and Planetology, USA. [3]Scottish Universities Environmental Research Center, East Kilbride.

Introduction: ALH 84001 is a meteorite from Mars, dominated primarily by a pyroxene matrix, defining it as an orthopyroxenite, but it also contains a variety of carbonates and glass, totaling ~1% wt [1]. The carbonates can be divided into three principle types: Mg-Fe-Ca zoned discs, carbonate globules within plagioclase glass and irregular carbonates in crush zones [2]. A number of competing models for carbonate formation exist in the literature:

1.) Biogenic model [3]. ALH 84001 $\delta^{13}C$ anomalies of ≤ 42 per mil were observed and noted to share similarity with terrestrial biogenic carbonates. This evidence was supported by an observed distribution of polycyclic aromatic hydrocarbons (PAH) > 1 ppm in ALH 84001. Visual textural interpretation was also considered to support biogenesis.
2.) Impact metasomatism model [4]. High temperature (>650°C) CO_2 saturated fluids interacted with silicate minerals following an impact. This model is based on calculated and observed phase relations in the $CaO\text{-}MgO\text{-}SiO_2\text{-}H_2O$ system, textural and morphological interpretations and C and O isotope analysis.
3.) Impact melt model [2]. Pre-existing carbonate and plagioclase feldspars were melted via intense localised impact induced crushing, redistributed and cooled in seconds, possibly in a single event. This model specifically rejects carbonates replacing glass. It is based on compositional K, Na, Ca analysis demonstrating local heterogeneity in the glass indicating stoichiometric deviation, supported by textural interpretation.
4.) Low temperature model. A low temperature (0-100°C) open system model whereby brine evaporates and precipitates to cement pore spaces [5] or is transported by hydrothermal circulation [6]; the model hypothesizes a multi-generational deposition of two carbonate types, with Mg carbonate precipitating ~0°C and Ca-Fe carbonate precipitating ~80°C. The model is based on O isotope analysis combined with textural interpretation.
5.) Mineral/glass replacement model [7]. States that carbonates replaced plagioclase glass in both clast and granular band settings; this process was followed by shock micro offsetting of petrographical features such as glass-carbonate stratigraphy and vein structures. The model is based on textural analysis.

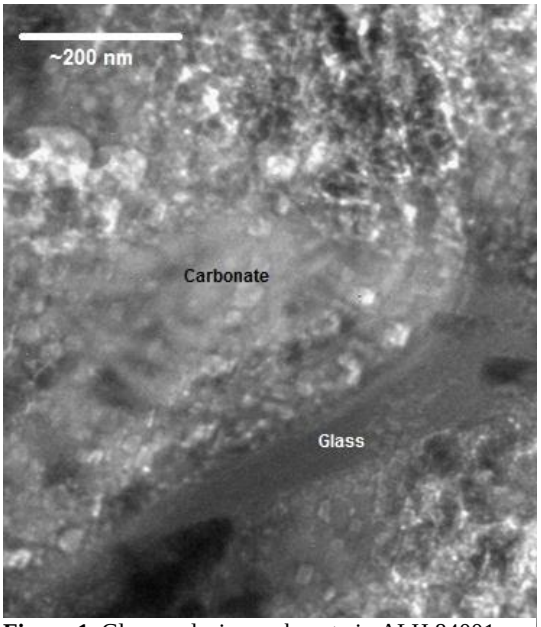

Figure 1. Glass replacing carbonate in ALH 84001.

Distinguishing between these models is important because they determine whether the carbonates are compatible with forming at low temperatures in the martian crust [5, 6], therefore potentially containing biosignatures within the carbonate globules [3]; or if the glass and carbonate formation is more indicative of high temperature and pressure impact shock melting ~4Ga ago [2, 7], which would likely preclude a biosignature. Our study looks at evidence for carbonate replacement of glass at the nano scale (figure 1), lending evidence for a mineral/glass replacement model, and as a corollary, helping to answer long-standing questions over the biotic origin of magnetite in the carbonate [8].

Methods: Our work has used thin section ALH84001, 173. SEM X-ray element maps of the sample were used to locate areas of carbonates that were spatially associated with plagioclase glass. With a FEI DuoMill focused ion beam (FIB) instrument, electron-transparent foils were cut across the plagioclase glass-carbonate interface for imaging and electron diffraction work using a FEI T20 TEM.

Results: SEM imaging and elemental mapping has revealed carbonates in a variety of contexts from fractures to distinct clusters of carbonate-glass patches (figure 1). These carbonate-glass patches, which are 0.1-0.2mm across, have carbonates inter-grown with plagioclase on a very fine scale. Each patch is composed of interconnected groups of zoned carbonate grains. These carbonates are intimately intergrown with the plagioclase in a manner that would be consistent with the carbonates replacing the glass, but other possibilities, such as shock melting, cannot be ruled out at this stage. Examination of the FIB-produced foils will focus on nanoscale petrographic relationships at the carbonate-glass and carbonate-pyroxene contacts.

References: [1] Score R. and Mittlefehldt D.W. 1993. *Antarctic Meteorite Newsletter* 16 (3). [2] Scott. E. R. D. et al. 1997. Nature, 387: 377–379 [3] McKay. D. and Gibson Jr. E. 1996. *Science* 273:924. [4] Harvey. R.P. and McSween. H.Y. 1996. *Nature*, 382, 6586, pp. 49-51. [5] Harvey. R.P. and McSween. H.Y. 1998. *International Geology Review*. 40. 774-783. [6] Romanek *et al*. 1994. *Nature* 372, 655 – 657. [7] Kring *et al*. 1998. *Geochimica et Cosmochimica Acta*, 62,12, pp. 2155–2166 [8] Treiman. A. and Essene, E. 2011.

Acknowledgements: We thank Dr Kevin Righter and NASAJSC for loan of ALH 84001, 173.

THE THERMAL AND ALTERATION HISTORY OF NWA 8114 MARTIAN REGOLITH.

J. L. MacArthur[1], J. C. Bridges[1], L. J. Hicks[1] and S. J. Gurman[2]. [1]Space Research Centre, Dept. of Physics & Astronomy, University of Leicester, LE1 7RH, UK, jm650@le.ac.uk [2]Dept. of Physics & Astronomy, University of Leicester, LE1 7RH, UK.

Introduction: NWA 8114 (a pair of NWA 7034) is a polymict [1] martian basaltic breccia [2] with a bulk-rock age of ~2.1 Ga [2] containing zircons dated at ~4.4 Ga [3]. It is the first sample of the martian regolith [3] with varied clasts bound in a fine grained matrix [4]. As the most hydrated martian meteorite identified to date [2], the majority of the water is thought to be hosted by hydrous Fe oxides [5]. The ferric phrases maghemite and goethite were detected [6], making this potentially the most oxidized known martian meteorite [1,6]. The oxygen isotope ratio of water shows $\Delta^{17}O$ values above the terrestrial fractionation line and the D/H isotope ratio analyses support the martian origin of water in NWA 7034 [2].

The meteorite was likely formed as a result of an impact event [7] which may have led to hydrothermal systems causing further alteration to it [6,8]. Our work characterises the partial breakdown, and mantling by fine-grained material, of pyroxene clasts, in terms of their oxidation state and related textures. We combine this with mineral thermometry to reveal the thermal history of the impact regolith within which the parent rock of this meteorite formed.

Methods: Three polished sections from the main mass of NWA 8114 were examined using a Hitachi S-3600N SEM with an INCA 350 EDX system and a JEOL 8600S EPMA. The I-18 beamline at the Diamond synchrotron was used for X-ray absorption near edge structure (XANES) analyses at sample points on a representative variety of clasts. A 5µm resolution map was taken over two zoned areas (Fig. 1) at 140 stepped energy levels to examine around the Fe-K edge. The data was normalised and deglitched using Athena before fitting the Fe-K edge energy and the 1s → 3d pre-edge features with a spline method for baseline subtraction [9].

Results: Over 1000 SEM and over 400 EPMA analyses points were taken, leading to a clast classification system of pyroxenes (pigeonite and augite, homogenous and exsolution), feldspars (plagioclase and alkaline), iron oxides (FeO, magnetite and Ti-rich magnetite) and phosphates (Cl-apatite), with some mixed clasts showing combinations of these. Applying px thermometry techniques [10] to the exsolution clasts yielded temperatures of 900-1050 °C, similar to 840-1000°C identified by [4]. The composition of cryptoperthite alkaline feldspar clasts, $Ab_{8\text{-}20}Or_{80\text{-}92}$, suggest that they experienced very slow cooling, as they separated nearly to the pure end members, albite and orthoclase.

The largest clast identified (Fig. 1a), pyroxene with bulk composition $Wo_{13}En_{30}Fe_{57}$, has a rim of material accreted to it (highlighted in Fig. 1a), which formed after the veins on the left of the image as it crosscuts them and is enriched in feldspar $An_{24\text{-}39}$ towards the edge. A basaltic clast (Fig. 1b) shows zonation with primarily pyroxene end member composition of $Wo_{31\text{-}38}En_{41\text{-}45}Fe_{19\text{-}24}$, with varying proportions of feldspar $An_{34\text{-}43}$ and pyroxene end members. These areas of accretion and zonation have been investigated using Fe-K XANES (Fig. 1c and d) to determine their oxidation state.

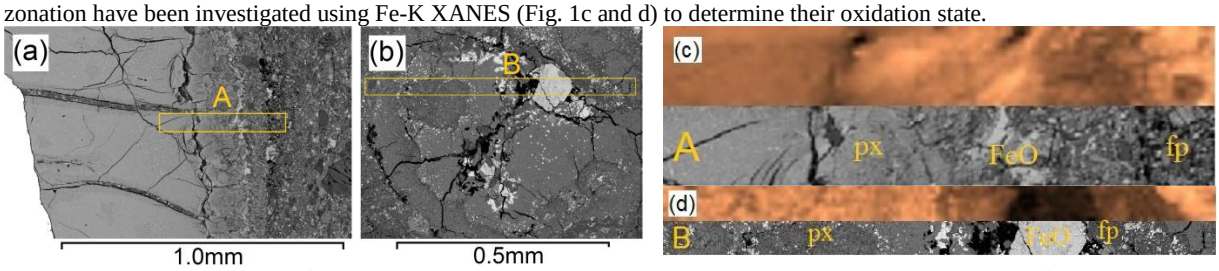

Fig. 1: (a) and **(b)** BSE images of pyroxene clasts showing sample regions A and B. **(c) (top)** Fe-K XANES map of A, 65 x 450 µm, showing normalized intensity measured at 7120.0 eV, light = Fe^{2+}, dark = Fe^{3+} **(bottom)** BSE image of A, showing varied pyroxenes (px) with the accreted rim between the iron oxide (FeO) and feldspar (fp). **(d) (top)** Fe-K XANES map of B, 40 x 640 µm, showing normalised intensity measured at 7120.0 eV, light = Fe^{2+}, dark = Fe^{3+} **(bottom)** BSE image of B, with augitic pyroxene, iron oxide and feldspar $An_{34\text{-}43}$.

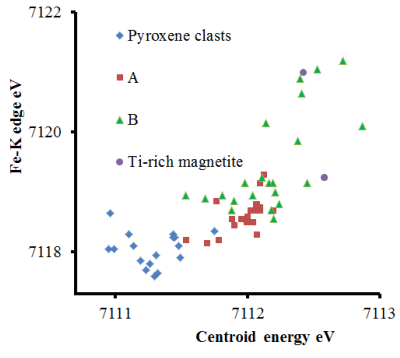

Fig. 2: Centroid vs Fe-K edge energies for different clasts and for different point samples from areas A and B (Fig. 1).

The two areas show higher Fe-edge and centroid energy positions than the more pristine pyroxene clasts (Fig. 2) and are thus more oxidized [9]. Area B is slightly more oxidized than area A (Fig. 2). This oxidation can be quantified using the $Fe^{3+}/\Sigma Fe$ silicate calibration scale developed in [9] which indicates that the pyroxene clasts have 0% $Fe^{3+}/\Sigma Fe$; while areas A and B have 18% - 40% $Fe^{3+}/\Sigma Fe$, with a few iron oxide areas reaching 60% $Fe^{3+}/\Sigma Fe$.

Discussion and Conclusions: The fine grained matrix associated with the accreted rim material (A) and the breakdown (B) of the basaltic pyroxene clast were associated with oxidation from the ferromagnesian minerals. SEM and EPMA examination of the pyroxene oxidation suggests the growth of iron oxide rich domains. This is consistent with the presence of a fluid within the regolith blanket for considerable time at high temperature, likely over 1000 °C, for pyroxenes to react. The zoned clasts are typically enriched in feldspar $An_{34\text{-}43}$ towards their edges. For the first time, this meteorite makes it possible to recreate the thermal history of a large regolith blanket on Mars and offers the potential to prepare a full thermal model.

References: [1] Stephen N.R and Ross A.J. 2014. LPSC XLIV, Abstract #2924. [2] Agee C. B. et al. 2013. Science 339, 780-785. [3] Humayun, M. et al. 2013. Nature 503, 513-516. [4] Santos A.R. et al. 2014. LPSC XLIV, Abstract #2513. [5] Muttik N. et al. 2014. GRL 41, p. 2014GL062533. [6] Gattacceca J. et al. 2014. GRL 41, 4859-4864. [7] Hewins R.H. et al. 2014. LPSC XLIV, Abstract #1416. [8] Humayun M. 2014. Meteorit. Planet. Sci. 49 Abstract #5413. [9] Hicks L. et al. 2014. GCA 136, 194-210. [10] Lindsley D.H. and Andersen D.J. 1983. JGR:Solid Earth 88 S02, A887-A906.

NOVEL FLUORESCENT SENSORS FOR THE DETECTION OF ORGANIC MOLECULES IN EXTRA-TERRESTRIAL SAMPLES.

Roy C. Adkin[1], James I. Bruce[2] and Victoria K. Pearson[1], [1]Department of Physical Sciences, [2]Department of Life, Health and Chemical Sciences, The Open University, Walton Hall, Milton Keynes, Buckinghamshire, The United Kingdom, MK7 6AA; Email address: Roy.Adkin@open.ac.uk; Twitter: @RCAdkin; Telephone: +44 (0)1908858372

Introduction: Organic compounds in extraterrestrial samples have mostly been elucidated by destructive analytical techniques [1 and references therein] which remove any information regarding spatial relationships between minerals and organic species. These relationships may infer in which cosmological provinces organic chemical evolution took place. We will describe progress towards developing fluorescent sensors that may resolve spatial discrimination and therefore the origins of organic species.

Rationale: Lanthanide (Ln) elements such as europium (Eu) and terbium (Tb) produce well defined line-like, high intensity and long lived fluorescent emissions [2] which may alter on interactions with organic molecules. In order to develop a sensor based on these principals, the Ln atom needs to be rendered chemically inert while remaining susceptible to these organic molecule interactions. An organic ligand must be employed to attain this. DOTA (1,4,7,10-tetraazacyclododecanetetracetic acid) was chosen as a plausible organic ligand because its structure, a tetra-substituted cyclen ring, and ability to chelate are well characterized. It is also commercially available. Fluorescent Ln-DOTA complexes are used in many biological and analytical imaging applications [3, 4] so it is logical to investigate their applicability to fluorimetric analysis of extraterrestrial organics. Ln-DOTA complexes are very stable [5, 6] because the Ln metal atom is enveloped within the DOTA structure. This is advantageous because, once prepared, the complex can be stored over time with little degradation and, once in solution, is unlikely to dissociate. The disadvantage of this is that the Ln is entirely shielded from any analyte, resulting in little or no analyte/Ln interaction. Experimental procedures were designed to investigate these theoretical advantages and disadvantages.

Methodology: A range of approximately 50 compounds were chosen giving a good representation of the organics identified in extraterrestrial samples and the most likely to interact with the Ln metal ion based upon their structure. A Eu-DOTA baseline fluorescent spectrum was obtained and compared against Eu-DOTA/analyte mixtures of a range of concentrations resembling those present in extraterrestrial samples. Upon collation and analysis of results a much reduced set of analytes were chosen for experimentation with Tb-DOTA.

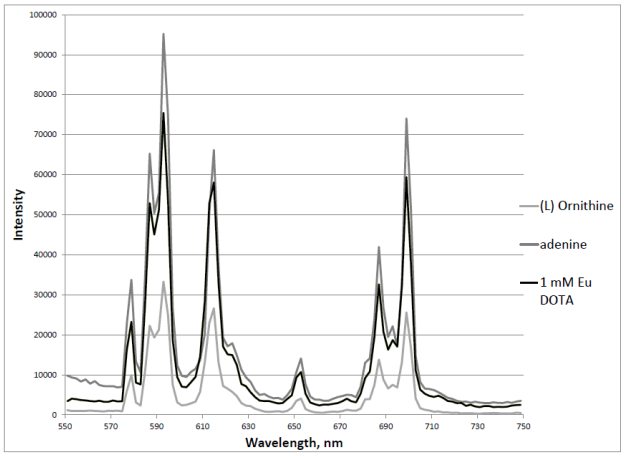

Figure 1. Fluorescent emission spectra of EuDOTA/adenine and EuDOTA/ornithine at equimolar concentrations of 1 mM, for comparison.

Results and discussion: As expected, results showed no change in fluorescent intensity or emission spectrum for any of the analytes at the concentrations found in extraterrestrial samples (μM to nM) with the Ln-DOTA complexes. This could be due to no interaction at any concentration of analyte or that there is an intrinsic limit of detection. Hence, experiments were conducted at equimolar concentration with fewer analytes and showed an increase in fluorescent intensity for some analytes and decrease for others (e.g. adenine and ornithine, respectively, Figure 1.). There was no discernible trend in behaviour according to analyte structure or how they might interact as a result. It is probable that any increase in intensity was due to displacement of water molecules from the complex coordination sphere. Any reduction could be caused by quenching by the analyte. Neither scenario necessarily indicates a direct analyte/Ln interaction; further investigation would help elucidate this. The first coordination sphere geometry for Ln is eight-coordinate. It is, therefore, most likely that the four nitrogen atoms of the cyclen ring and the four ethanoate pendant arms of the DOTA molecule occupy all eight coordination points. This reduces the ease with which the analyte can approach the Eu or Tb atom minimising any changes in fluorescent signal. Attention has now turned to the tris-substituted cyclen ring, DO3A, which has one less ethanoate pendant arm than DOTA. Although this reduces the stability of the Ln complex, it has the advantage of increasing ease of access for the analyte thereby facilitating ability to directly couple with the Ln atom.

Conclusion: DOTA, as was hypothesised, is an unsuitable ligand to use for the sensor. Experimentation has shown that neither Ln-DOTA complexes exhibited a change in fluorescent spectrum; the ligand therefore requires modification, not the choice of lanthanide. We will present results from the development and preliminary testing of the DO3A sensor.

References: [1] Pearson, V.K., et al., (2010) Astrobiology: Emergence, Search and Detection of Life, Basiuk, V.A., Editor, Am. Sci. Pub., 155-173. [2] Bruce, J. I., (2001) Photophysical aspects of lanthanide (III) complexes. [3] Schäferling, M., (2012) Angewandte Chemie Int. Ed., 51, 3532-3554. [4] Faulkner, S., et al., (2005) App. Spec. Rev., 40, 1-31. [5] Bruce, J. I, et al. (2000) J. Am. Chem. Soc., 122, 9674-9684. [6] Armelao, L., et al., (2010) Coord. Chem. Rev., 254, 487-505.

INVESTIGATING POROSITY IN ORDINARY CHONDRITES WITH X-RAY MICRO-COMPUTED TOMOGRAPHY (µCT)

N. V. Almeida[1, 2], C. L. Smith[1], D. Sykes[1], H. Downes[2], and S. S. Russell[1]. [1]Natural History Museum, London, UK. E-mail: n.almeida@nhm.ac.uk. [2]Birkbeck College, University of London, UK.

Introduction: Accurate characterisation of the porosity of meteorites is crucial for constraining models of parent body formation and evolution, revealing details such as permeability and hence providing insights into asteroidal processes, such as aqueous alteration [1]. Porosity is widely measured by a combination of the glass bead method and gas pycnometry [e.g. 2]. Pycnometry is, however, dependent on interconnected pore space. Other authors have investigated porosity by processing SEM images [e.g. 3], though this is limited to two-dimensional analyses. µCT is a non-destructive and non-contaminating analytical technique, capable of investigating the internal structure of samples in three-dimensions. Used previously to investigate porosity [e.g. 4], it can not only provide the modal porosity, but, unlike pycnometry, also allows visualisation of the location and nature of pore space. The aim of this work is to evaluate the ability of µCT to measure and characterise porosity within chondrites, and to investigate the relationship between porosity, metamorphic grade, and shock stage.

Methods: 20 H chondrites of varying metamorphic grade were chosen, primarily falls in order to minimise the effect of weathering. Each piece, of approximately 5 x 5 x 10mm (~1g) and without fusion crust, was scanned at 5-10µm/vox resolution, using the NHM Nikon HMXST 225 System. The greyscale data were thresholded using the Avizo software and porosity was calculated by the ratio of pore space to solid material in the samples. Porosity was also calculated for a random selection of slices in enable comparison between 2D and 3D data.

Results: The level of porosity in these samples varies widely, from less than 1% to 15%. Low porosity samples tend to exhibit porosity in veins, similar to well compacted samples analysed by Friedrich and Rivers [5], whereas higher porosities are found in samples dominated by interstitial porosity, such as Menow, Richardton, and Allegan, indicating they are incompletely compacted. More porous samples also tend to exhibit voids within chondrules. Although no firm trends are evident in this data set, we do witness a possible relationship of decreasing porosity with increasing shock. The four finds all have lower porosity than the falls, consistent with work by Bland et al. [6]. For the majority of cases, our values are within 15-20% of reported values, where available, although we note that our values are consistently lower than those calculated through the He pycnometry method from Britt and Consolmagno [7]. This is likely due to resolution limitations of the µCT system or heterogeneity of the meteorite.

Our initial results support the use of µCT as a crucial technique for characterising porosity in meteorites, demonstrating its ability to provide accurate and informed interpretations of porosity. Additional samples will be scanned to further clarify any trends and provide better statistical significance.

References: [1] Consolmagno G. J. et al. 2008. *Chemie der Erde - Geochem.* 68:1–29. [2] Consolmagno G. J. and Britt D. T. 1998. *MAPS* 33:1231-1241. [3] Strait, M. M. and Consolmagno, G. J. 2010. *41st LPSC,* Abs #2258. [4] Friedrich J. M. et al. 2008. *Planetary and Space Science* 56:895-900. [5] Friedrich J. M. and Rivers M. L. 2013. *GCA,* 116:63-70. [6] Bland P. A. et al. 2006. *Meteorites and the Early Solar System II,* 853-858. [7] Britt D. T. and Consolmagno G. J. 2003. *MAPS* 38:1161-1180.

A MICRO-CT APPROACH TO THE PALEOMAGNETIC CONGLOMERATE TEST APPLIED TO METEORITES

J. Shah[1,2], A. R. Muxworthy[1], M. J. Genge[1], S. S. Russell[2]
[1]Dept. Earth Science and Engineering, Imperial College London, South Kensington, London, SW7 2AZ.
[2]Dept. Earth Sciences, Natural History Museum, South Kensington, SW7
E-mail: js5809@ic.ac.uk

Abstract: Chondrules can provide insights into the physical history of the meteorite's parent body and the processes and conditions of the early solar system. We present a method that uses x-ray micro-computed tomography (micro-CT) scans to re-orientate ex-situ chondrules to their in-situ position, allowing a full-vector paleomagnetic study of the chondrules in Bjurböle (L/LL4) (BM1927,11). Following the logic of the paleomagnetic conglomerate test [1]: magnetic fields recorded by individual chondrules would be expected to be unique and random in direction, unless a field overprinted the initial nebular magnetization on the parent body. Previous work [2-4] has aimed to re-orientate chondrules to determine whether the magnetization is of nebular or parent body dynamo origin. Micro-CT is a non-destructive technique allowing the 3D visualization of a scanned object by reconstructing the x-ray attenuation of the object [5]. The 3D reconstruction can be used to accurately reorient ex-situ chondrules to their original in-situ positions, facilitating the conglomerate test to be conducted on samples with small clast sizes (i.e. chondrules in a chondrite). Bjurböle was heated to beyond the Curie point of its magnetic minerals on its parent body, so any pre-accretionary magnetization has been erased. Tetrataenite is a highly credible paleomagnetic recorder, and it is one of the primary magnetic minerals in Bjurböle [6]. As tetrataenite is a transformation of taenite, its acquired remanence is indicative of whether its parent body had an active magnetic field upon cooling below 320 ˚C, the reordering temperature [6]. By step-wise demagnetizing the chondrules, we were able to constrain paleomagnetic directions that could then be reoriented relative to their in-situ positions. When comparing these directions, we find that the magnetization present in the chondrules of Bjurböle is statistically random. The high anisotropy of tetrataenite likely resulted in its magnetization direction being governed by its crystallography rather than the presence of a unifying magnetic field. Future application of this method would be useful to investigate meteorites from parent bodies perceived to have had a magnetic dynamo [7,8].

References: [1] Graham, J. W. 1949. *J. Geophys. Res.* 54:2: 131-167. [2] Sugiura N. et al. 1979. *Phys. Earth Planet. Int.* 20**:**342–349. [3] Collinson, D. W. 1987. *EPSL* 84:369–380. [4] Fu R. R. et al. 2014 Abstract #1777 45th *LPSC*. [5] Elliott, J.C., and Dover, S.D. 2011. J. of Microsc. 126:2: 211–213 [6] Uehara M. et al. 2011 *EPSL* 306:241–252. [7] Weiss, B. P., and Elkins-Tanton, L. T. 2013 Ann. Rev. Earth Planet. Sci. 41:529-560. [8] Cournède, C., et al. 2014. LPICo. 1800:5292

COLLISIONAL FEATURES IN SATURN'S F RING

N. O. Attree, C. D. Murray, N. J. Cooper, and G. A. Williams
Queen Mary, University of London

Saturn's F ring is a dynamic and changeable environment that has long been suspected of possessing a population of small moonlet [1,2]. Previously we identified small (~50 km), linear features, observed in Cassini images, as produced by physical collisions [3]. Orbit determination suggests they consist of ring material displaced by ~1 m/s dissipative collisions with the nearby objects; which are likely tidally modified aggregates. Larger features are also visible in mosaics of Cassini images (see Fig. 1), some of which are associated with the moonlet S2004 S/6, and these are thought to involve higher velocity collisions (~70 m/s). Here we will present the latest results in cataloguing `jets' and `mini-jets' to examine their distribution, morphology and evolution with time. Comparisons between these observations and N-body simulations will then be presented in an effort to place constraints on the underlying moonlet population as well as on the physics of the collisions themselves.

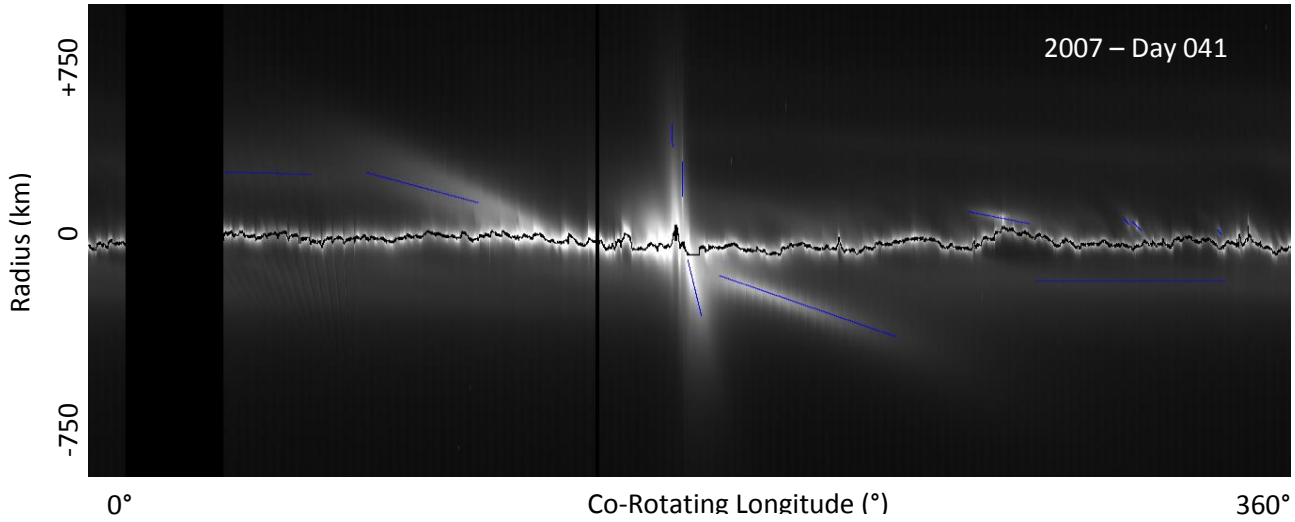

Figure 1: Mosaic of 124 Cassini images re-projected so that the y-axis is radius, relative to a model of the F ring core's orbit, and the x-axis is longitude in a frame co-rotating with said orbit. A number of jets are visible, either side of the bright core, and are highlighted with blue lines. Black vertical bars are a lack of coverage.

[1] J. N. Cuzzi, J. A, Burns, Charged particle depletion surrounding Saturn's F ring - Evidence for a moonlet belt? Icarus, 74(1):284 - 324, 1988. **[2]** B. K. Meinke, L. W. Esposito, N. Albers, and M. Sremevi. Classification of F ring features observed in cassini UVIS occultations. Icarus, 218(1):545 - 554, 2012. **[3]** N. O. Attree, C. D. Murray, N. J. Cooper, and G. A. Williams. Detection of Low Velocity Collisions in Saturn's F Ring. ApJ, 755 L27, 2012.

EXOPLANETARY SPECTROSCOPY WITH *HST*-WFC3/IR SPATIAL SCANNING: THE SUPER-EARTH HD97658B

A. Tsiaras[1], I. Waldmann[1] and G. Tinetti[1]. [1] University College London. E-mail: angelos.tsiaras.14@ucl.ac.uk

Introduction: Spatial scanning with *Hubble Space Telescope* WFC3/IR is a recently adopted technic for observing exoplanetary atmospheres. After having locked to the target, HST slowly slews along the y-axis of the detector in order to maximize the number of photons that are being collected. Although it is currently the most efficient technic, providing a very good signal-to-noise ratio, there are still some considerations about the systematics that are introduced from the scanning process. In this work we mainly studied, and tried to correct, the geometric distortions, which appear in a scanned spectrum. We applied these corrections to the spectrum of HD97658B from the observations of Knutson et al.,[1]. HD97658B is a super-Earth with a mass of 7.55 $M_{\oplus}$ and a radius of 2.25 $R_{\oplus}$ at 4.5 μm orbiting a low-mass (0.77 $M_{\odot}$) K1 (5170 K) dwarf star at 0.08 AU, [2].

Data Reduction and Sky Background: We downloaded the RAW datasets from the MAST Archive and followed the next steps in order to get clean images of the spectrum:

- Subtraction of the bias level from each sub-frame, the bias level is calculated as the mean value of the reference pixels, excluding those from the first five and the last five rows and those from the first and the last column.
- Subtraction of the zero-read from each sub-frame, this is because WFC3/IR has no shutter.
- Subtraction of a scaled to the exposure time version of the provided dark current frame for the specific observing mode.
- Division with the provided flat frame.
- Subtraction of a scaled to the exposure time version of the provided master-sky frame, the scale is calculated by fitting the master-sky frame to the out-of-spectrum area of the second-read.

Positioning Corrections: Since it is impossible to have exactly the same scanned spectrum from frame to frame, and WFC3 is an extremely sensitive instrument, it is vital to study how changes in position affect the final result. The two main factors that seem to affect the outcome are:

1) The IR detector has a tilt of 24° about its x-axis, which results in a different sky level along the y-axis and also in a slightly different wavelength calibration along the y-axis.
2) The detector is not being read as quickly as a CCD so the combination of reading speed, reading direction and scanning speed result in an effective exposure time which depends on the position of the spectrum on the detector.

Fitting the White Light-curve: After correcting for the above positioning issues, there is still the problem that the flux WFC3 collects from a stable source is not constant but a function of the orbital phase of HST. This behavior is known as “the ramp” and in order to correct this we fit a linear function together with an exponential trend to the out-of-transit light-curve Fig. 1.

Transmission Spectrum of HD97658B: The final step is to create the light curves for each wavelength and fit a transit model to each one in order to find the transit depth differences between each wavelength and the white light-curve Fig. 2.

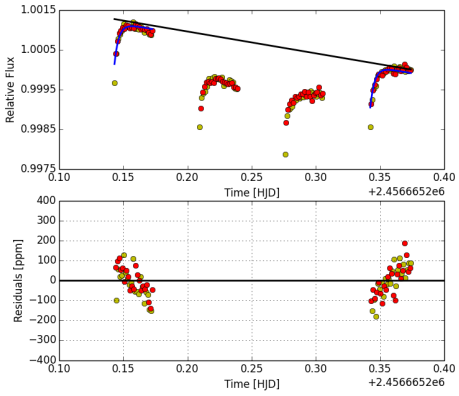

Figure 1: Linear and exponential correction for "the ramp".

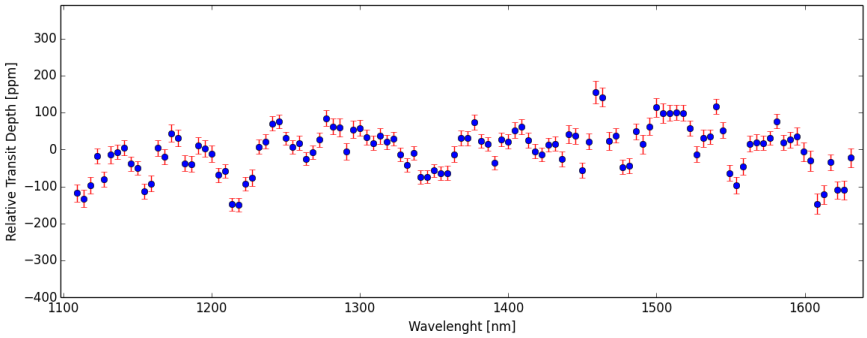

Figure 2: Transmission spectrum of HD97658b.

References:

[1] Knutson et al. 2014. *ApJ.* 794, 155.

[2] Van Grootel et al. 2014. *ApJ.* 786, 2.

BRIGHTNESS VARIATION DISTRIBUTIONS AMONG MAIN BELT ASTEROIDS FROM SPARSE LIGHT CURVE SAMPLING WITH PAN-STARRS 1

A. McNeill[1], A. Fitzsimmons[1], R. Jedicke[2] , R. Wainscoat[2], L. Denneau[2], P. Veres[2,3] and E. Magnier[2]. [1]Astrophysics Research Centre, Queen's University Belfast, Belfast BT7 1NN, Northern Ireland, UK; E-mail: amcneill11@qub.ac.uk. [2]Institute for Astronomy, University of Hawaii at Manoa, Honolulu, HI 96822, USA; [3] Department of Astronomy, Physics of the Earth and Meteorology, Comenius University, Mlynsk´a dolina, Bratislava, 942 48, Slovakia

Introduction: Through study and understanding of the rotational behaviour of main-belt asteroids, information relating to their physical and collisional evolution may be derived. For small asteroids, particularly those found in the inner main belt, the YORP rotational timescales are shorter than those for collisions, and, thus, we expect YORP to be the dominant effect. This makes the small-body population ideal for looking for evidence in light curves of spin-axis orientation due to YORP.

We have so far studied the light curve variations of >30,000 asteroids as obtained by Pan-STARRS 1. Asteroids were only considered with a formal uncertainty in w-band of 0.02 magnitudes or better. The majority of asteroids so far observed by Pan-STARRS have too few observations to allow light curve periods and amplitudes to be derived as proposed by Warner and Harris[1]. Hence we have analysed the cumulative distribution functions of the rate of magnitude change between pairs of observations separated by ~15 minutes. This was carried out for a range of asteroid diameters to observe the effect of size on magnitude variation in population samples in the inner and outer main belt. Analysis up to this point has shown that the rates of change in magnitude decrease toward lower rates with decreasing diameter for objects with diameters < 8 km in both the inner main belt (2.0 AU < a < 2.5 AU) and the outer main belt (3.0 AU < a < 3.5 AU). We propose this decrease towards slower rates of to be due to changes in the fraction of YORP-aligned spin axes caused by an increasing number of tumbling objects at small diameters. We will present these findings along with supporting comparisons to a simple statistical model.

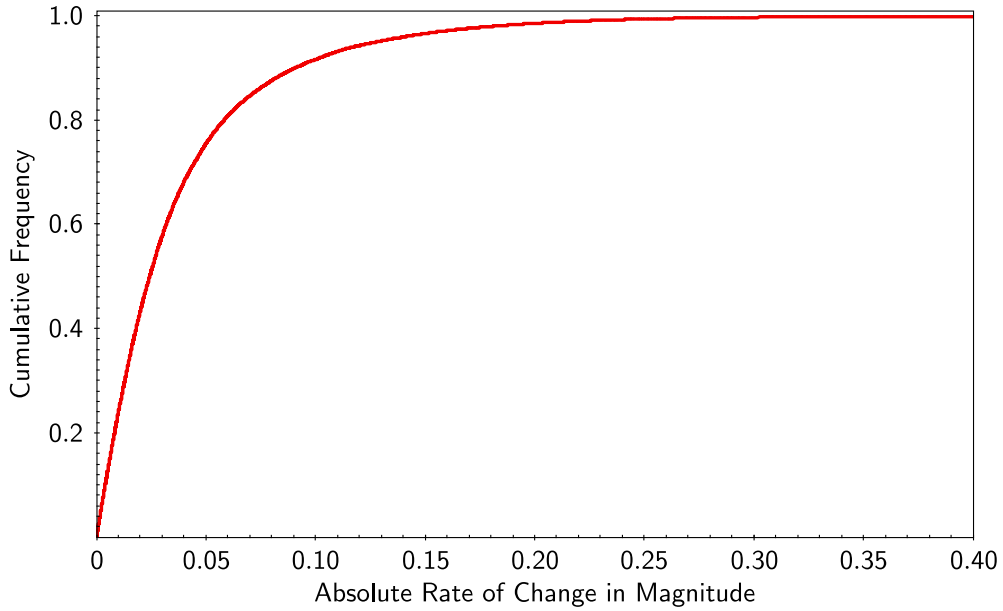

Figure: A sample cumulative frequency distribution of absolute rate of change in magnitude covering the entire reduced w-band data set from PS1

Acknowledgements: The Pan-STARRS Surveys have been made possible through contributions of the Institute for Astronomy, the University of Hawaii, the Pan-STARRS Project Office, the Max-Planck Society and its participating institutes, the Max Planck Institute for Astronomy, Heidelberg, and the Max Planck Institute for Extraterrestrial Physics, Garching, The Johns Hopkins University, Durham University, the University of Edinburgh, Queen's University Belfast, the Harvard-Smithsonian Center for Astrophysics, and the Las Cumbres Observatory Global Telescope Network, Incorporated, the National Central University of Taiwan, and the National Aeronautics and Space Administration under Grant No. NNX08AR22G and No. NNX12AR65G issued through the Planetary Science Division of the NASA Science Mission Directorate.

References: [1]Warner and Harris (2011) "Using sparse photometric data sets for asteroid light curve studies" (Icarus 216, 610).

SPIN-STATE AND THERMOPHYSICAL ANALYSIS OF THE NEAR-EARTH ASTEROID (8567) 1996 HW1

A. Rożek[1], S. Lowry[1], B. Rozitis[2], S. Wolters[3], M. Hicks[4], S. Duddy[1], A. Fitzsimmons[5], S. Green[3], C. Snodgrass[6], and P. Weissman[4].[1]Centre for Astrophysics and Planetary Science, University of Kent, UK, E-mail:ar377@kent.ac.uk. [2]Department of Earth and Planetary Sciences, University of Tennessee, USA, [3]Planetary and Space Sciences, Department of Physical Sciences, The Open University, UK, 4Planetary Science Section, Jet Propulsion Laboratory / Caltech, USA, [5]Astrophysics Research Centre, Queens University Belfast, UK, [6]Max Planck Institute for Solar System Research, Germany

Introduction: The asteroid (8567) 1996 HW1 is a near-Earth Amor-class asteroid. It has been a target of visual lightcurve observations during the two apparitions in 2005 [1,2] and 2008 [3]. The lightcurve datasets were complemented by the radar data obtained at Arecibo during the close approach in September 2008 [4]. The data was combined to constrain the shape and spin state of the asteroid. The sidereal spin rate and pole position were measured, with a complex rotation state not being ruled out. The shape of the asteroid resembles a contact binary with two components connected by a narrow neck. It was predicted that the asteroid's rotation rate is *decreasing* due to the Yarkovsky-O'Keefe-Radzievskii-Paddack (YORP) effect. We aimed to verify the predicted YORP-induced period change [4] and present a thermophysical model for the object.

Observing campaign: The asteroid (8567) 1996 HW_1 has been selected as one of the targets of an European Southern Observatory Large Programme (ESO LP) led by Dr. S. Lowry. The programme includes photometric monitoring, infrared thermal observations, and visual near-infrared spectroscopy of selected near-Earth asteroids. Within the ESO LP, the asteroid has been observed on six runs between April 2010 and April 2013 with ESO's 3.6-m New Type Telescope (Chile) to acquire optical lightcurves, and in September and December 2011 the infrared observations were performed with the VISIR instrument at the ESO's 8.2-m Very Large Telescope (Chile). The data set is completed by the visual lightcurve observations gathered from supporting programmes.

Spin-state analysis: The visual lightcurves from our 2010–2013 observing campaign were combined with the previously published lightcurves from 2005–2009, doubling the time span of the observations for the purpose of the potential YORP detection. The shape model developed from radar and lightcurve data [4] has been used in the spin-state analysis. The current spin-state model reproduces the shape of all the lightcurves obtained over the eight years very well. We do not detect any signature of YORP in our data despite the long time-base of our observations and the quality of the data obtained.

Thermophysical analysis: The thermal data was analysed using the Advanced Thermo-Physical Model (ATPM) [5,6]. The model is in a good agreement with infrared fluxes obtained with VISIR. We managed to confirm the radar-derived diameter of the object and constrain surface properties such as surface roughness and thermal inertia. The ATPM modelling indicates a small YORP-induced *acceleration* and an obliquity change. The current value of obliquity is close to the critical value, where the rotational component of YORP disappears. This result is in agreement with the results of our spin-state analysis. The detection of a period change at the predicted level may require a much longer observational time span. We note the difference in the sign between this prediction and the earlier estimates coming from the inclusion of large-scale self-heating in our analysis. For an object with a major concavity, it might occur that some parts of its surface will be irradiated by sunlight reflected off the other parts of the surface. This self-heating can significantly change the outcome of the YORP torque computation [7].

References: [1] Higgins, D. et al., 2006, Minor Planet. Bull., 33, 8. [2] Krugly, Yu. N. et al., 2007, In Proceedings of IAU Symposium No. 236, 385. [3] Benishek, V. & Protitch-Benishek, V., 2009, Minor Planet. Bull., 36, 35. [4] Magri, C. et al, 2011, Icarus, 214, 210–227. [5] Rozitis, B. & Green, S. F., 2011,MNRAS, 415, 2042. [6] Rozitis, B. & Green, S. F., 2012, MNRAS, 423, 367. [7] Rozitis, B. & Green, S. F., 2013, MNRAS, 433, 603.

SORTED PATTERNED GROUND ON EARTH AND MARS

A. M. Barrett[1], M. R. Balme[1]. M.R. Patel[1], A. Hagermann[1]. Open University Department of Physical Sciences. E-mail: alex.barrett@open.ac.uk.

Introduction: Sorted Patterned ground in common in cold climate environments on Earth. It occurs in places where the upper, active layer of permafrost thaws on a seasonal cycle, moving stones of different sizes into domains of coarse and fine material. Over many cycles a positive feedback is established and elaborate shapes, such as sorted circles, stripes and polygons emerge. Similar structures may be present on Mars. Clastic polygons and stripes have been observed across the northern plains by several studies [1, 2].These could have formed through the same processes that produce sorted patterned ground on Earth, namely the thawing of a permafrost active layer. However the cold dry environment of Mars would seem to make such thawing events unlikely.

It is possible that the presence of brines could depress the freezing point of water sufficiently for frequent thaw events to occur under martian conditions. Alternatively it is possible that they could have formed through a difference process and the similarities to terrestrial features are coincidental. It has been suggested that martian patterned ground could form through gravitational sorting, when clasts accumulate in the troughs produced by the erosion of thermal contraction cracks [3]. Another alternative is that boulders are locked into a layer of seasonal carbon dioxide frost and are moved due to the opening and closing of underlying contract cracks [4, 5]. Both of these mechanisms would require the presence of an underlying fracture net.

Methods: In this investigation a large scale survey of high resolution HiRISE images was conducted and the examples of possible patterned ground were mapped. These have been compared to terrestrial analogues to examine the likelihood that they are formed through any of the processes outlined above. The validity of the two fracture controlled mechanisms can be tested by determining which proportion of highly sorted patterns occur in proximity to fracture networks. The freeze-thaw sorting mechanism is harder to directly test. The best evidence for a periglacial formation mechanism would be the presence of clastic polygons within a coherent landform assemblage including other possible periglacial landforms. This would indicate that all of the landforms should have formed through related processes. If the most likely process to explain all of the observed morphologies is the thawing of ground ice then such a landscape could potentially provide a geomorphic marker for places where water has been liquid in the geologically recent past.

Results: Potential examples of clastic patterns were found across the martian northern plains. They were not found to be common, but occurred in each of the study areas examined and at lower latitudes than had been established by previous investigations. A particularly extensive region of sorted patterns were found in the north east of Acidalia Planitia, in the vicinity of Lomonosov Crater. This area had a sufficiently large number of sorted patterns to assess whether they formed through either of the fracture control mechanisms. It was found that the majority of sorted patterns appeared to be independent of underlying fractures, and many were not superposed on fracture networks at all. Very few examples of clasts within fracture troughs were recorded, although they were present in a few locations. Several examples of patterns ground were found as part of wider assemblages, however these were not common enough to unreservedly accept a periglacial explanation.

References: [1] Gallagher C, Balme MR (2011) Geol Soc London, Spec Publ 356:87–110. [2] Gallagher C, et al. (2011) Icarus 211:458–471. [3] Levy JS, et al. (2010) Icarus 206:229–252. [4] Orloff T, Kreslavsky M, Asphaug E, Korteniemi J (2011) Boulder movement at high northern latitudes of Mars. J Geophys Res 116:1–12. [5] Orloff TC, et al. (2013) P Icarus 225: 992–999.

ANALYSIS OF PRESOLAR SILICON CARBIDE GRAINS USING TOF-SIMS AND NANOSIMS.

A. Clarke[1], T. Henkel[1] and I. C. Lyon[1]. [1]School of Earth, Atmospheric and Environmental Sciences, The University of Manchester, Manchester, M13 9PL, UK. Email: alex.clarke-2@postgrad.manchester.ac.uk.

Introduction: Presolar grains are micron-sized dust grains which formed from the gas surrounding dying stars. They are identified by their highly anomalous isotope ratios (relative to solar compositions), which vary by a few orders of magnitude and are only explained by stellar nucleosynthesis. As a result, presolar grains must have formed before the solar system and survived extensive alteration before being incorporated into solar system bodies. These alteration processes include interaction with supernovae shockwaves and galactic cosmic rays, ion implantation [1], and aqueous alteration within asteroids. Analysis of presolar grains therefore provides information on stellar processes and environments, as well as processes which occurred in the interstellar medium, solar nebula and meteorite parent bodies.

Presolar silicon carbide (SiC) grains are found in relatively high abundances (up to 150ppm) in nearly all primitive chondrite classes. As a result of their abundance, relatively large size (~1 micron on average) and ease of extraction from meteorites, presolar SiC grains are well studied, with over 10,000 individual grains analysed [2]. However, the majority of these grains were separated from their host meteorites with the use of harsh acids, which have been shown to alter and damage the grain surfaces [3, 4]. For this reason, the presolar SiC grains analysed in this work will be separated using a Gentle Separation procedure, a method which minimizes damage to the grains during extraction.

Methods: 110mg of Murchison matrix material was processed using the Gentle Separation method to extract presolar SiC grains. The material was first broken down into individual grains using freeze-thaw disaggregation. Size and density separation were then carried out to increase the abundance of presolar SiC grains in the fraction of interest. Samples were prepared by distributing material onto a gold foil with a finder grid imprint. Each sample was then mapped for selected elements using the EPMA, in order to identify presolar SiC grains.

In order to calibrate measurements of presolar SiC grains, eight silicate standards (of known composition) were analysed using a Time-of-Flight Secondary Ion Mass Spectrometer (TOF-SIMS), to determine the variations in elemental and isotopic compositions as a result of instrumental fractionation

Future work: Presolar SiC grains will primarily be analysed for their elemental and isotopic compositions using a TOF-SIMS. This will allow the entire mass spectrum to be analysed simultaneously whilst depth profiling the grains, maximizing the information which is collected. Selected grains of interest will also be analysed using the NanoSIMS. This delivers higher precision isotope ratios than are possible with the TOF-SIMS, but is only capable of analyzing 7 species at once.

Results and Conclusions: Eight silicate standards were analysed using the TOF-SIMS in order to determine the suitability of the method for the analysis of presolar SiC grains. Relative Sensitivity Factors (RSFs) were determined with errors typically below 30% for the majority of elements. As many elements vary by up to three orders of magnitude in presolar SiC grains [1], these errors are small in comparison. In the silicate standards, isotope ratios for Li, B, Mg, Si, Ca and Cr were determined with errors of <33‰ (with many <20‰). In presolar SiC grains, many isotope ratios vary by between 1 and 4 orders of magnitude. As these errors are much smaller than the expected isotopic variation, the TOF-SIMS is suitable for the analysis of presolar SiC grains.

References: [1] Lyon I. C. et al. 2007. *MAPS*. 42:373-385. [2] Hynes K. M. and Gyngard F. 2009. Abstract #1198. 40th LPSC. [3] Bernatowicz T. J. et al. 2003. *Geochim Cosmochim Ac*. 67:4679-4691. [4] Henkel T. et al. 2007. *MAPS*. 42:1121-1134.

SURVIVAL OF THE IMPACTOR DURING HYPERVELOCITY COLLISIONS.

Ch. Avdellidou[1], M.C.Price[1], M. Delbo'[2] E-mail: ca332@star.kent.ac.uk
[1] Centre for Astrophysics and Planetary Science, School of Physical Sciences, University of Kent, Canterbury, UK.
[2] Observatoire de la Cote d'Azur, Nice, France.

Introduction:
Impacts have shaped asteroids, and their size frequency distribution, through 4.5 Ga of Solar System evolution. The appearance and morphology of asteroidal surfaces are also the result of impact processes, which are responsible, for instance, for the formation of craters and the production of regolith. Over the last four decades, a plethora of laboratory experiments and computer simulations have provided insights into collision processes, but our understanding of the fate of the impactor at impact speeds of several km/s is still poorly understood. This is because experiments were not focused on the study of the projectile and the fate of its fragments after the impact. However, interest has increased in the fate of the projectile and projectile debris to possibly explain phenomena such as the source of the olivine and dark material deposits observed on Vesta [1][2] and the formation of multi-lithology asteroids such as 2008 TC3 [3].

Considering an average impact speed of <v> = 5.3 km/sec for Main Belt asteroid collisions [4], we present preliminary results of our laboratory program devoted to measuring the survivability and state of impactors, covering initially a speed range of 0.4 - 3.5 km/sec. Peridot (Mg-rich olivine) projectiles were fired onto porous water ice targets (with strengths similar to those assumed for asteroidal regoliths), using the University of Kent's Light Gas Gun. The icy targets allow for an accurate quantification of the mass and size distribution of the projectile's fragments that were embedded in the crater, as we simply melt the crater and filter the water, leaving the debris from the impactor behind. Additionally, an ejecta collection system was built in order to capture the majority of the projectile's escaped fragments for analysis. Using Scanning Electron Microscopy and energy dispersive X-ray spectroscopy (EDX) we were able to discriminate the impactor's fragments and produce their size distributions. Raman spectroscopy was also used to examine the state of the largest surviving fragments; shifts in the position of the Raman bands are possible indicators of shock history.

References:
[1] Daly R.T. and Schultz P.H. 2013. 44th LPSC
[2] Reddy V. et al. 2012. *ICARUS*. vol.221
[3] Gayon-Markt J. et al. 2012. *MNRS*. vol.424
[4] Bottke B. et al. 1994. *ICARUS*. vol.107

A Search for Disintegrating Exoplanets

D. Staab[1] C.A. Haswell[1], J.R. Barnes[1], L. Fossati[1], G. Anglada-Escude[2], P. Arriagada[3] and J.S. Jenkins[4].
[1]The Open University E-mail: daniel.staab@open.ac.uk [2] QMUL [3] Carnegie Institution of Washington [4]Universidad de Chile

Introduction: For the vast majority of exoplanets only their most basic properties (mass, size and orbit) are known. Characterisation is easiest for transiting planets and even the planet's size is unconstrained for non-transiting objects. Thus transiting planets of all possible types are key to the study of the Galaxy's planet population. Currently, the dearth of known planets that are amenable to in-depth characterisation, i.e. orbiting nearby bright stars, significantly constrains the study of exoplanets. Our research aims to discover the subset of such objects that are suffering significant mass-loss through evaporation. These disintegrating exoplanets are ideally suited for follow-up work, focused on chemical composition.

Probing Planetary Composition: Chemical composition plays a key role in determining planetary structure and evolution. Several very different structures and compositions can match a particular mass and size [1]. To reveal mass-radius-composition relationships of the various planet classes it is crucial to make direct measurements of bulk compositions. The opportunity to go beyond atmospheric characterization and sample the bulk composition arises in particular when ultra-short period planets are being evaporated by intense irradiation from the host star. Detailed chemicalcharacterisation of the mass loss, using the transmission spectroscopy technique, is enabled by the extended spatial distribution of the gas.

Rocky Bodies: A prototype disintegrating rocky planet, KIC 1255b, was discovered in the Kepler dataset via variable-depth transits of a cloud of dust and metal-rich vapour fed by a ~0.1 Earth mass planet in a 16 hour orbit [2] . KOI 2700b is a second example [3], but also orbits a faint star. Modelling suggests these planets are in a short-lived, catastrophic final phase of evolution[4], so there are likely to be many more progenitor systems losing mass more gradually. If we can find them orbiting nearby bright stars, these progenitors will facilitate detailed characterisation. In any individual object, we are sampling the current surface layer, but as these planets are disintegrating we will be probing a variety of depths by observing a sample of objects.

Search Strategy: Our recent work on WASP-12b revealed that mass loss from short-period planets can produce a shroud of diffuse gas which engulfs the entire planetary system and produces noticeable absorption of the stellar spectrum in the resonance lines of abundant species [5,6]. By examining archival spectral data on bright stars we have identified about 50 which show signs of enshrouding gas [7]. Based on this, we are carrying out a highly targeted radial velocity planet search using SOPHIE and HARPS. The observing strategy enables detection of short-period planets down to about 2 Earth masses in a few nights of telescope time. Future space-based observations with the TESS, CHEOPS and PLATO missions will be able to detect smaller transiting objects.

References:

[1] Rogers L.A. & Seager S. 2010. *ApJ.* 712: 974R.
[2] Rappaport S. et al. 2012. *ApJ.* 751:1R..
[3] Rappaport S. et al. 2014. *ApJ.* 784:40R.
[4] Perez-Becker D. and Chiang E. 2013. *MNRAS.* 433. p.2294-2309.
[5] Haswell C. A. et al. 2012. *ApJ.* 760:79H.
[6] Fossati L. et al 2013. *ApJL.* 766:L20.
[7] Staab D. et al. 2015 in prep.

PROBING METEORITE MATRIX USING NON-DESTRUCTIVE TECHNIQUES.

E. Vaccaro[1,2], T. Goral[1], J. Najorka[1], S. S. Russell[1] [1]Dept of Earth Sciences, The Natural History Museum, London, UK. E-mail: e.vaccaro@nhm.ac.uk. [2]Planetary & Space Sciences, Open University, Milton Keynes, UK.

Introduction: The minute quantities or particle size of samples returned from future space missions makes it vital to develop non-invasive diagnostic research methods to study these precious materials. The mineralogy of such samples is a key parameter to determine, but presents many challenges when material is limited or high spatial resolution is required. In this study we have carried out a combination of several non-destructive analysis of selected matrix regions of primitive carbonaceous chondrites ALHA77307 and QUE 99177 to investigate their nature.

Experimental methods: Ultra high-resolution image maps were acquired using a Carl Zeiss Ultra Plus Field Emission SEM. Image manipulation software "Image J" was used to estimate the clast and pore abundances by thresholding different grey-scale values from the image maps. Element maps of the same matrix regions were acquired, at 15kV and 5kV using a FEI Quanta 650 SEM with an innovative XFlash QUAD 5060F Bruker detector. [1]. Micro-XRD analyses were directly collected from the selected areas on the thin section using the Rigaku D max Rapid II. A pin-hole of 30 μm was used to achieve an X-ray beam footprint on the sample of ~50 x 500 μm [2].

Results: The micro-XRD patterns indicate the presence of olivine, clinoenstatite, pyrrhotite, magnetite and kamacite in the matrix of the meteorites studied. Clast and pore abundances in 5 image maps of each meteorite (each map having an area of ~ 20 x10 μm) show the average abundance of metal grains in ALHA77307 and QUE 99177 is 3±2.3% and 2±0.8% respectively, the average porosity is 6±4.1% and 3±1.6% respectively, and the average abundance of crystalline silicates and oxides are 65±12.1% and 46±4.8% respectively. A groundmass of amorphous material accounts for 26±16.2% in ALHA77307 and 49±4.0% in QUE 99177. In both samples the element maps acquired show that the main cations of the amorphous groundmass are Al, Si and Fe, consistent with previous works e.g. [3], [4]. The matrix of ALHA77307 contains some acicular grains of Mg-silicate grains, a morphology indicative of condensation from solar nebular.

Conclusions: The phase identification using in situ micro-XRD demonstrates that this technique has the potential to be a useful tool in the characterization of minute samples or local areas of interest. The element maps acquired, using a FEI Quanta 650 SEM with an innovative Bruker detector, demonstrated to be capable of providing chemical information at spatial resolution down to a volume of 200 nm in depth by 100 nm in radius at 5kV,fig. 1. This has proved to be a useful tool for non-destructive chemical analysis at high spatial resolution.

References: [1] E. Vaccaro et al., Abstract #5327. *MetSoc 2014* [2] E. Vaccaro et al., Abstract #5348. *MetSoc 2014.* [3] A. Brearley, 1993, *Geochim. et Cosmochim. Acta* 57. [4] M. Neyda, A. Brearley, 2010, *Geochim. et Cosmo-chim. Acta* 74.

INTERACTIONS BETWEEN THE INTERIOR AND SURFACE RESERVOIRS FOR VOLATILES ON MARS AS RECORDED IN MARTIAN METEORITE NWA 7034

G. M. Jacobs[1]. M. Anand[1,2]. I. A. Franchi[1]. M. M. Grady[1,2]. [1] Planetary and Space Sciences, The Open University, Walton Hall, Milton Keynes, Bucks, MK7 6AA. [2]Department of Earth Sciences, The Natural History Museum, Cromwell Road, London, SW7 5BD, UK. E-mail: George.Jacobs@open.ac.uk.

Introduction: NWA 7034, popularly known as Black Beauty, is a relatively recent addition to our inventory of martian meteorites [1]. Martian meteorites were originally classified under Shergottites, Nakhlites and Chassignite (SNC) categories [2]; shergottites are further classified into basaltic, olivine-phyric, and lherzolitic types [3]. Nakhlites are clinopyroxenites; igneous cumulates consisting primarily of augite [4,5]. Chassignites are primarily olivine cumulates, a martian equivalent to the dunite [4,5]. The oldest martian meteorite, ALH 84001, is currently in a category of its own, an orthopyroxenite [5].

However NWA 7034 and its pairs belong to a new class, martian breccia [6]. The meteorite has been identified as martian based on a number of mineralogical and geochemical signatures; the pyroxenes of NWA 7034 are a good match for other martian meteorites [2], the $\Delta^{17}O$ value of the water present in NWA 7034 is distinct from terrestrial values, but within SNC ranges [6]; trapped gases, such as argon, krypton and xenon, are also a good match for modern martian atmosphere [6]. NWA 7034 also possesses a very similar bulk-composition to martian surface material [6] whilst retaining links to the shergottite class [1]. Its groundmass contains secondary alteration products such as ferric oxides that also host extra-terrestrial water [2]. Therefore geochemical investigations of NWA 7034 could assist in the understanding of interactions between the interior and surface reservoirs of volatiles on Mars.

Type and composition: NWA 7034 is believed to be a regolith breccia consisting of at least five distinct lithologies, from alkali basalt to trachy-andesite [6]. X-ray diffraction analysis performed at the University of New Mexico gives the modal abundances as ~38% plagioclase feldspar, ~25% low calcium pyroxene, ~18% clinopyroxene, ~9% iron oxides, ~4% alkali feldspar and ~3% apatite [2]. U-Pb dating on zircons, baddeleyite and phosphates give four age groups: 4.44Ga, 4.35Ga, 1.44Ga, and 1.35Ga [1]. Also of interest is the presence of macromolecular carbon [2]. Bulk carbon analysis has shown that mineral inclusions contain at least 22 ± 10 ppm of C [2].

Uniqueness: NWA 7034 shows greater REE enrichment than all but nakhlites' mesostasis [2]. Its major element compositions are a better match for Gusev crater rocks rather than other martian meteorites, being enriched in Na and K, along with having high Mg/Si, Al/Si and Ni/Mg ratios [2]. NWA 7034 also shows enrichment in $\Delta^{17}O$, with values of 0.58 ± 0.05 ‰, compared to the usual SNC range of 0.15 - 0.45 ‰ [2]. Extra-terrestrial water exists within NWA 7034 in concentrations of over 6000 ppm [6]. Analysis of trapped atmosphere shows elevated ^{40}Ar and ^{36}Ar values compared to other meteorites [6]. All of these attributes make NWA 7034 a unique Mars sample.

Martian Volatiles: Due to its lack of plate tectonics, Mars does not have a system for recycling crustal material [7]. Therefore, we expect the deuterium/ hydrogen (D/H) ratio, commonly expressed in terms of δD, in the martian interior to reflect the primordial ratio [7]. Hydrous primary igneous minerals, such as apatite, can provide such primordial signatures [7]. D/H signatures are also useful in evaluating the source(s) of water in the Solar System [7]. Martian atmosphere has a high δD value of ~4200 ‰ due to preferential loss of H over D from its atmosphere [7]. Meteorites derived from primitive magmas, such as Yamato 980459, show δD values similar to chondritic and terrestrial values, whilst enriched meteorites such as Larkman Nunatak 06319, show very high δD values closer to martian atmosphere [8].These results seem to suggest that Mars possesses a primordial interior reservoir of water (similar to chondritic and terrestrial-like δD), whilst surface processes introduced fractionated water to martian magmas, leading to D/H enrichment [8]. The $\delta^{13}C$ values for bulk carbon in NWA 7034 are -23.4±0.73‰; this is very similar to carbon found in shergottites [2]. Because the nature of NWA 7034 is quite different to other martian meteorites this suggests that there could be multiple light carbon reservoirs within Mars [2]. However its brecciated nature means comparison of individual lithologies could reveal multiple reservoirs.

Objectives: NWA 7034 represents a good match for the martian surface compared to other meteorites, representing multiple lithologies; it has a great potential to shed more light on interactions amongst martian surface processes, and the martian hydrosphere and atmosphere. Initially using thin sections of NWA 7034, apatite grains will be identified through SEM analysis, targeting grains high in phosphorus, calcium and chlorine. These apatite grains will them be analysed using NanoSIMS to measure H and C isotopes. The δD and $\delta^{13}C$ signatures of the various lithologies within NWA 7034 can then be compared with each other, the martian atmosphere, other meteorites, comets, and terrestrial samples. The project will then focus in on the C inventory of NWA 7034. This will allow for study of how surface fluids and atmosphere have interacted with igneous rocks on the martian surface, and how the various volatile reservoirs mix and are incorporated into martian rocks.

References: [1] Yin Q. –Z. et al. 2014. Abstract #1320. 45th LPSC. [2] Agee C. B. et al. 2013. *Science*. 339:780-785. [3] Howarth G. H. et al. 2014. Abstract #1310. 45th LPSC. [4] Grady M. 2006. *In McCall G. J. H. et al. 2006*. 256:405-416. [5] Papike J. J. et al. 2009. *GCA*.73:7443-7485. [6] Cartwright J. A. et al. 2014. *EPSL*. 400:77-87. [7] Hallis L. J. et al. 2012. *EPSL*. 359-360:84-92. [8] Usui T. et al. 2012. *EPSL*. 357-358:119-129.

DRAGONS – RESISTIVE GRID CALIBRATION

J. New[1], F. Giovane[2], R. Corsaro[3], M. Price[4], M. Burchell[5], M. Cole[6]
[1]University of Kent, UK; [2]Virginia Tech, USA; [3]Naval Research Lab, USA
jn287@kent.ac.uk

Keywords: Orbital debris, micrometeoroids, hypervelocity impacts, detector, LEO

The Debris Resistive/Acoustic Grid Orbital Navy Sensor (DRAGONS) is intended to be a large area impact sensor for in-situ measurements of micrometeoroids and orbital debris (MMOD) in the 0.05 mm to 1 mm size regime. MMOD particles in the 0.2 mm to 1 mm size regime are too small to be detected by ground based radars and optical telescopes, but large enough to jeopardise the safety of human space activities and autonomous missions in low Earth orbit (LEO). Although safety concerns are negligible for MMOD smaller than 0.2 mm in diameter, DRAGONS sensors can detect micrometeoroids as small as 0.05 mm for further study.

The proposed detection area of DRAGONS is four 0.5 m × 0.5 m panels with independent operations. DRAGONS' design combines three unique detection technologies that maximize the information extracted from each impact. The first technology is a resistive grid consisting of 62.5-μm-wide resistive lines, coated in parallel and separated by 62.5 μm gaps on a Kapton film. When particles a few hundred micrometers or larger strike the resistive grid, penetrations occur in the film and resistive lines are severed. The size of the damage area can be estimated from the increased resistance. The second technology employs a dual-layer, 25-μm-thick Kapton film with a 10 cm separation. By measuring the time difference between impacts on the two films, the impact speed can be calculated. The third technology is based on polyvinylidene fluoride (PVDF) acoustic impact sensors. Multiple PVDF sensors are attached to the backside of both Kapton films to provide impact timing measurements. The impact location on each film can be identified from the triangulation of signals received at different PVDF sensors. Combining the impact location on both films provides an estimate of the impact direction.

Calibration and testing of DRAGONS' resistive grid is currently being conducted at the University of Kent, where researchers are attempting to relate the impact-hole size and projectile diameter of high and low density spheres in the 0.05 mm to 1 mm size regime. The results presented in this poster include five projectile materials (Stainless Steel 420, Copper, Aluminium, Acrylic and Nylon) with incident impact angles ranging between 0° and 45° impacting 25 μm Kapton foils and replicas of DRAGONS' Resistive Grid.

PANSPERMIA SURVIVAL SCENARIOS FOR ORGANISMS THAT SURVIVE TYPICAL HYPERVELOCITY SOLAR SYSTEM IMPACT EVENTS. D. L. S. Pasini[1], M. C. Price[1]. [1]School of Physical Sciences, University of Kent, Canterbury, Kent, CT2 7NH, UK. (corresponding author: dp335@kent.ac.uk).

Introduction: Previous experimental studies have demonstrated the survivability of living cells during hypervelocity impact events, testing the panspermia and litho-panspermia hypotheses [1]. It has been demonstrated by the authors that Nannochloropsis Oculata Phytoplankton, a eukaryotic photosynthesizing autotroph found in the 'euphotic zone' (sunlit surface layers of oceans [2]), survive impacts up to 6.93 km s^{-1} (approx. shock pressure 40 GPa) [3, 4]. Also shown to survive impacts up to 5.49 km s^{-1} is the tardigrade species Hypsibius dujardini. [5, 6]. It has also been shown that they can survive sustained pressures up to 600 MPa using a water filled pressure capsule [7]. Additionally bacteria can survive impacts up to 5.4 km s^{-1} (~30 GPa) – albeit with a low probability of survival [1], and the survivability of yeast spores in impacts up to 7.4 km s^{-1} (~30 GPa) has also recently been demonstrated [8]. Other groups have also reported that the lichen Xanthoria elegans is able to survive shocks in similar pressure ranges (~40 GPa) [9]. Here we present various simulated impact regimes to show which scenarios are conducive to the panspermia hypothesis of the natural transfer of life (via an icy body) through space to an extraterrestrial environment.

Methodology: ***Shock Pressure Experienced During Impact:*** A series of simulated impacts were run using Ansys' AUTODYN software using a 2-D Lagrangian mesh solver with axial symmetry. 37 pressure tracking gauges were placed throughout the projectile to record the pressures during the impact event. The Optimal Point ('Op.P.') of lowest peak pressure during the impact was found to be gauge No. 1 in all instances. Thus, these pressure values are used for the 'best case' survival scenario (i.e. assuming significant numbers of an organism are distributed across the body such that survival depends only on the lowest peak pressure during impact). The simulations consist of an icy body impacting into an ocean and a rocky silicate body (Fig. 1). Float glass is used to simulate the silicate body, as work to validate a realistic basaltic analogue model is ongoing by the authors.

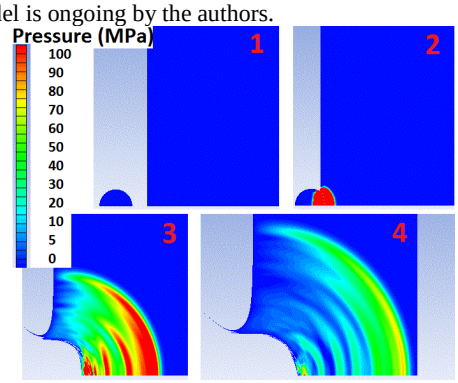

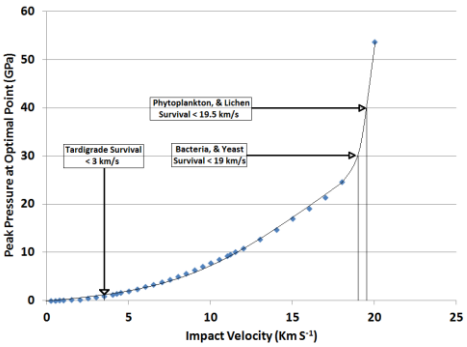

Fig. 1. Ansys AUTODYN simulation showing pressure contours for a 200 m water ice projectile impacting an ocean at 1.5 km s^{-1}. (Image timesteps - 0, 97, 390, & 560 ms into run). **Fig. 2.** Impact velocity vs. peak pressure at Op.P. for water ice projectile impacting icy body.

Results: ***Impact Velocities:*** An optimum situation is assumed of a projectile passing near to a target body and being captured by the body's own gravity well. Thus the impact velocity will be equal to the body's local escape velocity.

Results: ***Survival Within The Solar System:*** The results presented here indicate the tardigrade species could only survive oceanic and rocky impacts up to 3, & 2 km s^{-1} respectively (e.g. Fig. 2). Thus, impact survival can occur on bodies such as Enceladus, Ceres (and all asteroids), Pluto (and equal or smaller Kuiper Belt Objects), Europa, and any bodies similar to the Moon or Titan that have substantial liquid bodies on their surfaces. However, the other four organisms considered here show that impact survival can occur anywhere within the solar system with the exception only of the four outer solar system gas planets.

Results: ***Extrasolar Planetary Impacts:*** Two Super-Earth exoplanet candidates, KoI 82.02 & 115.02, are used as examples. If homogeneous, and composed primarily of the perovskite phase of $MgSiO_3$ (Earth-like), the radii of KoI 82.02 & 115.02 are expected to be 1.4 R_E, or 1.7 & 1.8 R_E respectively if Europa like [10], Survival is possible on Super-Earths composed of water/ice (and smaller rocky exoplanets) beyond our solar system. However, survival appears unattainable for larger rocky Super-Earths (where V_{esc} exceeds 15.9 km s^{-1}) without an aid, such as atmospheric drag forces lowering the impactor's speed.

Conclusions: The natural transfer of life throughout the solar system via impacts is possible for a variety of simple species. Some Super-Earths beyond our solar system are also within their survival tolerances. Oceanic impacts allow higher survival rates than rocky body impacts. However, atmospheres on bodies can lower an impactor's speed, increasing the probability of survival. Even the humble tardigrade (a complex life-form) could survive impacts onto small moons and asteroids.

References: **[1]** Burchell M. J. et. al. (2004). *MNRAS*, 352; 1273. **[2]** Ghosal S. et. al. (2002). *NASA/TM-2001-210935*, 88. **[3]** Pasini D. L. S. et al. *LPSC44*, 1497. (2013). **[4]** Pasini D. L. S. et. al. *EPSC2013*, 396. (2013). **[5]** Pasini D. L. S. et al. *LPSC45*, 1789. (2014). **[6]** Pasini D. L. S. et. al. *EPSC2014*, 67. (2014). **[7]** Seki K. et al. *Nature*, 395. 853-854. (1998). **[8]** Price M. C. et al. (2013). *Icarus, 222*, 263. **[9]** Horneck G., et al. (2008) *Astrobiology, 8*, 17. **[10]** Hadden S. and Lithwick Y. (2014) *ApJ*, doi:10.1088/0004-637X/787/1/80.

MULTISPECTRAL IMAGING OF HYDROTHERMAL ALTERATION TERRAINS USING AN EXOMARS PANCAM EMULATOR.

J. K. Harris[1], I. Crawford[1] and C. R. Cousins[2]. [1]Birkbeck University of London, E-mail: Jennifer.harris@bbk.ac.uk. [2]University of Edinburgh.

Remote Sensing and visible and near infrared (VNIR) reflectance spectroscopy are fundamental tools in the exploration of isolated environments on Earth and of our neighbouring planetary bodies, in particular Mars. One of the current objectives of the Mars science community is to identify regions of the planet that may have previously been habitable. This search is primarily focused on mineral assemblages and lithologies that form in the presence of liquid water. Key instruments that have already been utilised for this purpose include the multispectral cameras on both the Spirit and Opportunity rovers (Pancam) and MSL Curiosity (MastCam). The upcoming ESA/Roscosmos 2018 ExoMars rover will continue to use in-situ reflectance spectroscopy for geological target selection at the Martian surface, within which to search for signs of life. It is imperative therefore to conduct groundtruthed field tests of the ExoMars PanCam to ensure adequate target selection for the mission and reliability of PanCam datasets.

The Námafjall geothermal field in the volcanic Krafla region of Iceland was used to field test the current configuration of the Aberystwyth University PanCam Emulator (AUPE), a prototype of the ESA/Roscosmos ExoMars Panoramic Camera (PanCam). The minerals commonly found in this type of environment include phyllosilicates, iron oxides, and opaline silica, all of which have been detected on the surface of Mars making the region a suitable Mars analogue site. AUPE datasets are compared and groundtruthed to in-situ field spectroscopy data and laboratory spectral library data. The ability of AUPE to identify and characterise extreme habitable volcanic environments was examined and the accuracy of the AUPE multispectral datasets scrutinised.

ARAM DORSUM: A NOACHIAN INVERTED FLUVIAL CHANNEL SYSTEM AND CANDIDATE EXOMARS 2018 ROVER LANDING SITE.

M. Balme[1], **J. Davis**[2], P. Grindrod[3], E. Sefton-Nash[3], S. Gupta[4], P. Fawdon[1], P. Sidiropoulos[5], V. Yershov[5], & J-P. Muller[5]. [1]Dept. of Physical Sciences, The Open University, Milton Keynes, UK, [2]Dept. of Earth Sciences, University College London, UK., [3]Dept. of Earth and Planetary Sciences, Birkbeck, University of London, UK, [4]Dept. of Earth Science & Engineering, Imperial College, London, UK, [5]Mullard Space Science Laboratory, University College London, UK.

Introduction: The search for life on Mars is a cornerstone of international solar system exploration. In 2018, the European Space agency will launch the ExoMars Rover to further this goal. The ExoMars Rover's key science objectives [1] are to: 1) search for signs of past and present life on Mars; 2) investigate the water/geochemical environment as a function of depth in the shallow subsurface; and 3) to characterise the surface environment. ExoMars will drill into the sub-surface to look for indicators of past life using a variety of complementary techniques, including assessment of morphology (potential fossil organisms), mineralogy (past environments) and a search for organic molecules and their chirality (biomarkers). Our group proposed the Hypanis and Aram Dorsum sites [1,2]. Here, we present the science case for Aram Dorsum. The Aram Dorsum site in western Arabia Terra is situated about half way between Meridiani Planum and the dichotomy boundary, where Arabia Terra meets the northern lowlands. Aram Dorsum itself is a flat-topped, branching, sinuous ridge-like feature that is surrounded by smoother marginal materials (Fig. 1, 2).

Observations: The Aram Dorsum main channel system is sinuous to meandering and contains multiple channels. These are both laterally and also vertically separated from one another as shown by cross-cutting relationships and traces of older, now buried, channels alongside and underneath the main channel system. In the west of the study area, the channel system is a well-defined, single thread channel. In the east the plan-view pattern is more consistent with an anastomosing, or multi thread channel, sometimes separated by lozenge-shaped 'islands'. The main channel system is superposed upon a smooth, low relief channel-marginal unit that is also overlain by local and regional overburden materials. Inliers of this unit are seen in erosional windows within the overburden materials.

Interpretation: The presence of channels at different stratigraphic positions demonstrate that there was long-lived fluvial activity, not catastrophic flow. This is reinforced by the overall morphology of the channel, which is consistent with a river-like fluvial system, not a catastrophic flow. That channels are set within the channel marginal unit, as well as on top of it, suggests that the channel marginal unit is a sedimentary deposit. The main channel system is not braided, and there is little evidence of unconfined channel migration. Instead, there are several stable sinuous paths, with multiple lateral branches. This implies that, when the main trunk formed, the channel has competent banks and that channel migrated laterally by avulsions, or was anastomosing, rather than by unconstrained lateral 'sweeping'. In the absence of land plants [e.g., 3], other mechanisms that could stabilise the banks include ice-cementation or a high clay content. Aram Dorsum is a Noachian-era, aggradational, multithread/sinuous river-system, including small tributaries and extensive flood plain-like marginal deposits.

Relevance to ExoMars Science Goals: Aram Dorsum displays clear evidence for the long-lived action of water in the Noachian (possibly even early/mid Noachian). Although the inverted channel likely contains mainly coarse-grained sedimentary outcrops, the channel marginal unit is probably fined-grained sediments, or could contain lenses and/or 'islands' of fine grained material suitable for preserving biosignatures. Importantly, the system has been exposed from beneath >100s of metres of overburden materials; outliers of such overburden are still present. Such burial/exhumation greatly benefits preservation of biosignatures.

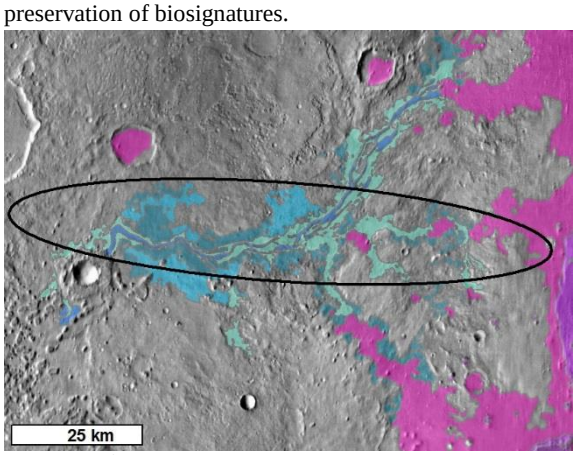

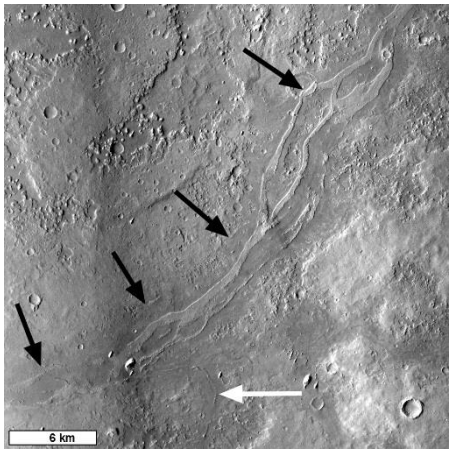

Figure 1 (left): Aram Dorsum site and 2018 landing ellipse. Blue/green areas are Aram Dorsum or its marginal units. Flow is inferred to be East-to-West. Purple areas are regionally extensive, Noachian-aged sedimentary units that superpose all other units within the study area.

Figure 2 (right): CTX mosaic showing the Aram Dorsum ridge system (black arrows).

References: [1] ESA ExoMars LSSWG (2013), http://exploration.esa.int/mars/53455-call-for-exomars-2018-landing-site-proposals/ Ref: EXM-SCI-LSS-ESA/IKI-001 [2] Sefton-Nash et al., (2015), *LPS XLVI*, Abstract #1414 [3]Cotter, E. (1978), in: Miall, A.D. (Ed.), Fluvial Sedimentology, *Can. Soc. Pet. Geol. Mem. 5*, 361–383

THE HISTORY OF WATER AT LYOT CRATER, MARS: POSSIBLE SURFACE MANIFESTATIONS OF ANCIENT GROUNDWATER AND/OR RECENT CLIMATE CHANGE.

Laura Brooker[1], Matthew Balme[1], Susan Conway[1], Gareth Collins[2], Axel Hagermann[1]. [1]Department of Physical Sciences, Open University, Walton Hall, Milton Keynes, UK. [2]Department of Earth Science and Engineering, Imperial College, London, UK.

Introduction: Lyot Crater, a 220 km diameter, Hesperian-aged martian impact basin, contains many landforms that appear to have formed by glacial, periglacial and fluvial processes [1][2][3]. Around Lyot are what appear to be flood-carved channels that could have formed by groundwater release during the impact event [1][2]. Hence, the landscape of Lyot crater appears to record the action of both ancient water sourced from underground, and more recent water sourced from the atmosphere. In this project landforms and landscapes in and around Lyot Crater will be documented and mapped to assess the case for their formation by water and ice-related processes; and hydrocode impact modelling will aid in determination of the conditions that created Lyot crater. The combination of the two parts of the project will determine the potential for the preservation of material of astrobiological interest. We will present the initial mapping-work for this project and discuss the potential avenues of future work.

References: [1] Balme M. R. et al. 2013 and Soare R. J. 2013. *EPSC Abstracts.* 8:EPSC2013-636-1. [2] Harrison T. N. et al. 2010. *Geophys Res Let.* 37. Doi:10.1029/2010GL045074. [3] Dickson J. L., Fassett J. W. and Head, J. W. *Geophy Res Let*. 36. Doi:10.1029/2009GL037472.

SURVEY OF THE PLASMA COMPOSITION IN SATURN'S MAGNETOTAIL

Marianna Felici[1,2,3], Christopher Arridge[3], Dan Reisenfeld[4], Michelle Thomsen[5], Andrew Coates[1,2].
1. Mullard Space Science Laboratory, University College London, UK; 2. The Centre for Planetary Sciences at UCL/Birkbeck, UK; 3. Department of Physics, Lancaster University, UK 4. University of Montana Missoula, MT; 5. Planetary Science Institute Los Alamos, NM

Email: marianna.felici.12@ucl.ac.uk

In 2006 the Cassini explored Saturn's deep magnetotail, reaching distances of about 68 Rs (where Rs is the equatorial radius of Saturn).

We have identified cold plasma in one event from 30 Rs in the tail which we interpret as polar wind outflow from Saturn's ionosphere and where the surrounding plasma sheet has an unusual composition (Felici et al., in preparation).

This event raises the question of what is the typical and atypical composition in different regions of the magnetotail. Previous compositional studies have mostly focused on regions of the magnetosphere inside of 17 Rs [1]. We present an extended survey of the bulk plasma composition using time-of-flight data from the CAPS/IMS instrument on Cassini. The results are organised by radial distance and local time in order to examine sources and sinks of plasma in the magnetotail and their time dependence. Our preliminary results show some agreement with previous studies ([2,3]) and interesting features (e.g important dusk dawn asymmetry).

[1] M. F. Thomsen et al., Survey of ion plasma parameters in Saturn's magnetosphere, J. Geophys. Res., 115, A10220, doi:10.1029/2010JA015267

[2] D. Reisenfeld et al., The ion composition of Saturn's magnetosphere
37th COSPAR Scientific Assembly. Held 13-20 July 2008, in Montréal, Canada., p.2593

[3] R. D. Di Fabio et al., (2011), Long term time variations of the suprathermal ions in Saturn's magnetosphere, Geophys. Res. Lett., 38, L18103, doi:10.1029/2011GL048841.

THE PHOTOMETRIC PROPERTIES OF THE TRANS-NEPTUNIAN OBJECT (145452) 2005 RN_{43}

M.G. Hyland[1], A. Fitzsimmons[1] and P. Lacerda[2]. [1] Astrophysics Research Centre, Queen's University Belfast, Belfast BT7 1NN, UK. Email: mhyland02@qub.ac.uk. [2] Max Planck Institute for Solar System Research, Justus-von-Liebig-Weg 3, 37077 Göttingen, Germany.

Introduction:

The region of space beyond Neptune is populated with small icy bodies with colours ranging from neutral to very red. These observed colours are related to the surface properties of the trans-Neptunian objects (TNOs). Therefore by making accurate measurements of the magnitudes and colours of TNOs we can begin to constrain their surface compositions and understand how these bodies have been affected by processes such as space weathering. The TNO (145452) 2005 RN_{43} is a classical Kuiper Belt object that is relatively large in size (diameter D ~ 679 km[1]). Previous observations of this object have allowed its absolute magnitude to be estimated[1], [2], [3], while its colour indices indicate that it is optically red in colour[4]. In this poster we will present recent analysis of this object that has been carried out on data obtained from observations of Medium Deep Field 9 using the Pan-STARRS 1 telescope in Hawaii. We will present the measured magnitudes as a function of phase angle for each of the filters used in the survey (see Fig. 1 for an example phase diagram) along with the absolute magnitudes and phase functions derived from these phase diagrams. Colour measurements for the object and constraints on the rotational lightcurve will also be shown.

References:

[1] Vilenius E. et al. 2012. *A&A.* 541, A94. [2] Ofek, E.O. 2012. *ApJ.* 749, 10. [3] Perna, D. et al. 2013. *A&A.* 554, A49. [4] DeMeo, F.E. et al. 2009. *A&A.* 493, 283-290.

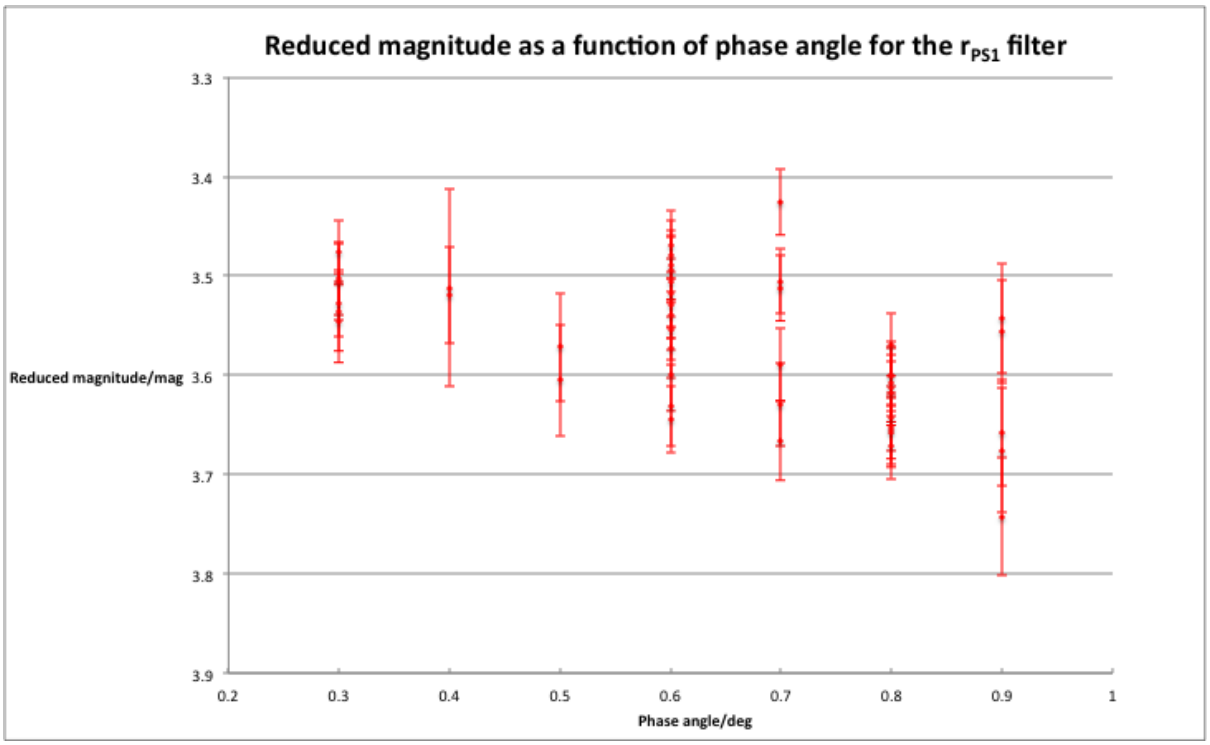

Fig. 1 - Reduced magnitude as a function of phase angle for the Pan-STARRS r_{PS1} filter.

USING THE MARTIAN METEORITES AS A GROUND TRUTH FOR SPACECRAFT DATA; A MULTIDISCIPLINARY APPROACH.

N. R. Stephen[1, 2, 3]; S. S. Russell[2]; M. J. Genge[3]: P. F. Schofield[2] & A. J. Berry[3, 4]

[1]Electron Microscopy Centre, Plymouth University, Drake Circus, Plymouth, Devon, PL4 8AA (Email: natasha.stephen@plymouth.ac.uk); [2] Department of Earth Sciences, Natural History Museum, South Kensington, London, SW7 5BD, UK; [3] Department of Earth Science & Engineering, Imperial College London, South Kensington, London, SW7 2AZ, UK; [4] Research School of Earth Sciences, Australian National University, Canberra, ACT 2601, Australia

Many databases containing spectral data from the Martian surface exist owing to many years of spectroscopic investigation by both orbiting satellites and rovers on the surface of Mars. The Martian meteorites, however, provide a unique opportunity to study true Martian material in the laboratory and therefore can be used as a ground truth for remotely acquired data. We have already shown that there are various mineral phases missing from the spectral libraries used to un-mix remote datasets, some of which are a major component of these Martian meteorites, e.g. the low-Ca clinopyroxene pigeonite, which is rare on Earth.

This study has used various non-destructive X-ray techniques (EDS, WDS, EBSD) to characterise the Martian samples in terms of their composition and crystallographic orientation before using targeted µ-FTIR to analyse specific mineral spectra to be used in direct comparisons. These µ-FTIR analyses focused on the mid-IR range (4000 cm^{-1} – 600 cm^{-1}) in order to characterise the silicate minerals using both bench-top systems as well as utilising the enhanced spatial resolution (8 µm rather than 50 µm) offered for µ-FTIR analysis at the Diamond Light Source in Oxfordshire, UK.

Three types of Martian meteorite were available to this study; various Shergottites, a Nakhlite and the polymict breccia NWA 7034. The samples represent a different type of Martian lithology and the samples are of various ages. The meteorites were analysed alongside terrestrial mineral standards similar to the Martian phases in question and to two synthetic Martian samples produced to a known bulk Martian composition. We present new, Martian-specific mineral spectra for the main silicate phases identified in the Martian meteorites and discuss implications for their use in spectral un-mixing at Mars.

PRESERVATION OF SOIL BIOMARKERS UNDER MARS-ANALOGUE CONDITIONS: ASTROBIOLOGICAL IMPLICATIONS

N.R.Thomas, J.L.Toney and V.R.Phoenix. University of Glasgow, School of Geographical & Earth Sciences. E-mail: n.thomas.1@research.gla.ac.uk.

Introduction: The question of the possible existence of life outside of the Earth has long held scientific interest, with particular interest on bodies potentially capable of harbouring liquid water. Mars is arguably the focus of the majority of current astrobiology research, as while its surface appears sterile it is yet possible that preserved evidence for life past or present may be uncovered. Mars features polar ice caps, and recent evidence suggests periodic surface water flows in the lower latitudes, as well as more obvious signs of ancient surface hydrological action through geologic features such as Valles Marineris. Direct in-situ study of Mars is difficult and expensive at present, making terrestrial analogue sites important for preliminary research and field testing of equipment. Classical analogue sites are the Atacama Desert and McMurdo Dry Valleys.

Project Aims: We present a novel Mars analogue site in the Chilean Altiplano, featuring a unique combination of Mars-like factors not available at other sites. Using the analogue we will examine the preservative effect of soil depth on molecular signs of life (biomarkers), to determine the likelihood of similar signs of life withstanding the hostile conditions of the Martian surface to sufficient extent that detection by future Mars surface missions is possible.

Methodology: Environmental data was gathered from several sites in the vicinity of the analogue site, and from a range of altitudes. Particular focus was placed on UV irradiance, temperature, moisture/humidity, and soil pH. Soil samples were also collected from a range of altitudes and depths below the surface. Soil samples will be analysed for abundance of nucleic acids and lipid-derived biomarkers such as ether membrane lipids and carotenoid pigments. 16S sequence analysis will describe relative microbial diversity in soils, and possible transcriptome sequencing may corroborate other biomarker findings such as photoprotective pigments and changes in abundance of unsaturated membrane lipids. Direct bacterial culture was attempted (Cyanobacteria first instance) from collected samples.

Preliminary Findings: Extracted DNA yield exhibits notable increase with soil depth up until a certain depth. Diurnal variation in soil temperature and moisture decreases in range concurrently with increased soil depth, with variation minimal at approximately the same depth as samples providing the greatest yield of extracted DNA, this suggests that the hostile surface conditions are indeed buffered in the shallow subsurface. Direct culture of Cyanobacteria from soil samples has been unsuccessful in first instance.

Future Work: 16S sequencing work is in progress at the time of writing. Second field trip to Chile planned for further experiment and sample collection. Further environmental measurements will be required to produce a penetration profile of UV light through soil depth. Extraction, identification, and characterisation of lipid-derived biomarkers will form the next major work package.

THE HYPANIS FLUVIAL DELTAIC SYSTEM IN XANTHE TERRA: A CANDIDATE EXOMARS 2018 ROVER LANDING SITE.

E. Sefton-Nash[1], **P. Fawdon**[2]*, S. Gupta[3], M. Balme[2], J. Davis[4], P. Grindrod[1], P.Sidiropoulos[5], V. Yershov[5] & J-P. Muller[5], [1]Dept. of Earth and Planetary Sciences, Birkbeck, University of London, UK, 2Dept. of Physical Sciences, The Open University, Milton Keynes, UK, [3]Dept. of Earth Science & Engineering, Imperial College, London, UK, [4]Dept. of Earth Sciences, University College London, UK. [5]Mullard Space Science Laboratory, University College London, UK.

Introduction: The search for life on Mars is a cornerstone of international solar system exploration. In 2018, the European Space agency will launch the ExoMars Rover to further this goal. The objectives of the ExoMars Rover are: 1) search for signs of past and present life on Mars; 2) investigate the shallow subsurface; and 3) characterize the surface environment. ExoMars will drill into the sub-surface to look for indicators of past life using a variety of complementary techniques, including assessment of morphology (potential fossil organisms), mineralogy (past environments) and a search for organic molecules and their chirality (biomarkers). Our group proposed the Aram Dorsum sites [1] and Hypanis [2] and led the scientific presentations about these sites at the workshops. Here, we present the science case for Hypanis. The Hypanis landing site in northern Xanthe Terra is situated on the boundary between the southern highland and northern lowlands. Our study area includes fluvio-deltaic deposits at the termini of Sabrina Vallis and Hypanis Vallis. The Sabrina terminal deposits are constrained to within the buried crater, Magong whilst the Hypanis deltaic system is more extensive (Fig. 1). The large crater population classifies the area as mid to late Noachian [3, 4]. Significant aeolian modification has occurred since delta formation; with crater counts [3, 4], supported by aeolian features, suggesting recent exhumation from overburden.

Geologic mapping and Hyperspectral analysis: Geologic mapping within the study area was performed using HiRISE, CTX and THEMIS coverage, including 13 stereo-derived HiRISE DEMs (Fig. 3). The landing ellipse is positioned to avoid landing directly on the upper delta units. Instead, smooth plains units, Sm and Em and related unit Le (interpreted as a mantling of Sm onto ancient crater ejecta). These units are less hazardous (Fig. 1) and are also compelling science targets if formed in low energy depositional environments caused by delta activity. Here we expect the finest grain sizes would have been deposited and any potential bio-signatures would be concentrated. Two CRISM observations lie within the Hypannis study area; FRS0003157E (Y fig. 1) shows a 1.9 μm hydration signature that aligns with exposed strata in eroded deltaic sediments, indicating putative hydrated minerals in discrete layers (Fig. 2). FRS0003134F (X fig, 1) shows the combined presence of the 1.9 μm absorption plus a strong 2.3 μm drop off, indicative of the presence of Fe/Mg-phyllosilicates [5, 6]. These signatures correspond to fractured areas within polygonally ridged terrain. CRISM coverage in Magong crater indicates weak Fe/Mg phyllosilicate signatures consistent with the presence of nontronite, verminculite or saponite in delta sediments [3].

Relevance to ExoMars Science Goals: The Hypanis landing site displays clear evidence for the long-lived action of water in the Noachian. Multiple exhumed and eroded lobes in the Hypanis delta are remnants of an extensive ancient avulsing system that was the result of sustained aqueous activity. This is supported by the interpretation that the total northward flow removed and deposited ~850 km^3 of material, of which the Hypanis deposits are estimated to comprise ~150 km^3 [7]. While upper delta units present traversability obstacles, the most rewarding science target lies in the Sm, Em and Le units, which are pervasive throughout the ellipse. These units exhibit fine-scale layering and the presence of phyllosilicates, suggesting a Low-energy depositional environment of delta-proximal materials. Exposures of these units may have concentrated any potential bio-signatures transported from the upstream Hypanis-Nanedi fluvial system. Crucially, there is growing geological and mineralogical evidence that the Hypanis delta was extensive and that habitable environments may have been prevalent over almost the entire landing ellipse.

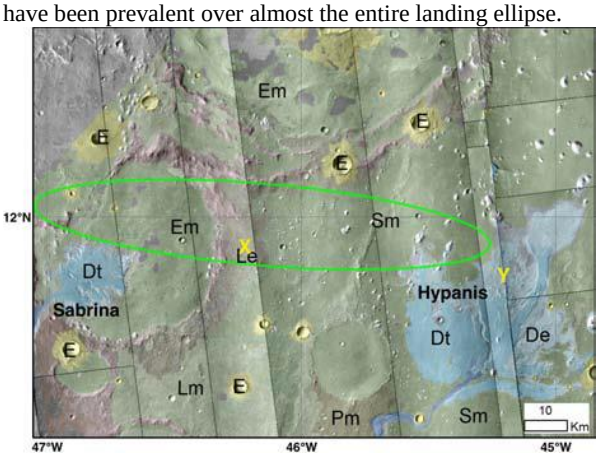

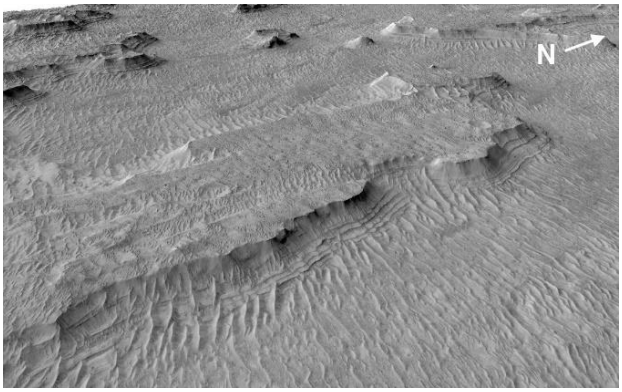

Figure 1 (left): *Geologic map of Hypanis study are overlaid on CTX. Geologic units are labeled. Deltaic units in shades of blue. The 2018 landing ellipse (104 x 19 km) is bright green. Pertinent CRISM observations are marked with yellow 'X' and 'Y'. Closely spaced transverse aeolian ridges (TARs) on top of units De and Dt (Fig. 2) prevent landing directly on upper delta material, because TAR morphology*

Figure 2 (right): *Perspective view of HiRISE 1m DEM at ~45.2°W, 11.7°N (observations ESP_21577_1920 & ESP_22434_1920). Note fine-scale layering and extensive erosion of upper delta units.*

References: [1] Balme, M. et al., (2015, this volume), LPS XLVI, Abstract #1321. [2] Gupta, S. et al., (2014), ExoMars 2018 First Landing Site Selection Workshop (LSS WS#1), ESAC, Spain. [3] Platz, T. et al., (2014) First Mars 2020 Landing Site Workshop, Crystal City, VA, USA. [4] Werner, S. (2014) Pers. Comm. [5] Pelkey, S. M. et al. (2007) J. Geophys. Res., 112, E08S14. [6] Viviano-Beck, C. E. et al. (2014), J. Geophys. Res. Plan. 119, p. 1403-1431. [7] Hauber, E. et al., (2009), Plan. SpaceSci. 57, p. 944-957.

SUBSURFACE HALOPHILES: AN ANALOGUE FOR POTENTIAL LIFE ON MARS.

P.F. Woolman, V.K. Pearson and K. Olsson-Francis. The Open University, Walton Hall, MK7 6AA, United Kingdom. Email peter.woolman@open.ac.uk.

Introduction:

Recent discoveries have reopened the idea that, in the past, Mars had a period of wetness where conditions were similar to those on Earth [1]. If this was the case then it is feasible that these environments may have harbored life. The martian surface today is dry, cold and heavily bombarded by UV radiation, making it an environment unsuitable for any known terrestrial life [2]; the martian subsurface might be considerably more hospitable. Subsurface microbial communities would not have access to sunlight for photosynthesis to drive their food chains, so primary production would have to be driven by chemolithoautotrophic organisms.

Every successful Mars landing site has been found to have abundant surface salt [3], and halite has been detected in Martian meteorites [4]. While subsurface halite deposits have not yet been detected on Mars, areas on the surface consisting of unidentified chlorine deposits have been detected with evaporation as one of the main theories to explain their creation [5]. On Earth, chloride evaporites are home to halophiles, and they have been suggested as an analogue for potential Martian life. Halophiles are micro-organisms which display a high salt tolerance. Despite being found in evaporite deposits, they are normally studied in surface brines. Brines form when the rate of evaporation of water is greater than the rate that water enters an area [6], so eventually most brines evaporate and form salt crystals. Halophiles in a brine are able to alter the size and formation rate of fluid inclusions within these salt crystals so as to entomb themselves inside until the crystals can re-dissolve [7]. It is uncertain how long halophiles can spend entombed within crystals, but there are some who speculate that it could be up to millions of years, if not longer [8].

If life had arisen on Mars during an earlier, more hospitable, wet period, as it did on Earth, then when the planet cooled, organisms analogous to terrestrial halophiles might have had the greatest potential for survival [9]. As the atmosphere left the planet, any large pools of water would have gradually evaporated, with the remaining fluid becoming increasingly brine-like. The only organisms that could survive these high salt conditions would have to be halophilic. The possibility exists that, even if there are no free-living martian halophiles remaining now, as the brines crystallized, halophiles could have been entombed inside mineral grains. It is feasible that their biomarkers and/or DNA could be extracted by instruments onboard future Mars landers [10].

It is also interesting to consider that, even though known terrestrial halophiles could not survive the high UV on the Martian surface today, they are still some of Earth's most UV tolerant terrestrial organisms. This is because, on Earth, briny environments tend to be created by evaporation of water brought on by intense sunlight; therefore organisms living in them get a high dose of UV [11]. It seems reasonable to suggest that a martian halophilic organism would, prior to the loss of Mars' atmosphere, initially have evolved in environments similar to the ones in which they evolved on Earth and so might share similar adaptations. There is some evidence to suggest that there is still periodic liquid water on Mars in the form of brines [3]. Any surface-dwelling organism remaining on the planet would need to have UV and salt tolerance and be able to enter periods of dormancy during the long dry spells. Since terrestrial halophiles have all three of these attributes, they are probably good candidates for use as analogues of martian life.

Boulby Salt and Potash mine in Yorkshire is 1.4 km underground and the second deepest mine in Europe. Despite this depth and the darkness, Norton et al., isolated halophiles from the halite deposits [12]. In this project we will be attempting to isolate and characterize halophiles from halite, as well as from other salt-rich sediments such as potash, sylvinite, anhydrite and polyhalite, in order to gain an understanding of potential life in the subsurface of Mars. Although the Boulby mine is used as a martian analogue environment [13], it does possess certain key differences from modern Mars, in particular its aerobic environment. Our long-term goals, once we have characterized the micro-organisms present, is to expose them to Mars conditions (past and present) to determine their survival potential. We will also investigate differences between their growth in the mine and in the simulated martian brine environments. To detect the presence of potential extinct or extant life on Mars, we will also focus on attempting to define biomarkers that may be left by halophile growth and degradation in these Mars-like conditions.

References:

[1] Mahaffy, P., et al., Science, 2014. [2] Hassler, D.M., et al., Science, 2014. 343(6169). [3] McEwen, A.S., et al., Nature Geoscience, 2013. [4] Sawyer, D.J., et al., Meteoritics & Planetary Science, 2000. 35(4): p. 743-747 [5] Osterloo, M., V. Hamilton, J. Bandfield, T. Glotch, A. Baldridge, P. Christensen, L. Tornabene and F. Anderson (2008). Science 319(5870): 1651-1654. [6] Jones, B. and D. Deocampo, Treatise on geochemistry, 2003. 5: p. 393-424. [7] Grant, W. D., R. T. Gemmell and T. J. McGenity (1998). Halophiles. Extremophiles: Microbial Life in Extreme Environments. K. Horikoshi and W. D. Grant, Wiley. [8] Adamski, J. C., J. A. Roberts and R. H. Goldstein (2006). Astrobiology 6(4): 552-562. [9] Fendrihan, S., et al., Astrobiology, 2009. 9(1): p. 104-112. [10] Sankaranarayanan, K., et al., PLoS One, 2011. 6(6): p. e20683 [11] Landis, G.A., Astrobiology, 2001. **1**(2): p. 161-4. [12] Norton, C.F., T.J. McGenity, and W.D. Grant, Journal of General Microbiology, 1993. 139(5): p. 1077-1081. [13] Cockell, C.S., et al., 2013. 54(2): p. 2.25-2.27.

THE EFFECTS OF TEMPERATURE ON THE RAMAN SPECTRUM OF HIGH PURITY QUARTZ CRYSTALS.

R. Hibbert[1], M. C. Price[1], T. M. Kinnear[1], M. J. Cole[1] and M. J. Burchell[1], [1]Centre for Astrophysics and Planetary Science, School of Physical Sciences, Univ. of Kent, Canterbury. (E-mail: rh443@kent.ac.uk).

Introduction: Quartz (SiO_2) is known to be present on Mars and has been identified to be in its crystalline form near Antoniadi Crater on the northern edge of the Syrtis Major shield volcano [1]. The *ExoMars* rover, due to launch in 2018, will carry the first Raman spectrometer to be deployed on another planetary body [2, 3].

Rationale: Raman spectroscopy is generally regarded as a nondestructive technique; this statement is incorrect. Concentrated laser power can generate localized heating leading to devolatisation, crystalline changes, and even melting of the sample [3]. These heating effects, coupled with the large fluctuation of Mars' surface temperature over the course of one Sol, could lead to misinterpretation of spectral data. This study aims to investigate how changes in temperature affect the Raman spectrum of quartz; either due to changes in the ambient temperature, and/or changes due to localized heating caused by the exciting laser. Further work is also ongoing [4] looking at how shock affects the Raman spectrum of quartz with the ultimate goal to being able to disentangle the two effects of heating and shock.

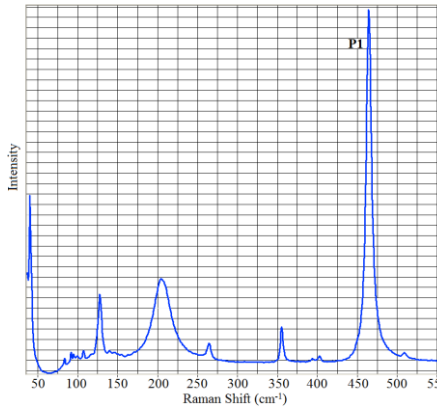

Fig. 1: Raman spectrum of quartz at 25°C with the main peak at 464 cm^{-1} labelled 'P1'

Raman spectroscopy uses monochromatic laser light to illuminate a sample. When the laser light strikes a molecule in the sample, most of the light is unaffected and is detected at its original wavelength. A very small amount of the light, however, shifts due to interaction with the molecule and is detected at wavelengths specific to the composition of the sample. This is known as Raman scattering [5]. Because the Raman scattering is specific to the composition of the sample, Raman spectroscopy can be used to identify specific molecular bonds within the sample.

The University of Kent's Raman spectrometer is a Horiba LabRam-HR equipped with four lasers: near infrared (785 nm), red (633 nm), green (532 nm), and blue (473 nm). In addition, it has a *Linkam* temperature controlled stage which can be used to cool/heat samples to between -180°C and 600°C. The work carried out in this investigation used the 532 nm green laser that mimics the laser which will be carried on *ExoMars*. The Raman spectrum for quartz at 25°C can be seen in Fig. 1, with the main peak located at 464 cm^{-1} labelled as 'P1'.

Methodology: A 9.03 ct quartz gemstone was placed in the *Linkam* temperature stage and heated to 30°C at a rate of 1°C per minute. Once 30°C had been reached the sample was allowed to stabilise for one hour before Raman spectra were obtained. The sample was then heated by 10°C at a rate of 1°C per minute and again allowed to stabilise for one hour before another spectrum was acquired. This process continued up to a maximum temperature of 300°C. To obtain data for temperatures below room temperature the quartz sample was cooled in the *Linkam* stage using a liquid nitrogen pump. At the beginning of this experimental run, the sample was first heated to 30°C (in the same manner as before) to allow for a comparison between the two experiments. Once this first datum was obtained, the sample was then cooled by 10°C at a rate of 1°C per minute and the sample was allowed to stabilise for one hour before Raman data was obtained. This process continued down to -40°C where a second datum point was obtained before the final run of experiments continued to a minimum temperature of -100°C.

This Raman data were then processed using a Python script which uses the least-squares fitting routine to find the exact position of the P1 peak at each temperature and then plot this position against the sample temperature.

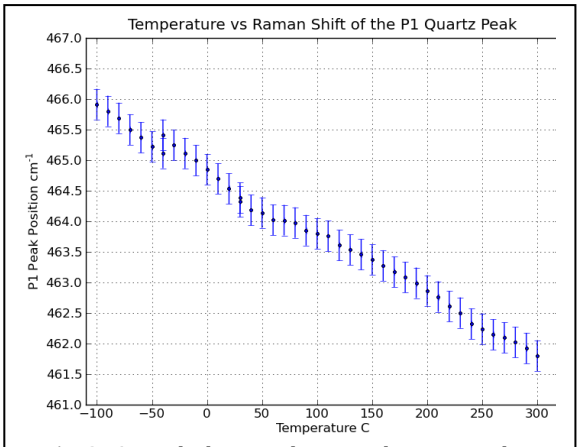

Fig. 2: A graph showing the P1 peak position when the quartz sample is subjected to varying temperatures.

Results: The graph of temperature vs P1 position can be seen in Fig. 2. The plot shows a definite trend indicating that as the temperature of the sample is increased the P1 position decreases in wavenumber. The P1 position at -100°C is 465.92 cm^{-1}, while at 300°C it is 461.80 cm^{-1}, giving a total variation of 4.12 cm^{-1} across a 400°C temperature difference.

Conclusion: As can be clearly seen in Fig. 2, there is a strong negative trend showing the P1 position, decreasing in wavenumber as the temperature increases. Further work will expand the temperature range to test the sample at temperatures between -180°C and 600°C. Using the Stokes and anti-Stokes ratio, the temperature of the sample itself will be calculated to compare with the ambient temperature of the stage to see how much laser heating has occurred.

References: [1] Bandfield J.L. et al (2004a) *J. Geophys. Res.*, 109, E10009 **[2]** Rull F. et al. (2011). *42nd LPSC* abstract #2400. **[3]** Rull F. et al. (2013). *44th LPSC* abstract #3110. **[4]** Hibbert R. et al (2015) *LPSC (these proceedings)* **[5]** Raman C.V. (1928). *Indian J. of Phys.*, 2, 387-389.

Acknowledgments: RH thanks Uni. of Kent for receipt of a PhD. tuition fees scholarship. MCP thanks the STFC, UK.

SIMULATING JUPITER'S GLOBAL ATMOSPHERIC DYNAMICS AND CLOUDS USING A GENERAL CIRCULATION MODEL

R. M. B. Young[1] and P. L. Read[1]. [1]Atmospheric, Oceanic and Planetary Physics, Department of Physics, University of Oxford. E-mail: young@atm.ox.ac.uk.

Abstract: We have been developing a model of Jupiter's atmosphere using the MIT general circulation model (MITgcm) to study its dynamics, clouds, and moist convective events. In particular we are interested in how various phenomena contribute to the formation and maintenance of the ubiquitous zonal jet structures. Jupiter and Saturn have superrotating equatorial jets (unlike Uranus and Neptune), which require an additional source of momentum flux into low latitudes, as superrotation cannot arise using angular momentum conservation arguments alone. Various effects may be at work, including baroclinic instability driven by differential heating between equator and poles, an internal planetary heat source, latent heat release from condensation, and heating via moist convection.

Building on earlier work by other groups [1, 2] and on a previous version of our simulation that used the Met Office Unified Model [3, 4], we present the current state of our research after a series of simulations were run using the Darwin cluster, part of the STFC DiRAC facility. Our model includes phenomena such as small-scale vertical mixing and dry convective adjustment, a simple 2-stream radiation scheme, realistic solar differential heating, internal heating from below, and an optional drag term reflecting possible MHD drag. These simulations investigated the spin-up of Jupiter's jet streams and cloud features under various combinations of these effects, chosen to isolate the effects of individual phenomena. The model shows spontaneous development of Jupiter-like zonally banded jet stream and layers of ice clouds formed of ammonia, ammonium hydrosulphide, and water at different levels (Fig. 1).

References: [1] Lian Y. and Showman A. P. 2008. *Icarus.* 194:597-615. [2] Schneider T. and Liu J. 2009. *JAS.* 66:579-601. [3] Zuchowski L. C. et al. 2009. *Icarus.* 200:563-573. [4] Zuchowski L. C. et al. 2009. *PSS.* 57:1525-1537.

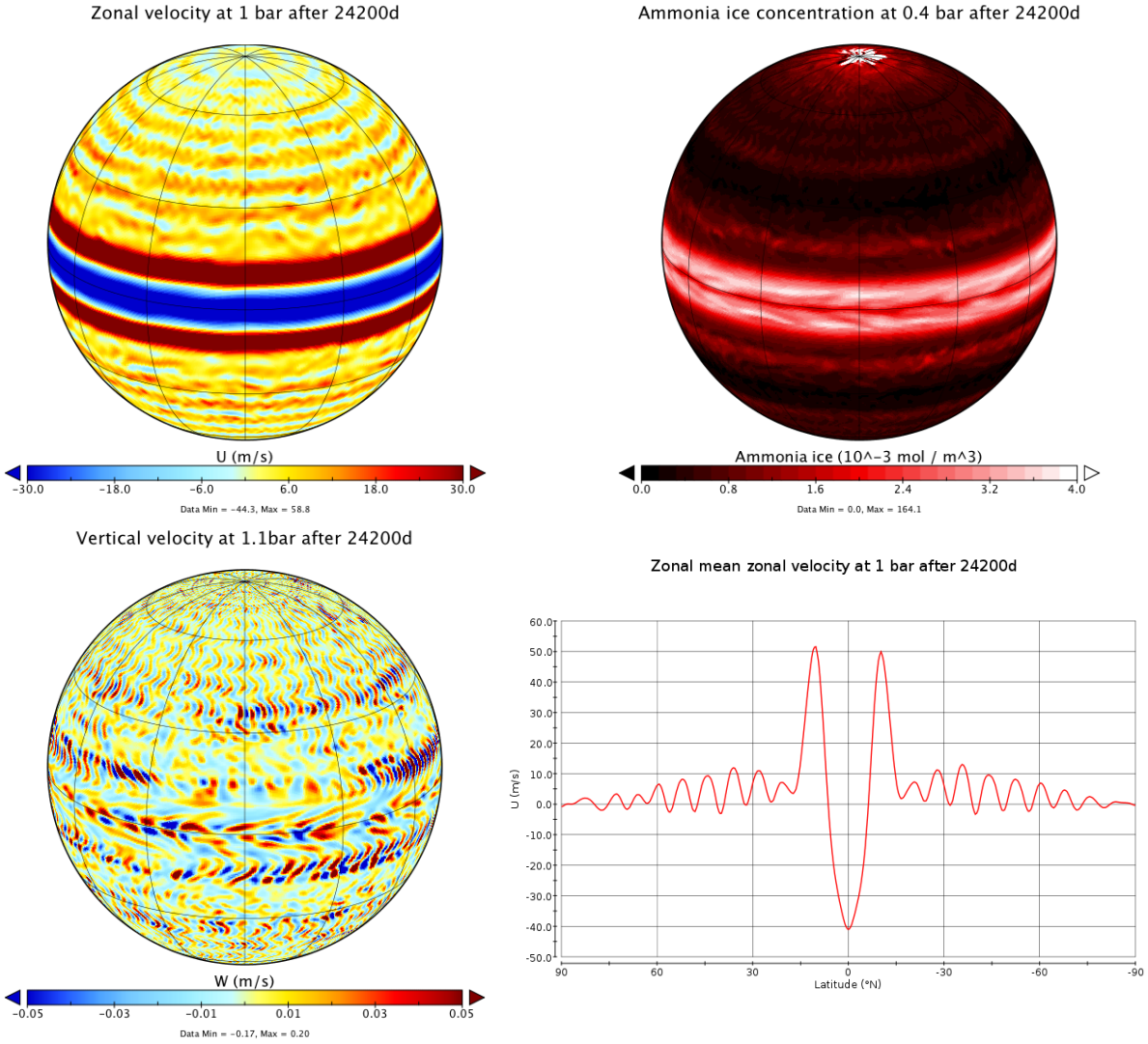

Figure 1: Jupiter simulated using MITgcm after 24200d simulated time, with realistic solar differential heating, 5.6 W m^{-2} internal heat flux, and MHD drag. Zonal and vertical velocities are shown at 1 bar, and ammonia ice concentration at 0.4 bar.

The Origin of water and other volatiles in the inner solar system as shown by Howardite-Eucrite-Diogenite (HED) meteorites.

T. J. Barrett[1], R. Tartèse[1, 2], J. J. Barnes[1], M. Anand[1, 3], I. A. Franchi[1], M. M. Grady[1], R. C. Greenwood[1], B. L. A. Charlier[1]
[1]Department of Physical Sciences, The Open University, Milton Keynes, MK7 6AA, UK. E-mail: thomas.barrett@open.ac.uk. [2]Muséum National d'Histoire Naturelle, Laboratoire de Minéralogie, 61 rue Buffon 75005, Paris, France. [3]Department of Earth Sciences, Natural History Museum, London, SW7 5BD, UK.

Introduction: Volatile elements play a fundamental role in planetary formation and evolution through their influence on melting, silicate melt viscosity, magma crystallization and eruption processes. The Howardite-Eucrite-Diogenite (HED) suite of meteorites represents the largest suite of crustal rocks available from a differentiated basaltic asteroid and account for between 2-3% of all meteorites collected globally [1]. This group of meteorites are also some of the oldest igneous rocks in the solar system, remaining relatively unaltered since their formation ~8 to 20 Ma after the formation of the solar system, and offer insight into the planetary accretion process(es). Therefore, by investigating the abundance and source(s) of volatiles they contain we can begin to constrain the timing when water (H_2O) existed in the inner solar system. Knowing precisely when water accreted in the inner solar system also has implications for how and when life emerged on Earth and possibly beyond.

The source of volatiles in planetary bodies can be investigated in a number of different ways. For water, the ratio between the two isotopes hydrogen (deuterium, D or ^{2}H and hydrogen, ^{1}H) has been widely used, since measured D/H ratios in different objects, formed in different regions of the solar system, vary widely (~25-fold variation in D/H ratios) [2]. Isotopic measurements of other volatile elements such as C and N can also provide additional constraints on volatile source regions. Recent advances in analytical instrumentation and techniques have enabled high-precision *in situ* measurements in volatile-bearing minerals such as apatite [e.g. 3-5].

Apatite [$Ca_5(PO_4)_3(OH,F,Cl)$] is a widely distributed mineral, albeit in trace amounts, in planetary materials which acts as a recorder of volatile abundances in magmas and magmatic source regions [6] and is the most common volatile-bearing phase in lunar rocks [7,8] and eucrites [6]. New apatite data has shown that eucrites have similar D/H ratios to those measured in terrestrial rocks and in CI chondrites, implying that water could have accreted early in the inner solar system [5] as opposed to dry accretion and subsequent late delivery of water [9,10].

The putative parent body of the HED meteorites is the asteroid 4 Vesta [11, 12], which is believed to have experienced a similar differentiation history as the Moon, making it an excellent analogue [13]. We are currently undertaking a detailed study of HED meteorites using *in-situ* Secondary Ion Mass Spectrometry (SIMS) on apatites and Step Combustion Mass Spectrometry on whole-rock samples to better constrain the volatile inventory and evolutionary history of 4 Vesta.

Methods & Results: We used the Cameca NanoSIMS 50L at the Open University to measure H_2O abundances and D/H ratios in apatite grains from four basaltic eucrites (DaG 844, DaG 945, Millbillillie, Stannern) using the protocol described in [3]. In total, 21 measurements were made on 15 different apatite grains. Apatite H_2O abundances range from ~50 to ~3450 ppm, and are associated with a weighted average δD values of -9 ± 55 ‰ (2σ).

Discussion: Our results are within error of and extend the range of data reported by [5] and are consistent with a common source of water for Vesta, the Earth, the Moon, Mars and carbonaceous chondrites [9, 14, 15]. No systematic variation is seen between H_2O abundance or δD and different geochemical trends and metamorphic grades. DaG 945 contains less water and is believed to have undergone granulitic metamorphism and at least some partial melting [16], which could explain the low water contents measured in apatite in this sample.

Other volatile elements. We are currently in the process of obtaining samples for C, N and noble gas isotope data for a small selection of eucrites to complement our SIMS studies.

References: [1] Janots E. et al. 2012. *MAPS*. 48(11):2135-2154. [2] Robert F. et al. 2000. *Space Sci Rev.* 92:201–224. [3] Barnes J. J et al. 2013. *Chem. Geol.* 337-338:480-55. [4] Tartèse R. et al. 2014. *MAPS*. 1-24. [5] Sarafian A. R. et al. 2014. *Science*. 346:623-626. [6] Sarafian A. R. et al. 2013. *MAPS*. 48(11):2135-2154. [7] McCubbin F. M. et al. 2011. *GCA*. 75(17):5073-5093. [8] McCubbin F. M. et al. 2010. *Am. Mineral*. 95(8-9):1141-1150. [9] Tartèse R. et al. 2013. *EPSL*. 361:480-486. [10] Albarède F. 2009. *Nature*. 461:1227-1233. [11] McCord T. B. et al. 1970. *Science*. 168:1445-1447. [12] Binzel R. P. and Xu S. 1993. *Science*. 260:186-191. [13] Mandler B. E. and Elkins-Tanton L. T. 2013. *MAPS*. 48:2333-2349. [14] Usui T. et al. 2012. *EPSL*. 357-357:119-129. [15] Robert F. 2006. *MESSII*. 341-351. [16] Yamaguchi A. et al. 2009. *GCA*. 73(23):7162-7182.

Acknowledgements: This work was funded by an STFC PhD studentship (to TJB). We would like to thank Francis McCubbin at the University of New Mexico and Alex Bevan at the Western Australian Museum, for allocation of samples without which this work would not have been possible.